Development of a Passive Check Valve for Cryogenic Applications

by

Bradley D. Moore

A thesis submitted in partial fulfillment of
the requirements for the degree of

Master of Science

(Mechanical Engineering)

at the

UNIVERSITY OF WISCONSIN – MADISON

2013

This page intentionally left blank

APPROVED BY

_____

PROFESSOR FRANKLIN K. MILLER
(Advisor)

_____

PROFESSOR JOHN M. PFOTENHAUER
(Co-Advisor)

DATE:_____

This page intentionally left blank

Acknowledgements

First and foremost, I would like to thank my family. Without your love and patience with a "head in the sky" son and brother, none of this would have been possible. Thanks to my siblings: Ben, Becca, Brianne, and Brendan for each providing me with a unique example to learn from and follow. Mom and Dad, you have always been there to love and support me. The greatest thanks of all is to my little buddy Andrew, the strength you taught me can never be put into words. I'll never regret getting to spend one more month with you.

Special thanks to my advisor, Prof. Franklin Miller, I have you to thank for my current career path. It's been a long journey from introductory Thermodynamics my junior year, but I have enjoyed every moment of it. Our conversations have spanned economics to superfluid Helium and if I can retain even a quarter of it I'll be a far more intelligent individual. Thanks to my co-advisor, Prof. John Pfotenhauer, for reminding me to take a step back and take the time to do things right. Thanks to Professors Nellis and Klein, I entered into your classes a boy and left a man.

Thanks to all of the folks I've worked with over the past few years: Jim Maddocks, for passing along a good deal of your vast wisdom in Cryogenics and life in general; Amir Jahromi, for patiently teaching me most of my experimental skills, even if they came with a few scars; Ser Eric of the Alar, for keeping me humble, entertaining, and entertained; Rogelio, for putting up with my terrible accents; Russell, for reminding me that I'm not really all that hippy; Diego, engage number one; The new guys in the office, Nate, Tom, and Brian, best of luck getting work done without me distracting you; The rest of the folks on the

13th floor who I have worked with, John E., Wenjie, Dongsheng, Rodrigo, Greg, Kendra, Doug, Bryant, Amanda, John D. and anyone else that I may have missed.

Special acknowledgment goes to the Wisconsin Space Grant Consortium, NASA SBIR program, and the UW Mechanical Engineering Department for financial support.

Abstract

Detectors requiring cryogenic cooling, such as transition edge sensor (TES) bolometers, microwave kinetic inductance detectors (MKIDs) or microcalorimeters on X-ray spectrometers, represent the state of the art for Infrared and X-ray astrophysics missions. To achieve the highest degree of resolution, cooling to temperatures below 1 K is required. A Cold Cycle Dilution Refrigerator (CCDR) is a continuous refrigerator capable of cooling to temperatures below 100 mK by using a novel thermal magnetic pump developed by Prof. F.K. Miller. This novel pump requires check valves to operate. This research is devoted to the design, fabrication, modeling and testing of a passive check valve for cryogenic applications, specifically for the CCDR. This thesis contains the check valve physical design as well as a laminar flow model predicting the performance of the valve. The facility design, operation and test results in both liquid nitrogen and on a Pulse-Tube Cryocooler are also included. The results of those tests where then compared to the model and a scaling argument was created for the performance of the valve in the actual CCDR.

Table of Contents

List of Figures

List of Tables

Nomenclature

Section 1

T_{valve}	Temperature of check valve (K)
ΔP_s	Sealing pressure difference supply by CCDR (kPa)
ΔP_{ff}	Forward Flow pressure drop allowable in CCDR (Pa)
$\dot{m}_{ff}$	Forward Flow rate of ^{3}He-^{4}He mixture (mgs^{-1})
$\dot{m}_{lb}$	Acceptable Leakage rate in CCDR (µg-s^{-1})

Section 2

$\Delta L_{inner,net}$	Net change in length of inner components (in)
$\Delta L_{brass,abutment}$	Change in length of brass abutment (in)
$\Delta L_{Teflon,seat}$	Change in length of Teflon seat (in)
$\Delta L_{steel,reed}$	Change in length of steel reed (in)
$\Delta L_{copper,washer}$	Change in length of copper washer (in)
$\Delta L_{stainless,screen}$	Change in length of stainless mesh screens reed (in)
$\Delta L_{shell,net}$	Change in length of outer shell (in)
$L_{brass,abutment}$	Length of brass abutment (in)
$L_{Teflon,seat}$	Length of Teflon seat (in)

$L_{steel,reed}$	Length of steel reed (in)
$L_{copper,washer}$	Length of copper washer (in)
$L_{stainless,screen}$	Length of stainless mesh screens reed (in)
$L_{brass,shell}$	Length of outer shell (in)
T_1	High temperature of integration for thermal contraction (K)
T_2	Low temperature of integration for thermal contraction (K)
α_{brass}	Thermal expansion coefficient for brass (K^{-1})
α_{Teflon}	Thermal expansion coefficient for Teflon (K^{-1})
α_{steel}	Thermal expansion coefficient for steel (K^{-1})
α_{copper}	Thermal expansion coefficient for copper (K^{-1})
α_{SS304}	Thermal expansion coefficient for stainless steel 304 (K^{-1})

Section 3

Re	Reynolds number (-)
ρ	Density of fluid ($kg\text{-}m^{-3}$)
v	Velocity of fluid ($m\text{-}s^{-1}$)
d_h	Hydraulic diameter of duct (m)
μ	Viscosity of fluid (Pa-s)

Per	Perimeter of duct (m)
A_c	Cross-Sectional area of duct (m^2)
$\dot{m}_{tot}$	Total mass flow rate through all micro channels ($kg\text{-}s^{-2}$)
n_{ch}	Number of micro channels
d_{ch}	Average diameter of micro channels
L_{ch}	Average length of micro channels

Section 4

$\dot{m}_{He}$	Actual mass flow rate of helium through omega flow meter (slpm)
$\dot{m}_{meas}$	Measured mass flow rate of helium through omega flow meter (slpm)

Section 5

w_{max}	Max deflection of circular plate (m)
v	Poisson's ratio (-)
F	Distributed load on plate ($N\text{-}m^{-2}$)
a	Radius of plate (m)
E	Young's modulus material (Pa)
th	Thickness of plate (m)
m	Geometric constant for laminar scaling argument (m^{-4})

1 Introduction

This thesis is devoted to the design, fabrication and modeling of a passive check valve for cryogenic applications. Check valves are common flow control devices in many conventional fluid systems. The basic function is to block flow in one direction, and allow it in the opposing direction. Often the operation is passive, actuated by the fluid flow itself with aid from mechanical features such as springs. In general, check valves are designed within the parameters of a specific system. The forward flow rate, acceptable leakage rate, and acceptable pressures are all important design criteria for valve design and are uniquely dependent on the application and working fluid of the system itself. It is this specificity that makes the design of a passive cryogenic check valve difficult. The limited literature available is tailored to certain applications with very different pressures, flow rates, and even fluids. This research was initially motivated by the need for passive check valve for application in a novel cold cycle dilution refrigerator (CCDR) proposed by Prof. F.K. Miller at the University of Wisconsin. As will be discussed in greater detail, the CCDR is a specific application which requires low flow rates, low sealing pressures, and low temperatures. As it became clear that passive valves would be difficult to implement in the CCDR, the investigation evolved into a study of the performance of the check valve through a broad temperature regime, serving to improve the general understanding and expertise of check valves of the UW Cryogenic Engineering Group.

1.1 Cold Cycle Dilution refrigerator

This research was initially motivated by the CCDR, so its design and requirements merit discussion. The CCDR is a sub-Kelvin refrigeration system for space based applications,

specifically in Infrared and X-ray astrophysics missions. Detectors requiring cryogenic cooling, such as transition edge sensor (TES) bolometers, microwave kinetic inductance detectors (MKIDs) or microcalorimeters on X-ray spectrometers, represent the state of the art for these missions. To achieve the highest degree of resolution, cooling to temperatures below 1 K is required. Current space flight technologies used to obtain sub-Kelvin temperatures are the Adiabatic Demagnetization Refrigerator (ADR), the single shot, space-pumped dilution refrigerator and the ^{3}He evaporation refrigerator. A continuous refrigerator capable of cooling to temperatures below 100 mK by implementing a cold cycle dilution refrigerator (CCDR) using a novel thermal magnetic pump developed by Prof. F.K. Miller provides an alternative to these technologies.

1.1.1 System Overview

The cold cycle dilution refrigerator will consist of a pump, a heat rejection stage, a set of four flow rectifying check valves, two recuperative heat exchangers, a phase separation chamber, a mixing chamber and a throttle detailed in Figure 1.1. A Temperature vs. ^{3}He concentration diagram corresponding to this system can be found in Figure 1.2.

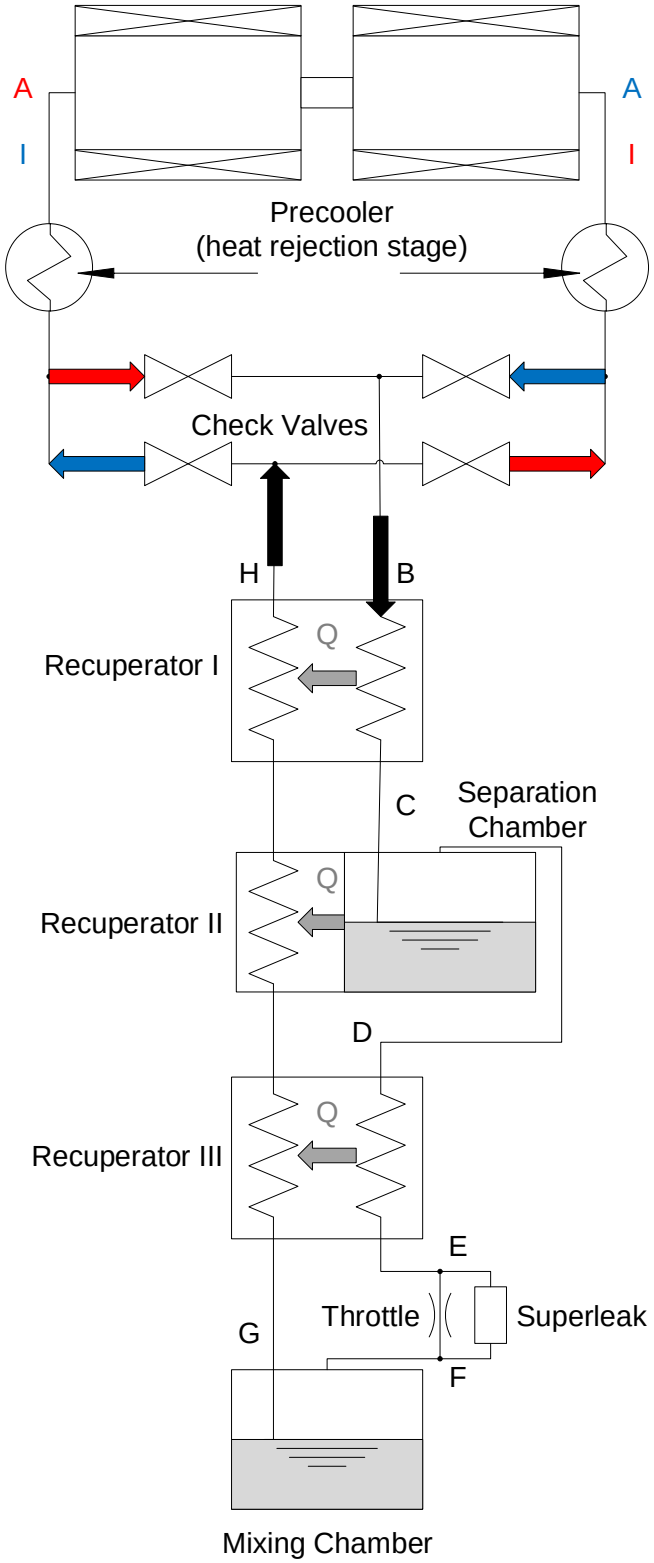

Figure 1.1: Schematic of the cold cycle dilution refrigerator.

The system fundamentally operates on the properties of mixtures of two isotopes of Helium, ^{3}He-^{4}He. At low temperatures, these mixtures can be separated into 2 phases, dilute (low concentration of ^{3}He) and concentrate (high concentration of ^{3}He). The endothermic mixing of these two phases at temperatures below 0.7 K is ideally suited for sub Kelvin cooling. The superfluidity of the ^{4}He component below 2.17 K is another important aspect. An exhaustive explanation of superfluidity can be found in various texts, such as W. E. Keller's Helium-3 and Helium-4, but for the purposes of this report the chief property is the lack of viscosity. The entire CCDR operates at temperatures below 2.17 K, also referred to as the Lambda point, so the ^{4}He component can flow unimpeded through the system, while the flow of ^{3}He can be managed. The ^{3}He component can said to be operating in a quasi-vacuum of ^{4}He. (Keller, 1969)

With the basic fundamentals of the working fluid established, the cycle as a whole can be described. As will be discussed later, the pump utilizes the well-known superfluid fountain effect to drive the mixture of dilute ^{3}He-^{4}He (^{3}He concentration ~ 6%) out of the pump at state A. The dilute stream rejects the load and pumping heat to a precooling stage, comprised of a cryocooler or pumped ^{4}He bath. The pump is an oscillating flow device, so it is necessary to rectify the flow by a system of 4 check valves to maintain the systemic flow direction indicated by the black arrows in Figure 1.1. The blue and red arrows into and out of the check valves indicate the alternating flow directions produced by the pump before the valve system. The fluid enters into a recuperative heat exchanger at state B and is cooled as it exchanges heat with the low concentration stream. The high concentration stream cools along a line of constant ^{4}He chemical potential as shown in Figure 1.2. Therefore, the concentration of this stream increases as the temperature decreases through the recuperator.

The working fluid exits the cold end of the recuperator as a 2-phase mixture and enters a separation chamber where the ^{3}He rich phase (D) is separated from the ^{3}He dilute phase. For ground- based applications this separation is achieved by gravity due to the density difference between the phases, as is typical in traditional dilution refrigerators. In microgravity, surface tension forces will be used to accomplish the separation. The use of surface tension for phase separation has been developed at the NASA Ames Research center. (Roach & Helvensteijn, 1999)

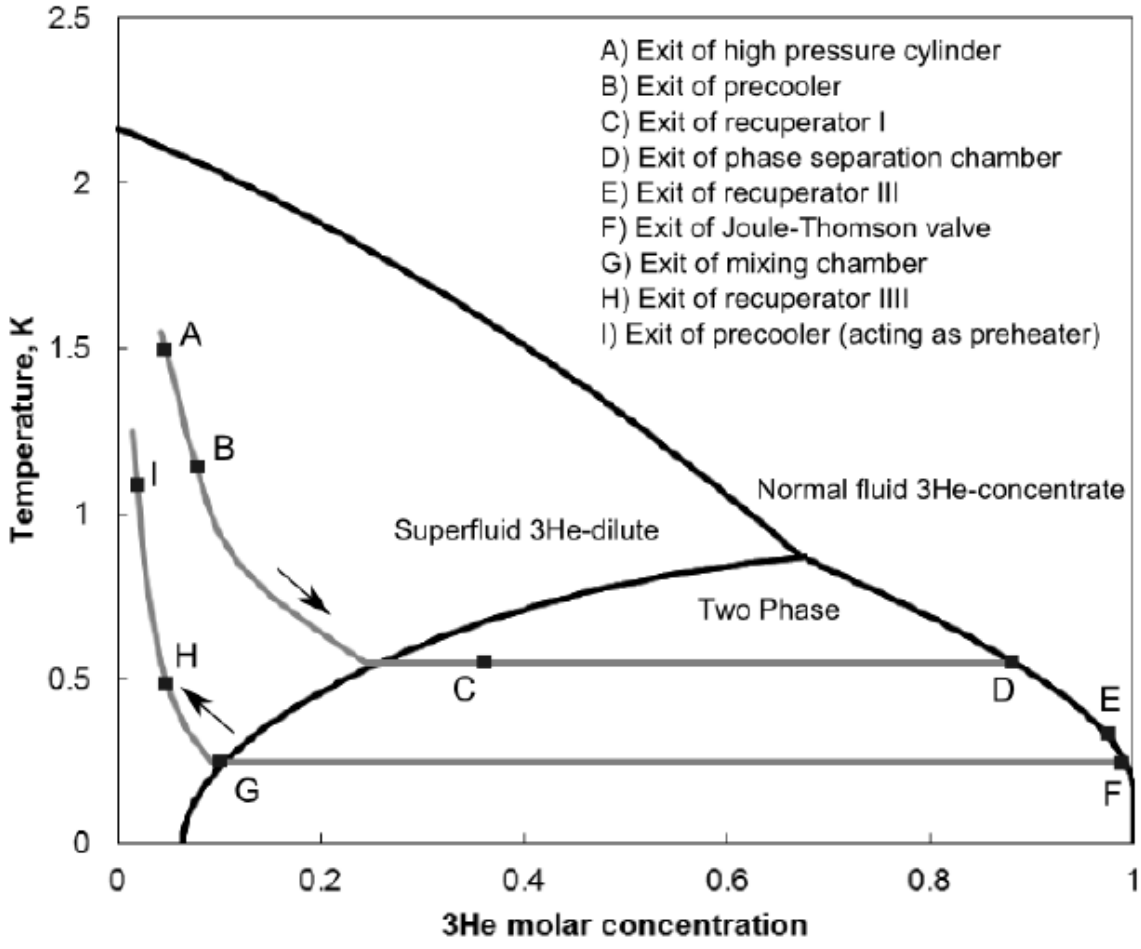

Figure 1.2: Plot of the cold cycle dilution refrigerator cycle on a T- x_3 diagram

Next, the ^{3}He rich phase exits the separation chamber and enters another recuperative heat exchanger and is cooled by the low concentration stream to state E. The fluid is then throttled through a capillary, producing a pressure drop and temperature drop to state F. The high ^{3}He concentration mixture enters a mixing chamber and is diluted with ^{4}He. The process of mixing ^{3}He into ^{4}He is endothermic therefore heat is absorbed from the load, providing the primary cooling at sub Kelvin temperatures. The dilute mixture (G) exits the mixing chamber and returns to the pump via the two recuperative heat exchangers, rejecting heat to the high concentration stream. The dilute stream then reenters the pumping subsystem (I and H), completing the cycle.

1.1.2 Pump Subsystem

At NASA-Goddard Spaceflight Center, Miller developed a thermodynamically reversible fountain effect pump shown in Figure 1.3. (Miller & Brisson, A Superfluid Pulse Tube Driven by a Thermodynamically Reversible Magnetic Pump, 2009) The pump consists of two canisters packed with Gadolinium Gallium Garnet (GGG) spheres connected by a piece of Vycor glass, called a superleak. A superconducting magnetic coil surrounds each of the canisters. The operation of the pump can be simplified into 4 primary steps shown in Table 1.1. At the beginning of the pump cycle (process step I), the current in the coil around cylinder A is increased while the current in cylinder B is decreased. This causes the magnetic field in A to increase while the magnetic field in B decreases. As the field increases in the paramagnetic GGG spheres the magnetic entropy decreases causing the thermal entropy in the spheres and the surrounding fluid to increase (the temperature increases) consistent with process step I.

At the same time the field in the other bed is decreasing, thereby allowing the magnetic dipoles of the GGG to disorder and increase the magnetic entropy, decreasing the thermal entropy of the fluid. The temperature gradient across the superleak results in a pressure gradient that causes the configuration to act like the well-known fountain effect pump. When the pump contains a dilute mixture of ^{3}He-^{4}He, the low temperature side is gradually depleted of ^{4}He because the ^{4}He flows out through the superleak to the high temperature side to maintain constant chemical potential, while the ^{3}He is blocked by the superleak staying behind at the cold side (step II). The ^{4}He flowing across the superleak drives the flow forward in the loop.

Eventually the cold side ^{4}He concentration drops to the point that it becomes necessary to reverse the direction of flow, which is accomplished by simply reversing the direction of the current in the superconducting magnetic coils, entering into process step III for cylinder A, and process step I for cylinder B. This causes the magnetic field and hence the temperature of the warmer bed (A) to begin decreasing while the field and temperature of the colder bed (B) begin increasing, thus reversing the direction of the pumping action and leading into step IV, when the ^{3}He is replenished in cylinder A and depleted from cylinder B. This configuration allows cyclic thermodynamic cycles to be driven without using pistons or moving parts.

Process Step	Process Description	Pump Concentration	Pump Temperature	Magnetic Field
I.	Raise temp at constant concentration	High	Rapidly increasing	Rapidly increasing to intermediate
II.	Discharge ^{3}He at constant temp	Decreasing	High	Ramp increase to maximum
III.	Lower temp at constant concentration	Low	Rapidly decreasing	Rapidly decreasing to intermediate
IV.	Replenish ^{3}He at constant temp	Increasing	Low	Ramp decrease to zero

Table 1.1: Pumping Process description

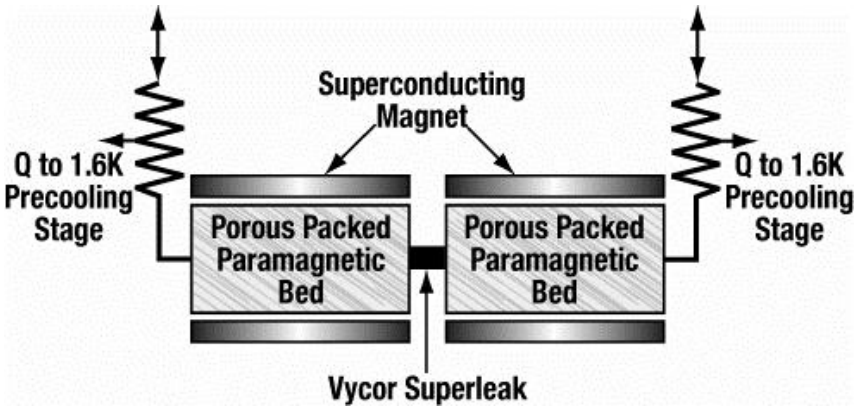

Figure 1.3: Schematic of the reversible pump.

Because of the requirement that the flow be reversed periodically, the pump is inherently an alternating flow device. However, it can be adapted to work with continuous flow thermodynamic cycles such as the proposed cold cycle dilution refrigerator by adding low temperature check valves, as discussed in the next section, to rectify the alternating flow.

1.1.3 Check Valve Requirements

The operation of the check valves in the system is best illustrated by a series of diagrams, Figure 1.4, Figure 1.5, Figure 1.6 and Figure 1.7. White valves are sealed; black valves are open, with arrows to indicate flow direction.

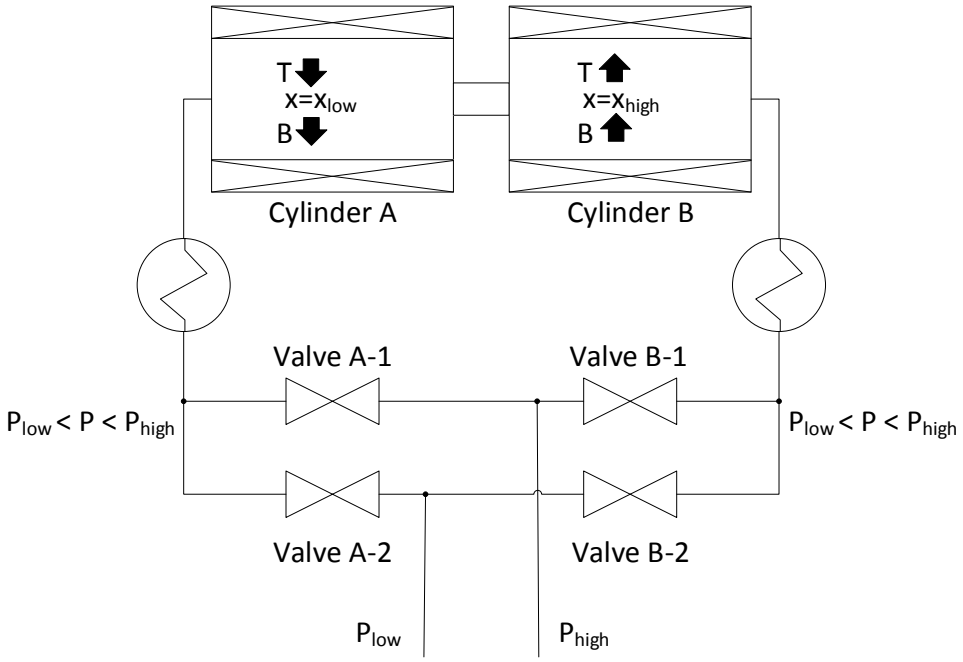

Figure 1.4: Process I, Cylinder A: Lowering temp at constant concentration, $P_{low}<P_A<P_{high}$, Cylinder B: Raising temp at constant concentration, $P_{low}<P_B<P_{high}$

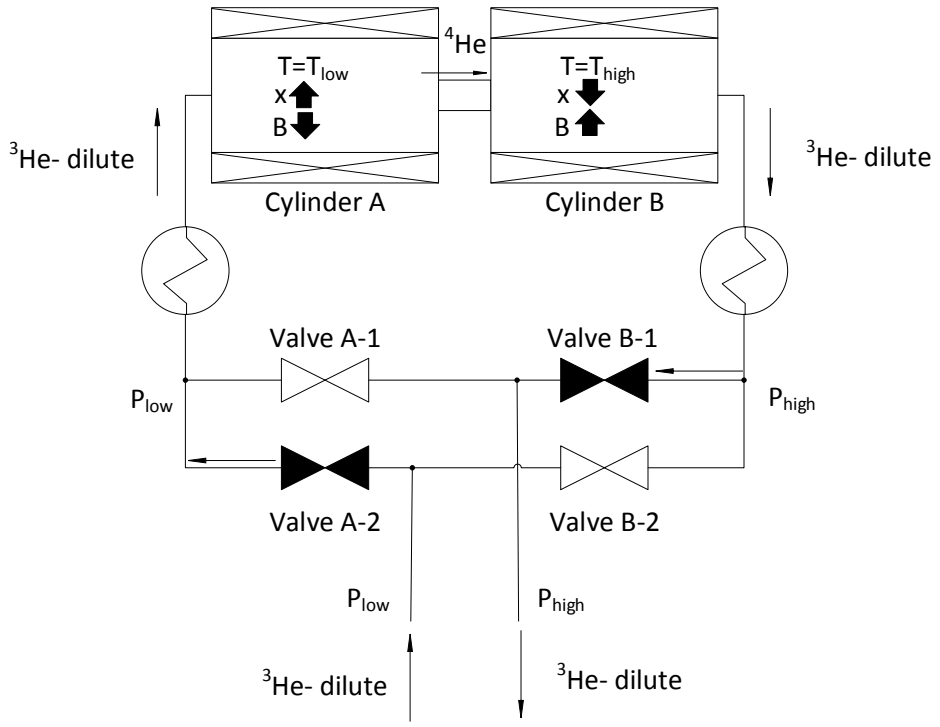

Figure 1.5 Process II, Cylinder A: Replenish ^{3}He at constant temp, $P_A = P_{low}$, Cylinder B: Discharge ^{3}He at constant temp, $P_B = P_{high}$

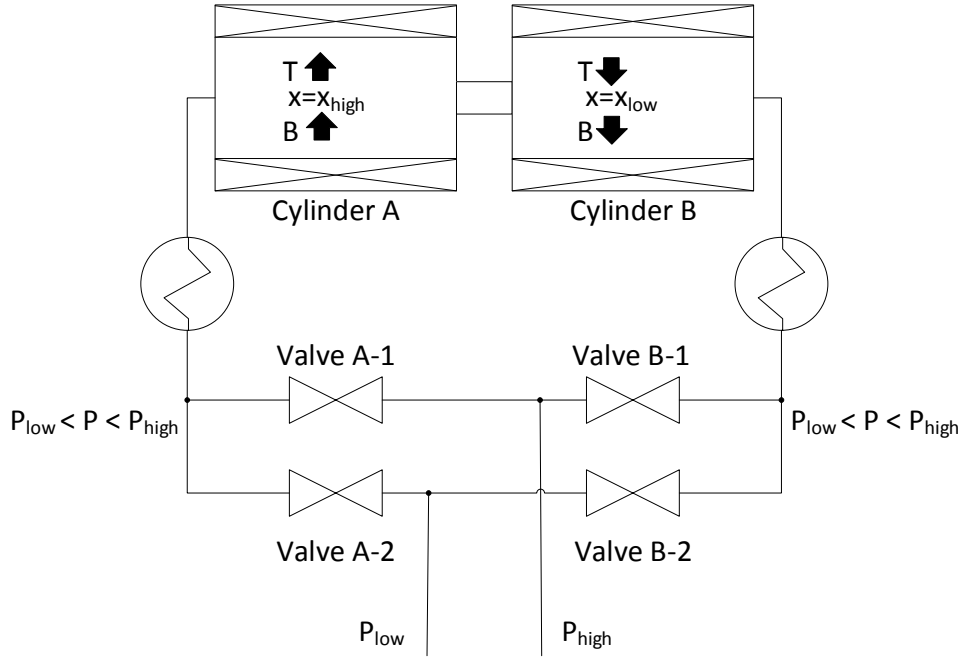

Figure 1.6 Process III, Cylinder A: Raising temp at constant concentration, $P_{low} < P_A < P_{high}$, Cylinder B: Lowering temp at constant concentration, $P_{low} < P_B < P_{high}$

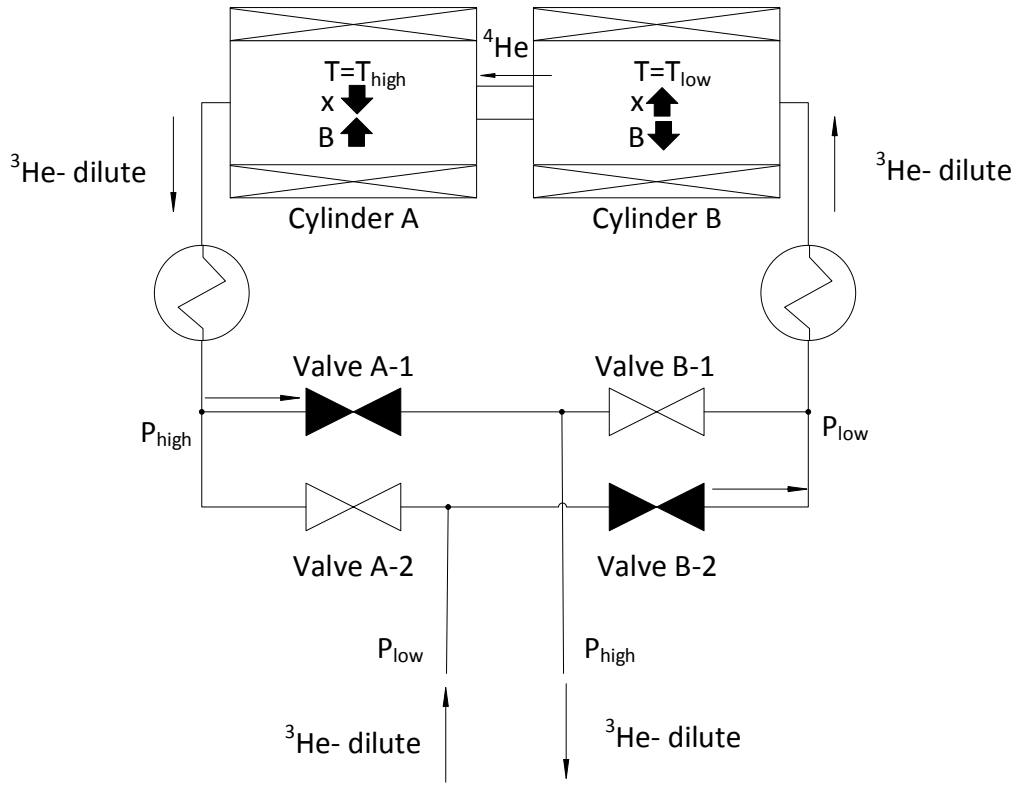

Figure 1.7 Process IV, Cylinder A: Discharge ^{3}He at constant temp, $P_A = P_{high}$, Cylinder B: Replenish ^{3}He at constant temp, $P_B = P_{low}$

Based on the process description and figures, valve A-1 must remain closed when the pressure in cylinder A is lower than the high pressure side of the cycle. A-2 must remain closed when the pressure in cylinder A is higher than the low pressure side of the cycle. In the same fashion, B-1 must close when the pressure in cylinder B is lower than the high pressure side and B-2 must close when the pressure in cylinder B is higher than the low pressure side. According to this set of criteria, all valves are closed in process I and III when the pressure in both cylinders is between the high pressure and low pressure sides of the cycle. It is also assumed that there is no significant cracking pressure to open the valves.

A numerical model of the CCDR was created as the Master's research of Bryant Mueller, another student working under Prof. Miller. Several parameters were varied in the model so

only selected results are shown in Figure 1.8, Figure 1.9 and Figure 1.10 to establish the design constraints of the valve.

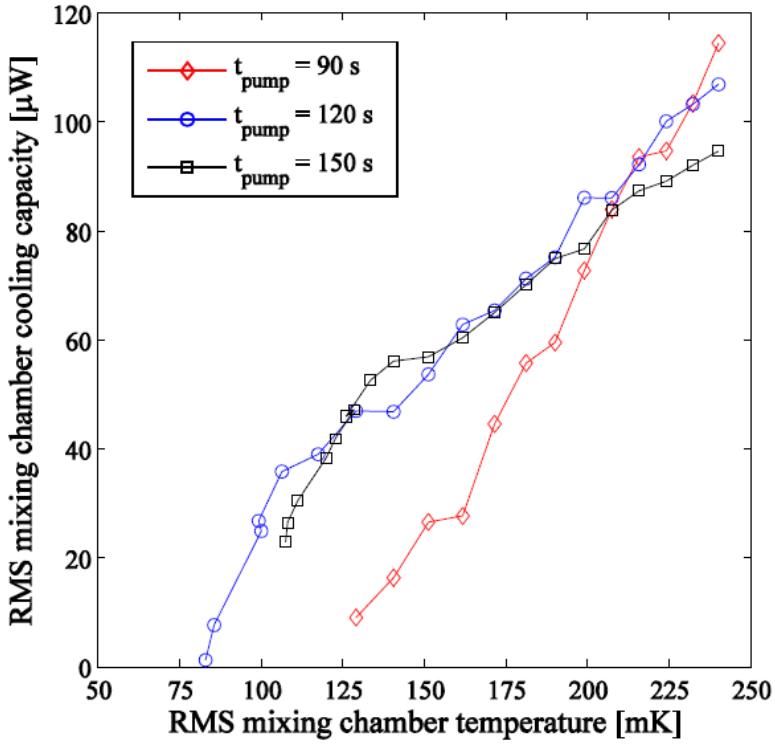

Figure 1.8: RMS mixing chamber cooling capacity

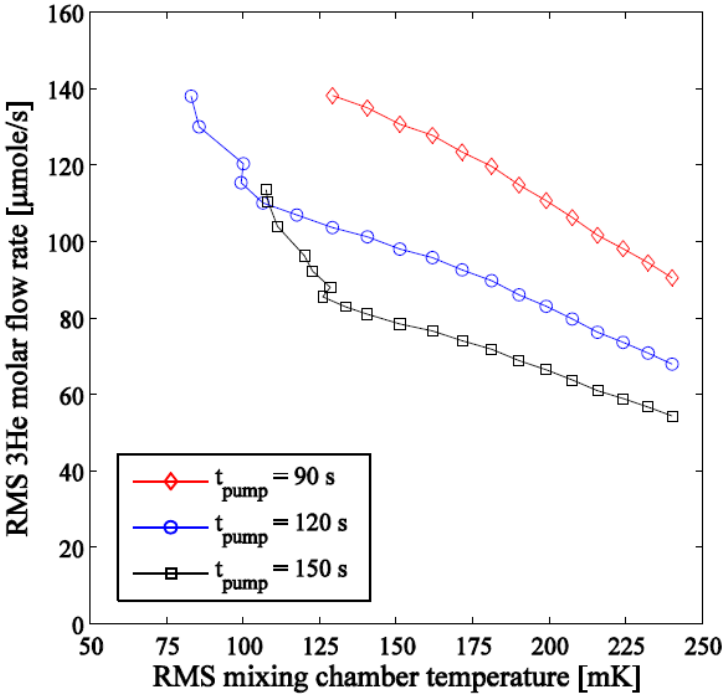

Figure 1.9: RMS ^{3}He molar flow rate variation with RMS mixing chamber temperature for multiple pump periods

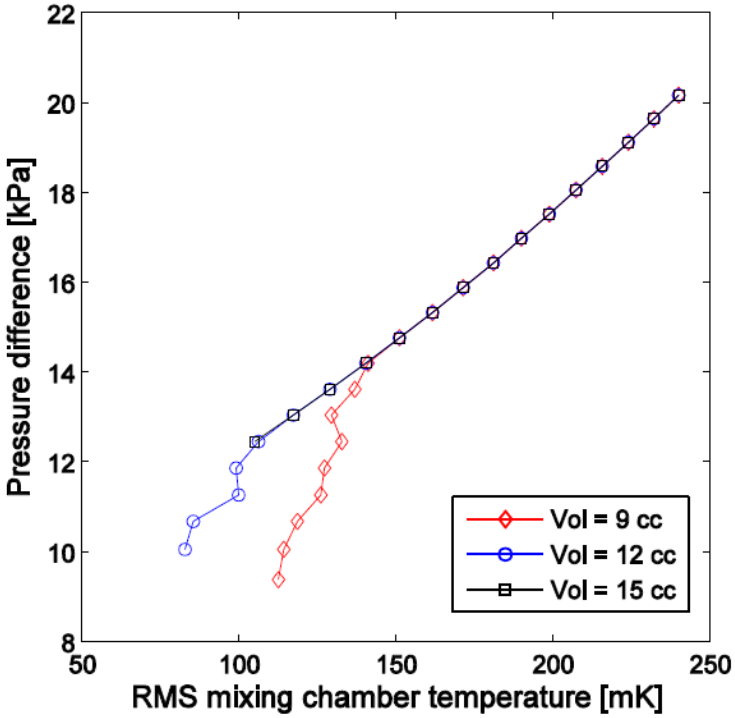

Figure 1.10: RMS pressure differentials for multiple cylinder volumes

The results of the model indicate that a pressure difference of approximately 10-20 kPa (1.45-2.9 psi) with a ^{3}He molar flow rate of 60-140 µmole/s will provide a cooling capacity of approximately 0-120 µW through a temperature range of 0.075-0.25 K. Assuming ^{3}He molar concentration leaving the pump is approximately 6%, the net mass flow rate of the mixture will be 3.94-9.20 mg/s. (Mueller, 2012)

Requirement	**Symbol**	**Value**
Working fluid		^{3}He-^{4}He mixture
Operating Temperature	T_{valve}	1.8 K
Sealing pressure difference	ΔP_s	10-20 kPa
Forward Flow pressure drop (1% of sealing ΔP_s)	ΔP_{ff}	100-200 Pa
Forward Flow rate	$\dot{m}_{ff}$	3.94-9.20 mg/s
Leakage rate (1% of forward flow)	$\dot{m}_{lb}$	39.4-92.0 µg/s

Table 1.2: Check valve requirements

As discussed earlier in this section, the design of a check valve is heavily dependent on the specific application. Utilizing the modeling efforts of Mueller, the requirements of the check valves can be fully specified as shown in Table 1.2. With these parameters established, the suitability of a passive check valve designed for the CCDR can be assessed.

1.2 Literature review

As discussed earlier, check valve design is very application specific. However there is previous work on cryogenic check valves intended for other systems that must be discussed. The following section will cover two other cryogenics check valve designs, one by Dr. James Maddocks of the Madison Cryo Group and the other by Veenstra et al at the University of

Twente in the Netherlands. Both have similar geometries to the valve presented in this thesis so they provide a good basis for comparison.

1.2.1 Sorption Compressor Check Valve

At the University of Twente development work was done on check valves to satisfy the requirements of a sorption compressor that would drive a 4.5 K Joule Thomson Cryocooler. The requirements of this system relevant to check valve design can be found in Table 1.3.

Requirement	**Value**
Working fluid	^{4}He
Operating Temperature	50 K
High pressure side sealing pressure difference	1.6 MPa
Low pressure side sealing pressure difference	.13 MPa
Forward Flow pressure drop	1 kPa
Forward Flow rate	1 mg/s
Leakage rate (at 16 bar)	3 µg/s

Table 1.3: Sorption Cooler Check Valve requirements

The valve consists of four main components shown in Figure 1.12, the vacuum seal, the spring disc, the valve seat, and the boss and valve spring. The vacuum seal is a standard copper seal to prevent leakage of helium out of the system. The remainder of the system is fabricated from AISI –SS316L to prevent differential thermal contraction. The spring serves to hold the boss and valve spring in place when the valve is pushed open from forward flow. Sealing occurs between the remaining two components, the seat and the boss. Both are polished to extremely high surface finishes, with height variations on the boss of less than

130 nm and height variations of the seat less than 80 nm shown in Figure 1.11. The valve seat also has a 15 µm gold layer to prevent a cold weld, as well as trap small particulates. Another way particulates are mitigated is the presence of filters embedded in the inlet and outlet lines which block any particles larger than .5 µm.

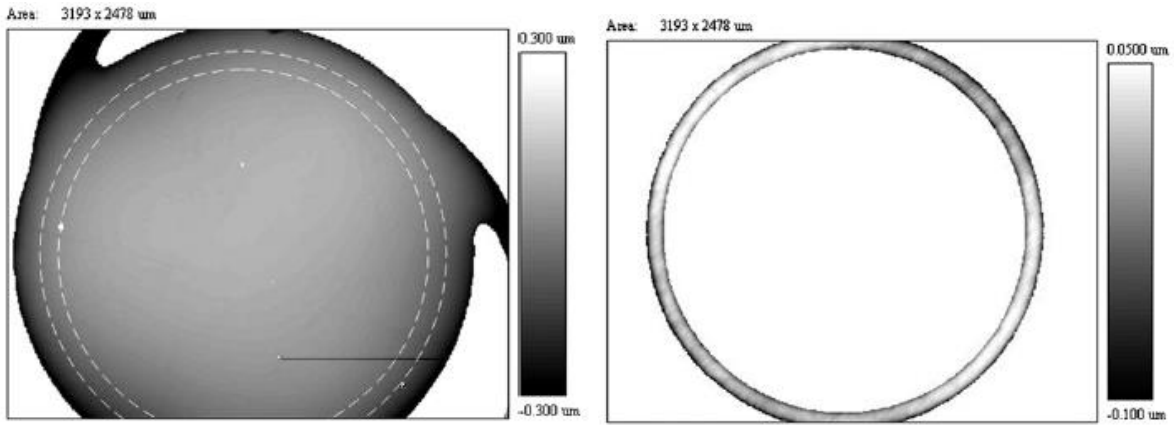

Figure 1.11: Surface finish of the boss (left) and the valve seat (right)

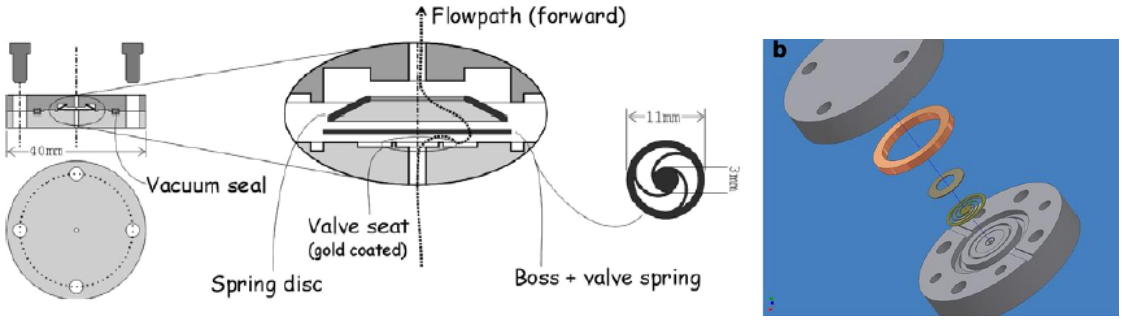

Figure 1.12: Schematic of check valve developed at the University of Twente (Veenstra, et al., 2007)

The results of tests at 50 K are shown in Figure 1.13. It is clear that the valve leak rate remained below the required leak rate through the entire pressure range. The forward flow pressure drop was also measured and found to be acceptable at approximately 100 mbar (10 kPa) at 1 mg/s. This is much higher than the design, but was deemed acceptable for the purpose of the valve.

It is clear that the check valve designed at the University of Twente must be fabricated with extremely tight tolerances and advanced techniques. It is also intended for higher pressures and much lower flow requirements than the CCDR, which is why this design was not replicated and tested. However, based on the analysis in this thesis, it became clear that this valve could present a possible alternative to utilizing actuated valves for the CCDR. Further investigation into this valve design is merited.

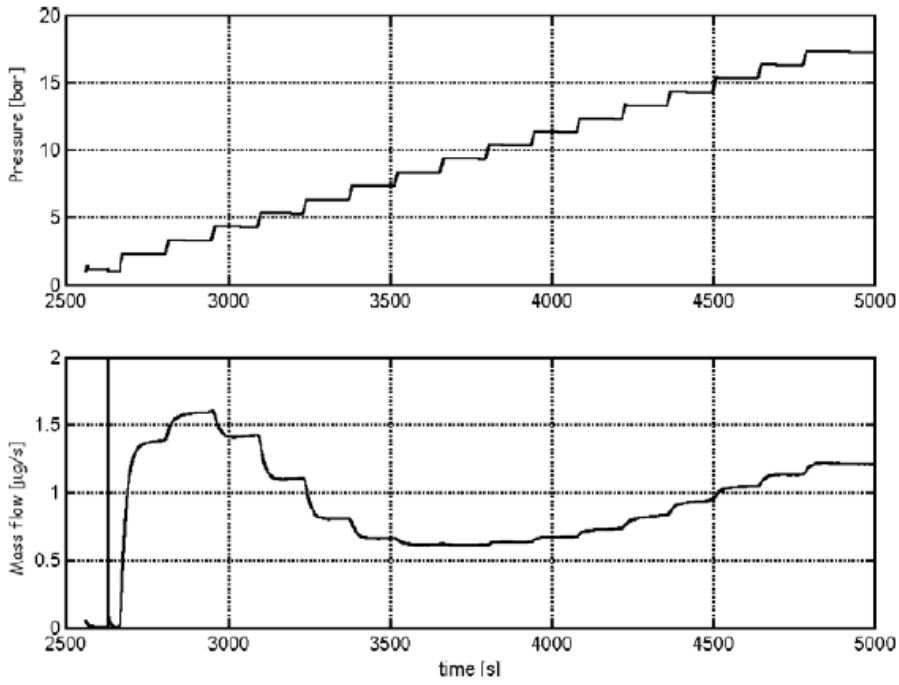

Figure 1.13: Cold test results from the University of Twente (Veenstra, et al., 2007)

1.2.2 Pulse Tube/Reverse Brayton Cryocooler Check Valve

The reed style design of the check valve in this thesis was heavily influenced by Dr. Jim Maddocks of the Madison Cryo Group (during the time of this work of Atlas Scientific). Maddocks gained a great deal of experience with reed style check valves while developing a

rectifying interface for a hybrid Pulse Tube/Reverse Brayton (PT/RB) cryocooler. In fact it was the surplus reeds from those tests that were used in this research. The pulse tube cycle can provide a large amount of cooling at higher temperatures, while the Reverse Brayton cycle can provide distributed cooling using helium as a working fluid. A portion of the oscillating pulse tube flow is rectified by check valves and provides continuous flow for the Reverse Brayton cycle.

The requirements of the valve are tabulated in Table 1.3. The additional fields of flow resistance in Pa-s/kg represent the data presented in the reference itself, with the conversion to actual pressure and leakage presented for convienience.

Requirement	**Value**
Working fluid	^{4}He
Operating Temperature	50 K
Sealing pressure difference (ΔP between high and low pressure)	.15 MPa
Leakage resistance	$9x10^8$ Pa-s/kg
Leakage rate	.167 g/s
Forward Flow resistance	$6x10^5$ Pa-s/kg
Forward Flow rate	28.7 g/s
Forward Flow pressure drop	17.2 kPa

Table 1.4: PT/RB check valve requirements

The valve is comprised of a brass seat and spring steel reed shown in Figure 1.14. Not shown in the figure are the copper washer and wave spring used to compensate for differential thermal contraction and to hold the reed in place when subjected to forward flow. Both the

seat and seal were polished to near a mirror finish, though measurements where not taken of the actual surface roughness. A high level of flatness was also required, although a qualitative assessment of this property was deemed adequate.

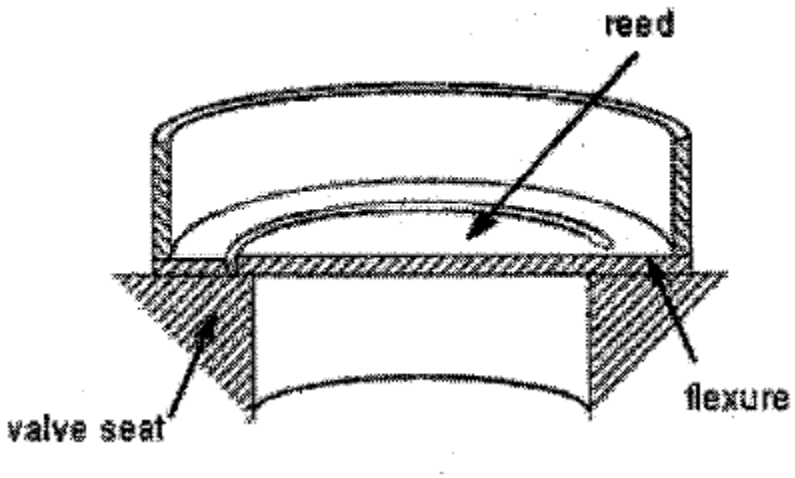

Figure 1.14: Schematic of check valve for PT/RB cryocooler (Diab, Nellis, Maddocks, & Yarbrough, 2004)

Upon testing the valve, it was found that the leakage rate of the check valve was below the range of the flow meter used in the experiment of .01 g/s. This was well below the required leakage rate, so further testing was not employed to determine the exact rate. Figure 1.15 illustrates the flow rate of the valve in the forward and sealing directions. The forward flow resistance was then extrapolated from this curve as $3x10^6$ Pa-s/kg, also below the required resistance.

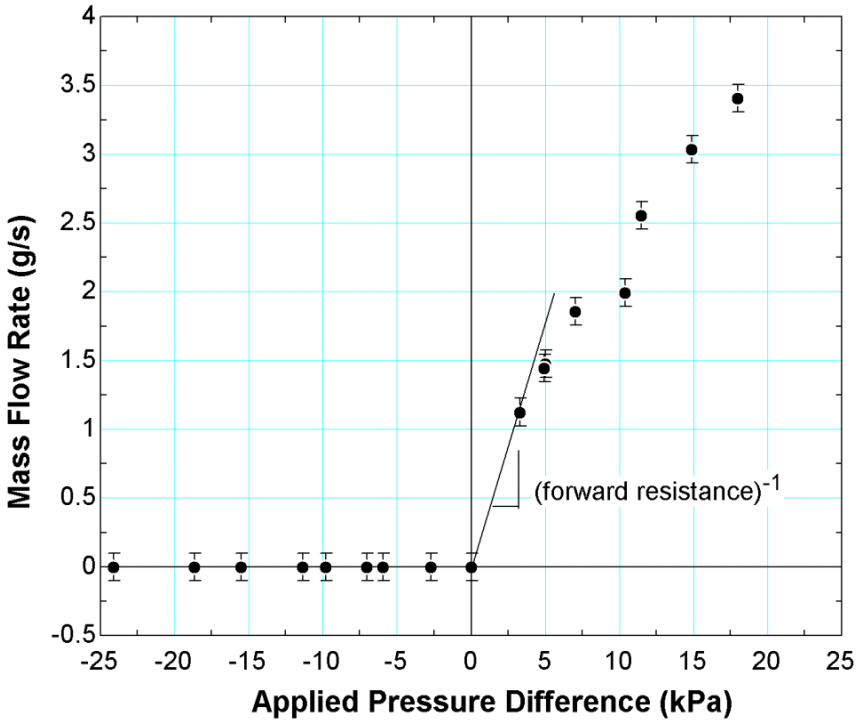

Figure 1.15: Forward flow and leakage rate of the PT/RB check valve (Diab, Nellis, Maddocks, & Yarbrough, 2004)

Though the valve design for the PT/RB cryocooler provided inspiration for the valve design contained in this thesis, it is clear that the flow rates and pressures involved are orders of magnitude higher than is required for the CCDR and, as a result, this valve cannot be employed directly. (Diab, Nellis, Maddocks, & Yarbrough, 2004)

1.3 References

Diab, A. K., Nellis, G. F., Maddocks, J. R., & Yarbrough, S. (2004). Development of a Rectifying Interface for a Hybrid Pulse Tube/Reverse Brayton Cryocooler. *AIP Conference Proceedings* (p. 710). American Institute of Physics.

Keller, W. E. (1969). *Helium-3 and Helium-4.* Plenum Press.

Mueller, B. (2012). Thermodynamic Modeling of a 3He-4He Cold Cycle Dilution Refrigerator. University of Wisconsin - Madison.

Miller, F. K., & Brisson, J. G. (2009). A Superfluid Pulse Tube Driven by a Thermodynamically Reversible Magnetic Pump. *Cryocoolers 15.* 15th International Cryocooler Conference.

Roach, P. R., & Helvensteijn, B. P. (1999). Progress on a Microgravity Dilution Refrigerator. *Cryogenics 39*, 1015-1019.

Veenstra, T. T., Venhorst, G. C., Burger, J. F., Holland, H. J., ter Brake, H. J., Sirbi, A., & Rogalla, H. (2007). Development of a Stainless Steel Check Valve for Cryogenic Applications. *Cryogenics*(47), 121-126.

2 Valve Design and Fabrication

2.1 Initial iterations

The original valve design was proposed by Miller based on work done at MIT on a manually actuated low dissipation valve for application in an earlier iteration of the CCDR concept. (Miller & Brisson, 1999). A key difference between the valve work done at MIT and the initial check valve iteration in this research is the use of annular flow and a spring to take the place of the weights and manual actuation used at MIT.

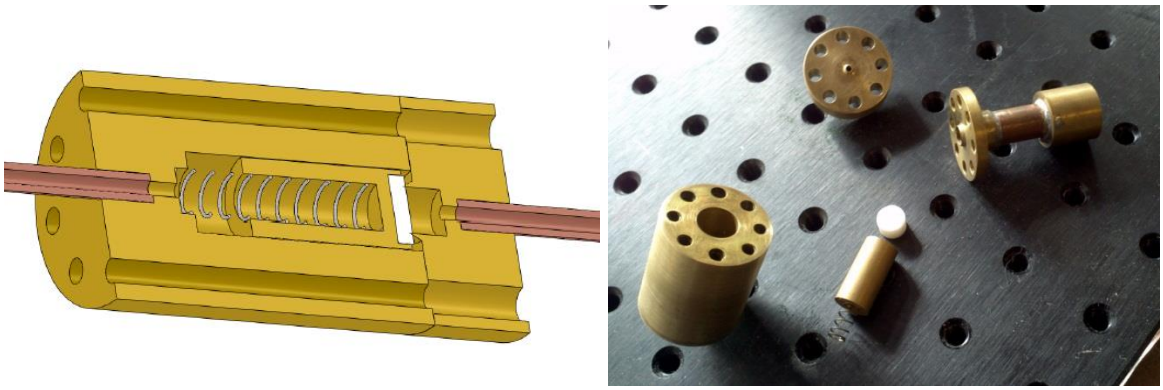

Figure 2.1: Initial iteration of poppet style valve

As seen in Figure 2.1, the initial iteration had poppet style geometry. A very tight tolerance between the poppet and body of the valve was required to maintain laminar flow through the annulus. The annular flow prevents the poppet from tilting and reorienting in flow, it also assists in maintaining a steady flow in the forward direction, counteracting possible instability due to the spring. The sealing occurs between the flat Teflon seat mounted in the poppet and the brass knife edge cut into the body of the valve. The Teflon seat was polished

to a near mirror finish and the knife edge was carefully machined to the limits of sharpness attainable by the available tools.

The first issue that surfaced with this geometry was preload. Miller's paper indicates that a force of approximately 98 N would be required to seal the valve and achieve acceptable leak rates. The springs available could not physically achieve this within reasonable limitations of initial length. This left the option of pressure preload. With the dimensions of the seat and knife edge, a pressure of approximately 230 psi would be required to achieve an acceptable leak rate. However, though unpublished, Miller had attained better sealing at lower pressures than the published results and so room temperature testing was pursued with this geometry. The leak back flow was higher than the range of the flow meter even as the applied back pressure was ramped up to 100 psi. It became clear that extremely high preloads were indeed required as indicated by the published results on the MIT valve. Several modifications of this poppet style geometry were attempted to lower this required pressure, such as a Teflon knife edge on flat brass, as well as various styles and sizes of the knife edge in both Teflon and brass. As all of these tests swamped the flow meter it became clear that the poppet style geometry would not provide adequate sealing for the CCDR.

The results of the initial poppet valve development returned the valve to the basic design phase. At this point Dr. James Maddocks's experience with reed style check valves became critical. With metal seated valves and surface finishes rough relative to the poppet valve seat, he had achieved better sealing at lower pressures than any of the poppet valve tests. However, as discussed earlier, the back flow rate on the metal seated reed valves employed in the Pulse Tube/Reverse Brayton Cryocooler was far too high for the CCDR. At this point

the polymer seat concept could be employed to improve the sealing of the reed style geometry.

2.2 Reed Valve

The principle of a reed valve is simple. As illustrated in Figure 2.2, a metal tongue is pressed over an orifice to seal against backflow. The sealing surface is then the overlap area between the diameter of the reed and the orifice. To open, the flow is reversed and the reed lifts allowing flow through a slit with varying area.

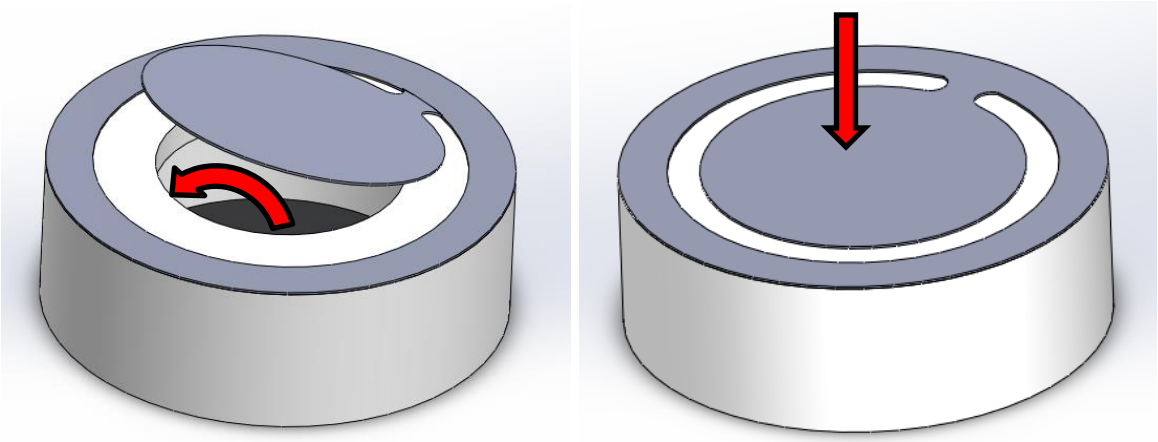

Figure 2.2: Open reed valve forward flow (left) and closed reed valve back flow (right), the red arrows indicate direction of flow

The valve itself consists of several components shown in Figure 2.3: the valve base, particulate screens, Teflon seat, spring steel reed, copper washer, steel wave spring, valve top, and indium O-ring. Detailed drawings of these components can be found in Appendix A.

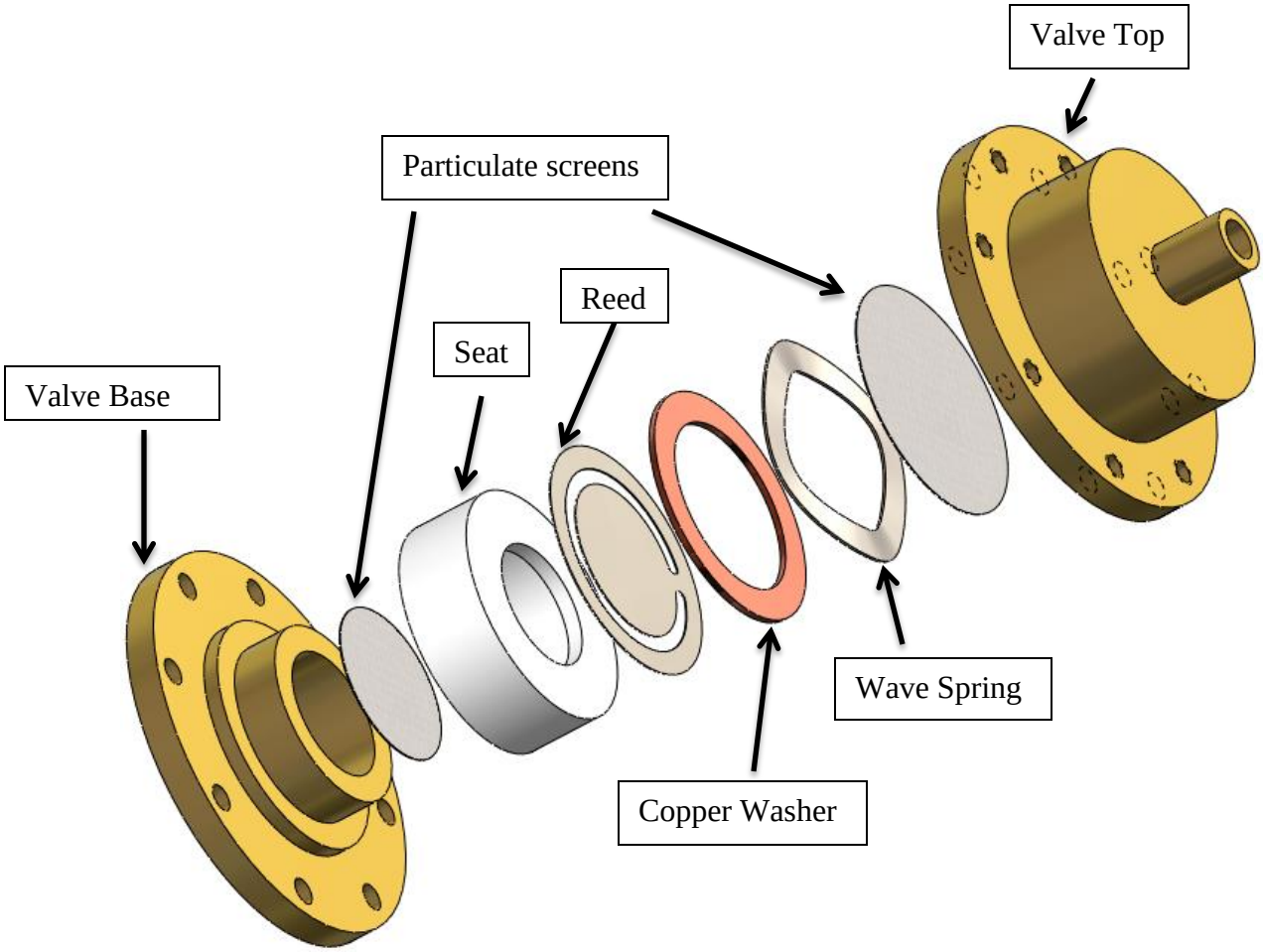

Figure 2.3: Exploded view of reed valve

2.2.1 Valve Base

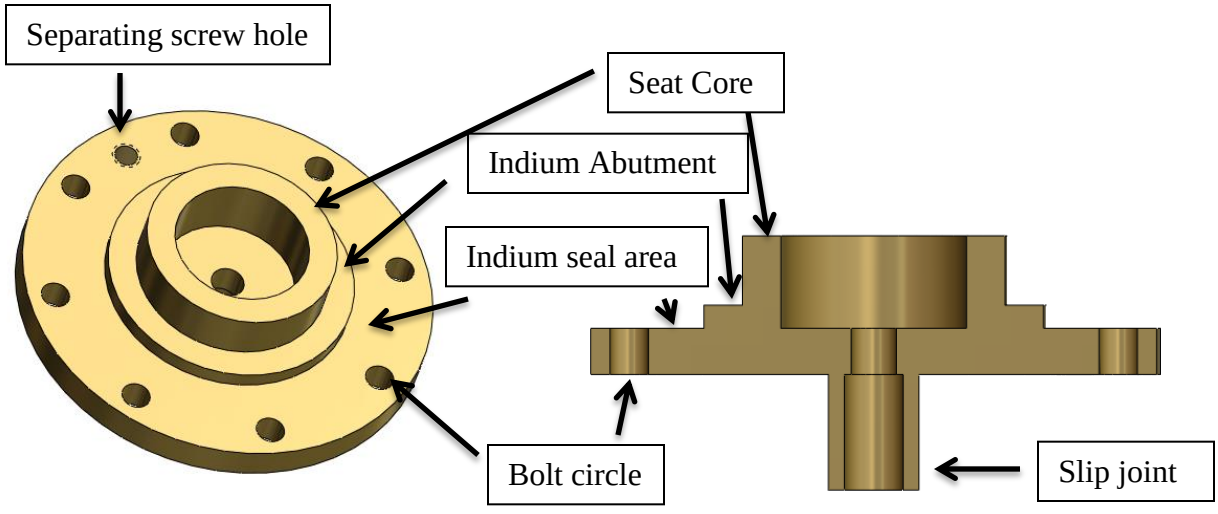

Figure 2.4: Reed valve base

Figure 2.5: Fabricated reed valve base

The valve base was fabricated from brass and can be found in Figure 2.4 and Figure 2.5. At the bottom of the part, there is a sleeve of brass to create a slip joint for 1/8" copper tubing. The wide flat section of the base serves to provide space for a bolt pattern of #2-56 screws with a radial gap remaining for the indium O-ring. The next feature is the abutment coming out of the wide flat section. It provides a feature for the indium to flow against, preventing it from pressing into the Teflon seat. The final feature of the valve base is the seat core. The Teflon seat is epoxied over this feature to prevent the Teflon seat from sliding off or slipping and to provide sealing at higher temperatures where the viscosity of Helium is high relative to the low temperature tests. Another important design consideration in the seat core feature is differential thermal contraction. The thickness of the walls of the brass seat is the same as the thickness of the corresponding walls on the seat itself. As the Teflon and brass cool, the Teflon will contract more than the brass, squeezing against it and providing a hermetic seal. The epoxy also serves to prevent the seat from being pushed off of the core by the

contraction. To find the overlap of the two materials as they cool down, a simple calculation was performed. Equation 2.1 provides the basis for computing the linear thermal contraction of a solid. (Pobell, 2007)

$$\alpha(T) = \frac{1}{L}\frac{dL}{dT} \tag{2.1}$$

It can be integrated through a temperature range to yield Equation 2.2 with ΔL as the change in length, L as the initial length, α as the thermal expansion coefficient, and T_1 and T_2 the temperature range.

$$\frac{\Delta L}{L} = \int_{T_1}^{T_2} \alpha(T)dT \tag{2.2}$$

The linear thermal expansion coefficient α is experimentally determined, and an integration must be performed to determine the net change in length over a temperature range. An often employed assumption here is that the radial contraction can be simulated as a linear contraction with the radius taken as the length. Conveniently, EES (Engineering Equation Solver) has a built-in function (TotalThermalExp('Material name', T=Temperature)) that return the ratio of the net change in length to the original length from 293 K to a temperature provided to the function. Multiplying the radius of the interface between the Teflon seat and the brass core by the value provided by this function will yield the final radius of each of the parts at a given temperature. The difference between the two radii will give the interference. The surface finish of both of the parts is less than .001" as machined, so an interference of more than .001" will ensure a hermetic seal. This interference was plotted in Figure 2.6 as a function of temperature from room temperature (293 K) down to the lowest temperature available for this function in EES (4 K).

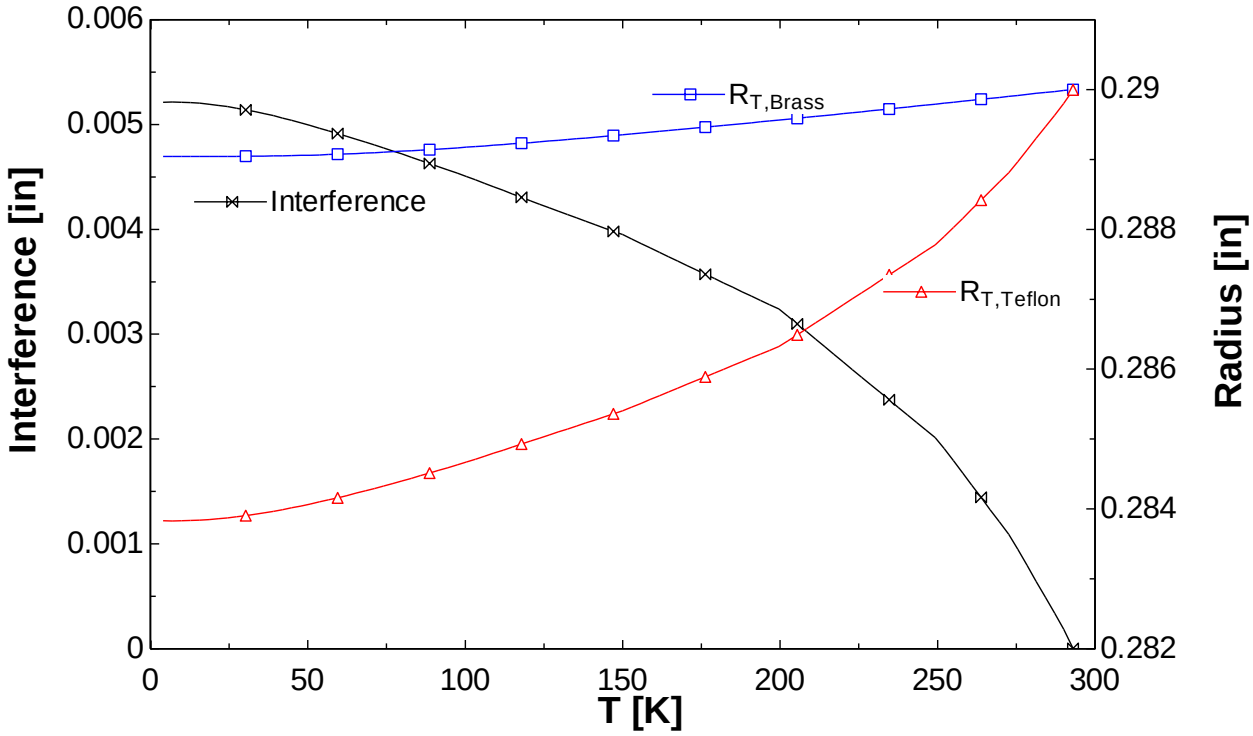

Figure 2.6: Outer radius of brass core and inner radius of Teflon seat and interference between the two plotted as a function of temperature

It is clear from this plot that after a drop in temperature of 20 K from ambient, the interference between the two parts increases beyond .001" and hermeticity is ensured. For the range of 293 K to 273K the epoxy provides adequate sealing.

2.2.2 Particulate screens

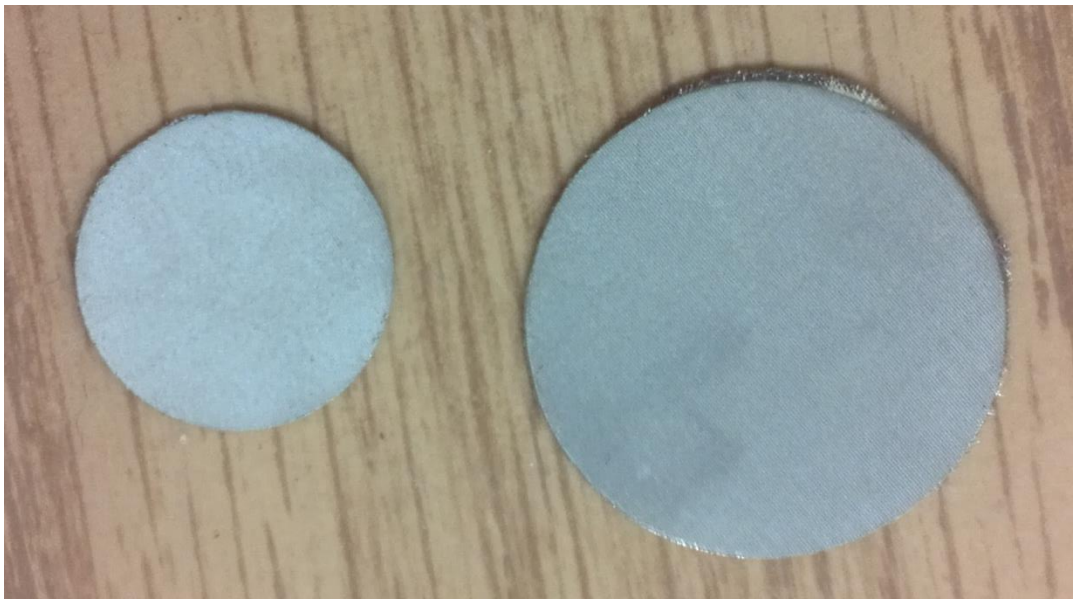

Figure 2.7: Particulate screens, small (left) and large (right)

In the experimental environment available, some form of particulate contamination was expected. None of the setup was fabricated in a clean room, and in spite of the care taken in construction small particulates continually appeared on the valve seat during the actual experiment. Thus, later in the design, particulate screens shown in Figure 2.7 were installed to attempt to mitigate this effect. Further discussion of these particulates and their implications will be discussed in the results section of this thesis. The late installation of the screens prevented the purchase of custom extremely fine screens. Ideally the screen would filter out all particulates larger than the average surface finish of the mating surfaces (in this case ~1-2 microns). However the finest screen available in an acceptable time frame and price range was a stainless steel 304, 200x1400 per square inch weave from McMaster-Carr. With a horizontal wire diameter of .0028” and a vertical wire diameter of .0016” this screen blocks particles larger than 10 microns in diameter. McMaster did not provide a specification for the open area of the screen and overlapping wires make estimation of the open area by

wire diameter and density alone difficult. However it was estimated that the open area was at least 10% based on the specifications of similar meshes available. For the small screen this would yield a net open area for flow of 0.0126 in^2 versus a cross sectional area of only 0.003 in^2 of the 1/16" inner diameter tubing leading to the valve. Therefore the pressure drop due to the screen can be considered negligible. Even so, the pressure drop across the screen was experimentally measured and found to be much less than 1 psi. The installation of the smaller particle screen was much more involved that the larger screen. The larger screen is simply placed between the valve top and the wave spring. It was created to have the same diameter as the inner diameter of the valve top using a sheet metal press. The pressure of the wave spring holds the screen in place blocking particulates in the back flow direction. However the spacing between the top of the brass core and the bottom of the valve seat prevents a similar press fit to be employed for the small screen. It was epoxied to the top of the brass core using Stycast 1266. However the fine mesh size coupled with the high viscosity of unset Stycast 1266 caused the epoxy to wick into the mesh. To prevent the epoxy from wicking and blocking the screen, the valve base was connected to a compressed air hose and air was blown through the screen until the epoxy had set. A Teflon ring was clamped over the screen to prevent the air pressure from blowing the screen off of the valve base. As will be discussed in the next sub section, untreated Teflon is very averse to bonding and the ring was easily removed after the epoxy had set. Figure 2.8shows the bonding setup for the small screen. After the screen was bonded, the Teflon seat was bonded over the core described in the next section.

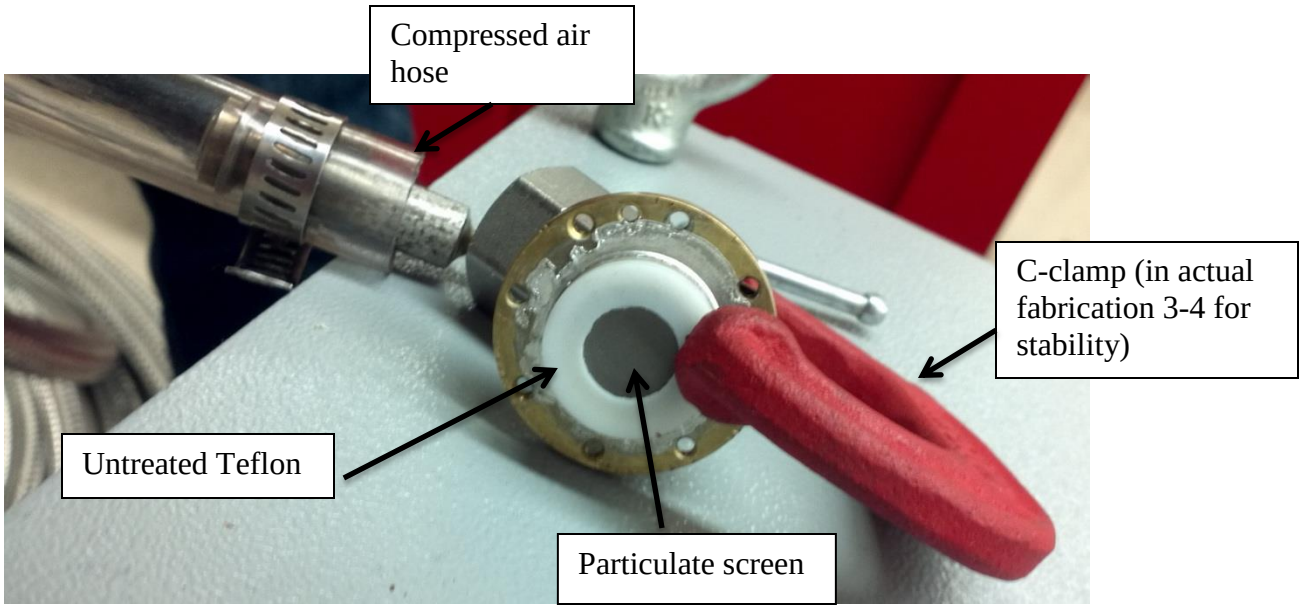

Figure 2.8: Small screen bonding setup

2.2.3 Valve Seat

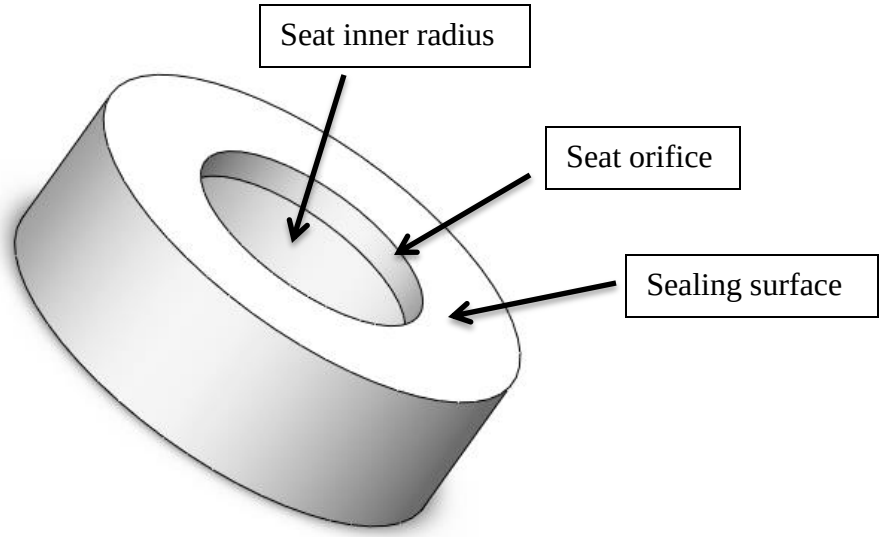

Figure 2.9: Teflon seat

The Teflon (Polytetrafluoroethylene, or PTFE) seat of this valve is the primary feature that differentiates the design from other cryogenic check valves. It can be seen in Figure 2.9. Teflon was selected based on Miller's experience with flouropolymer seats at MIT. These materials are advantageous due to their toughness and chemical inertness. A further

advantage for this application are the various relaxation peaks at temperatures of approximately -100 C, 20 C, and 127 C, as can be seen from Figure 2.10. Each of these relaxation peaks results in a phase transition of the internal structure of the Teflon, with the lowest temperature transition resulting in a phase with high toughness and little relaxation. (Rae & Dattelbaum, 2004) Therefore, if the Teflon seat can be preloaded and "formed" at a higher temperature and then cooled to cryogenic temperatures, when the preload is released the seat will retain its shape.

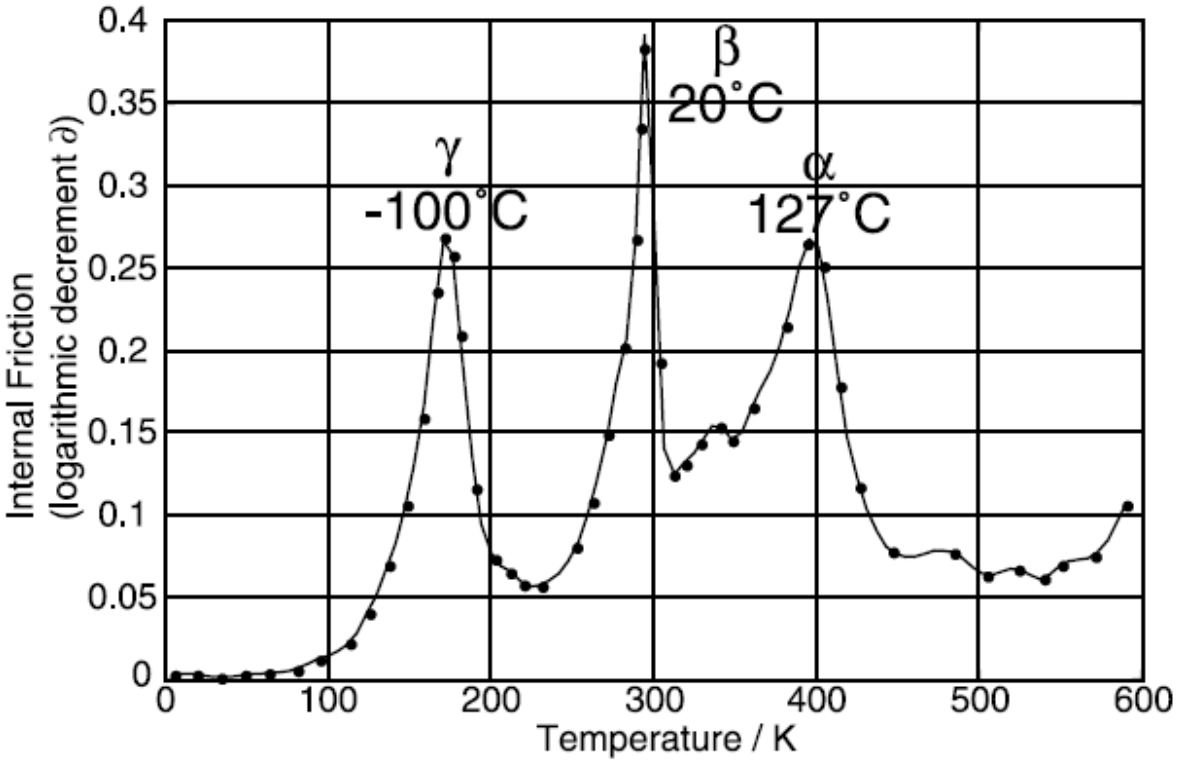

Figure 2.10: Relaxation peaks of Teflon (PTFE)

The dimensions are governed by constraints with other parts. The inner radius fits over the brass core of the valve base and must have the same radius as the outer radius of the core. The two parts must hold a close tolerance to ensure the press fit described in the valve core

section. The seat orifice is governed by the size of the reed tongue. A radial overlap of .05 in was selected, causing the orifice to be .4” in diameter.

A second consideration must be made for differential thermal contraction. As well as contracting in the radial direction, the Teflon and brass will contract in the axial direction at different rates with respect to temperature. The analysis of this difference was done assuming the bottom of the Teflon seat is fixed to the top of the indium abutment such that the inner radius of the Teflon is not fixed to the outer radius of the brass. The two initial lengths being compared are the valve core height vs. the seat inner radius height referred to in Figure 2.12. Utilizing the same assumptions and functions in EES as the radial analysis discussed earlier, but with the respective heights rather than radii, Figure 2.11 was generated.

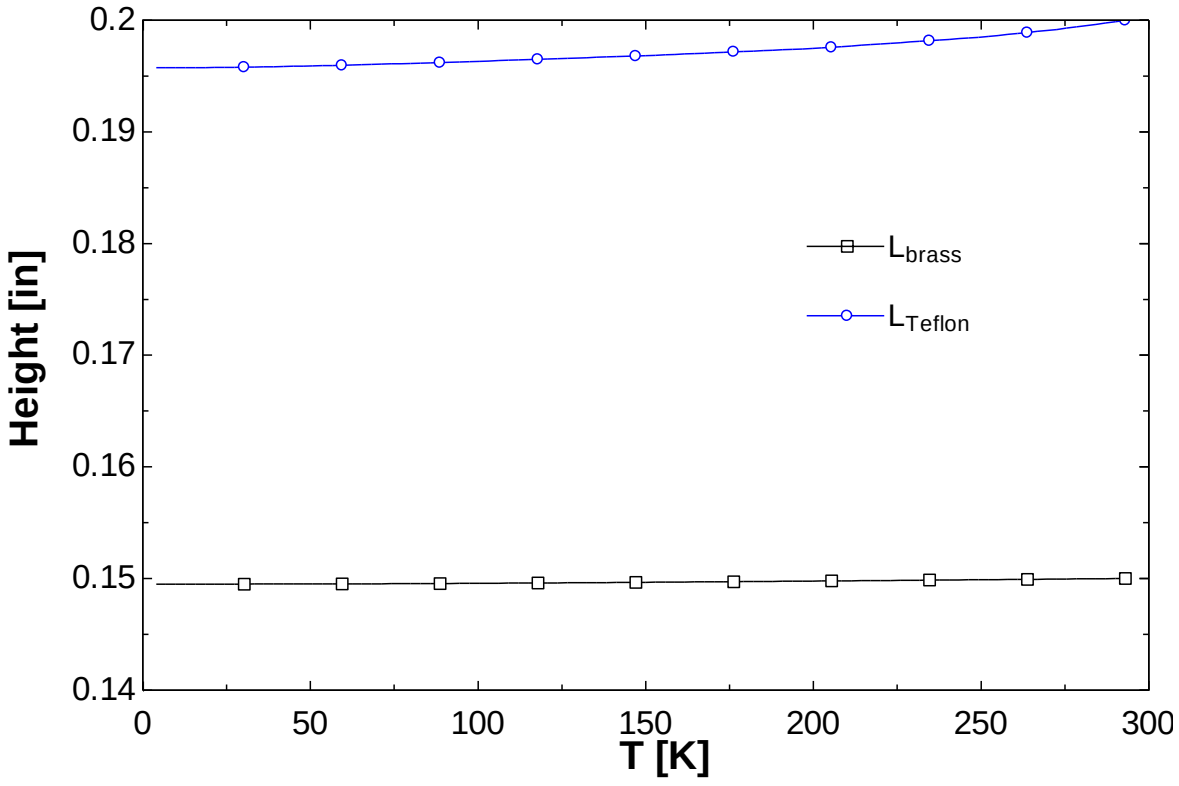

Figure 2.11: Difference between the seat inner radius height and the valve core height

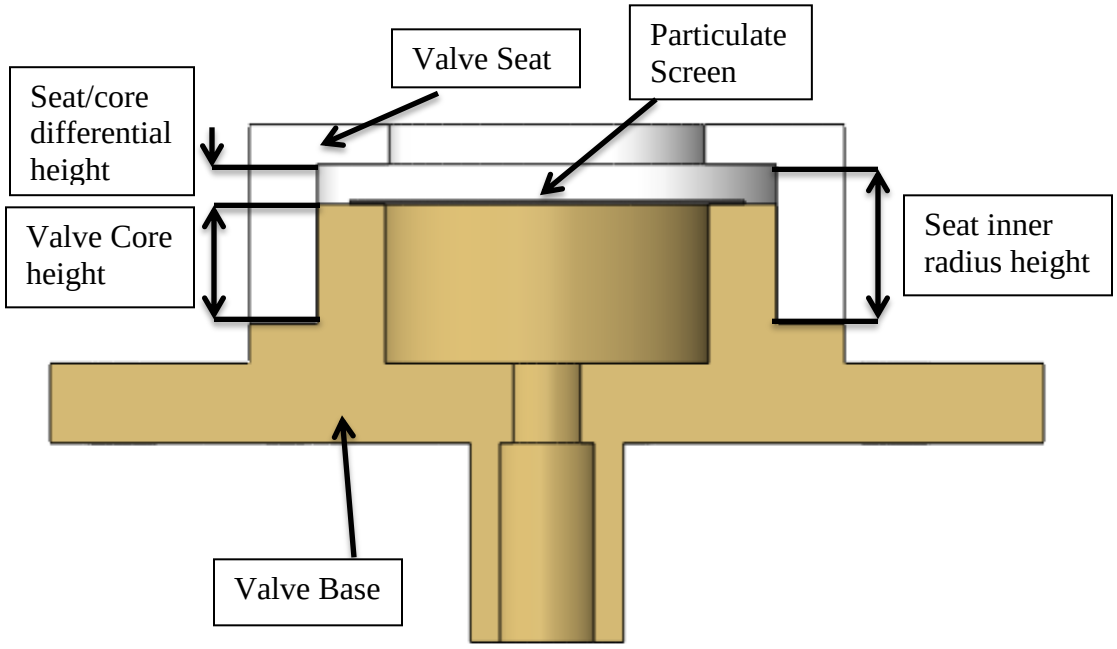

Figure 2.12: Section view of seat

It can be seen that the seat/core differential height remains high throughout the temperature range and there is no interference. This extra difference provides a margin for epoxy seepage from the inner radius joint and the particulate screen (which also has an epoxy joint of not negligible height). Thus the deformation of the seat due to valve core contracting at a different rate can be avoided.

Another critical aspect of the Teflon seat design and fabrication is the bonding of the Teflon to the brass seat core. The Teflon was epoxied over the brass core with Stycast 1266. However, Teflon is extremely chemically inert due to the extremely strong carbon-fluorine interatomic forces. Thus, a common method to bond Teflon is to prepare the surface by stripping the fluorine atoms with a chemical etchant. For the fabrication of this valve, Fluoroetch from Acton Technologies was employed. After treatment, a brown carbonaceous

layer remains on the etched surface leaving it favorable for bonding. Care must be taken to avoid splashing the etchant on or near any of the sealing surfaces, since it chemically alters the surface also increasing the roughness and decreasing the ductility. (Du Pont) (Acton Technologies, 2003)

Figure 2.13: Etched Teflon seat

Note that the surface is only etched on the lower portions of the valve seat. This not only helps avoid contamination of the sealing surfaces as mentioned earlier, but also avoids shear in the joint due to the axial differential thermal contraction. It also serves to provide an unaltered Teflon surface to radially contract around the brass and provide a hermetic seal while the epoxy along the etched bottom edge prevents the seat from shifting or sliding off during cool down.

The Teflon seat was polished after it was mounted to the valve base and the epoxy had set. It was manually polished with 3M Aluminum oxide polishing paper. The paper is precision micron graded in incremental steps of 30 micron, 15 micron, 9 micron, 3 micron, 2 micron, and 1 micron roughness, allowing the surface to be polished by stepping through each of these increments. The paper was placed on a granite slab certified to a surface flatness of less than .000005" (.127 micron) per inch. To prevent harder steel particles from embedding in the Teflon seat, special care was taken to ensure that the different sets of polishing paper were employed for the Teflon seat and the steel reed. To polish the seat, first it was cleaned using methanol and compressed air. The largest particle size paper (30 micron) was then placed on the granite slab. The valve base provided a stable grip to ensure uniform flatness during polishing and "figure 8" motions were utilized to ensure uniform finish. The pressure must be modulated based on experience, too much pressure will deform the seat, to little will result in a poor surface finish. Visual inspection determined when the seat was polished to the uniform surface finish obtainable with the given polishing paper. Following the largest grit paper, the part was cleaned again using methanol and compressed air to prevent larger particles from traveling to the smaller grit sized polishing papers. The next level of polishing paper (15 micron) was then placed on the granite slab and the same polishing procedure was repeated. This was repeated with the remaining polishing paper grit steps, with cleaning between each paper.

2.2.4 Reed

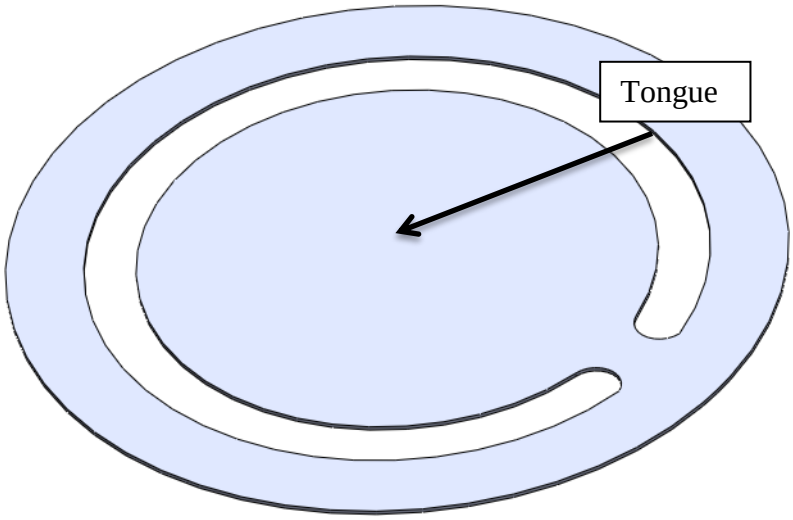

Figure 2.14: Reed solid model

The reed itself was fabricated out of spring steel by an offsite machinist. It was cut from a .004” thick sheet of spring steel using wire EDM (electrical discharge machining). This process uses an electrical discharge through a constantly fed brass wire to heat and remove material. Thicker reeds were also available in varying thicknesses of .006” up to .012” from previous valve work by Atlas Scientific. The thinnest reed available was .004” and this was selected to achieve two aims. First, thinner reeds cause a lower pressure drop in the forward flow direction. With thicker reeds, more force is required to bend the tongue a given amount based on beam theory. Assuming the helium is incompressible the cross sectional area required for a given mass flow rate should remain the same for both a thinner and thicker reed. However, more force is required to displace the tongue by a given amount, resulting is a greater pressure drop for the thicker reed. The second reason is based on Maddocks’ previous work. He had found that the thinner reeds sealed at lower pressures than the thicker counter parts.

The process by which the reed was fabricated proved to be the first obstacle in preparing the reed for use. It was found that the heat added by the EDM process caused slight warping of some of the reeds, specifically on the thinner reeds. Before proceeding to preparing the surface, each reed had to be tested for flatness. If the reed is not flat, it will not align with the flat Teflon seat and the sealing will be poor. To test each reed for flatness, it was placed on the same granite slab used for polishing the Teflon seat and visually inspected by pressing lightly on various points and checking for obvious deflection.

Another important aspect is the surface finish of both the seat and the reed. As indicated in the literature review, the valve both for the Hybrid PT/RB cooler and the Sorption compressor required very low roughness on the sealing surface. In fact, the valve from the University of Twente had height variations of less than 130 nm on the boss, which is an equivalent part to the reed in this valve, and variations of less than 80 nm on the seat. To achieve these finishes for the Twente valve, the techniques for polishing optical lenses were employed. However within budget restrictions, such methods could not be employed and it was deemed acceptable to utilize similar polishing methods to the valve developed by Miller at MIT and the valve developed by Maddocks with Atlas Scientific.

The reed was manually polished with 3M Aluminum oxide polishing paper. As mentioned in the seat section, the polishing paper used on steel must be kept separate from the paper used for Teflon to prevent contamination. As mentioned previously the paper precision micron graded in incremental steps, allowing the surface to be polished by stepping through each of these increments. The paper was placed on the flat granite slab starting with the 30 micron (highest roughness) polishing paper. The reed was polished by lightly applying pressure in

the center of the tongue with one finger to ensure uniform flatness and polishing in figure 8 motions to provide uniform surface finish. A latex glove was also employed to both provide a better grip on the reed and protect the polisher's hand. After visual inspection that the surface was uniform, the reed was cleaned with Methanol and blown dry with compressed air to prevent larger particles from traveling with the reed to the smaller particle size polishing paper. This was repeated with each polishing paper of 15 micron, 9 micron, 3 micron, 2 micron, and 1 micron roughness, with the same cleaning procedure between. Figure 2.15 shows a polished reed.

Figure 2.15: Finished reed

Following polishing the surface finish of the reed was analyzed with a Zygo New View 6300 optical profilometer available at the UW Materials Science Center. Optical profilometers can provide a very accurate measure of surface height variation by utilizing the wave properties of light. In a profilometer, the source light is split into 2 beams, one reflects off of the piece itself and the other off of a reference mirror. The interference pattern caused by the two

beams provides the height of a given point, and precise piezoelectric positioners provide a scan accurate to below 1 nanometer (in the case of the Zygo New View 6300). (Optical profiling: how optical profilers work)

The resolution of the scan can also be improved by selecting higher magnification lenses, resulting in a smaller field of view. Based on the expected surface finish obtainable with the 3M polishing paper, a focal lens of 10x was selected to give a horizontal resolution of .95 microns. For each scan this resolution produced a field of view of .7x.53 mm. The software associated with the profilometer allowed for stitching of multiple scans together. However there is a limit to the number of these scans that can be stitched together based on the sheer number of points required in the scan (average size of the files was 100 MB with 1.8 million points). Therefore an entire surface profile of the reed could not be generated, so a narrow band consisting of 4 separate scans was taken across the centerline of the tongue. An accurate depiction of surface finish at each radial point of the reed could then be analyzed. Figure 2.16 shows a 3-D model of the first of these scans and the most critical, since the sealing surface is the last .05" (1.27 mm) of this scan. Figure 2.17 was generated with a scale in a different orientation. For closer analysis, a surface profile was generated in Figure 2.18 a. The surface profile shows the height profile along the line indicated in the top view of Figure 2.18 b. The sharp drop off at the left edge of the surface profile is the edge of the reed. Neglecting that edge, a flatness of approximately +/- 1 micron is apparent. Also from this surface profile, it is clear that there are few height variations (beyond flatness) that approach 1 micron with the average much less 1 micron. Given that the sealing surface is only 1.27 mm from the edge, a second linear profile was taken in Figure 2.19. This figure further

illustrates that the surface variation is much less than 1 micron with a single feature on the sealing surface approaching 1 micron in height. Inspection of this plot yields an approximate variation of .2 micron. The height variation of the sealing surface in the radial direction appears to be approximately .5-.6 microns. The remaining three scans can be found in 6Appendix B and indicate approximately the same flatness and surface variation.

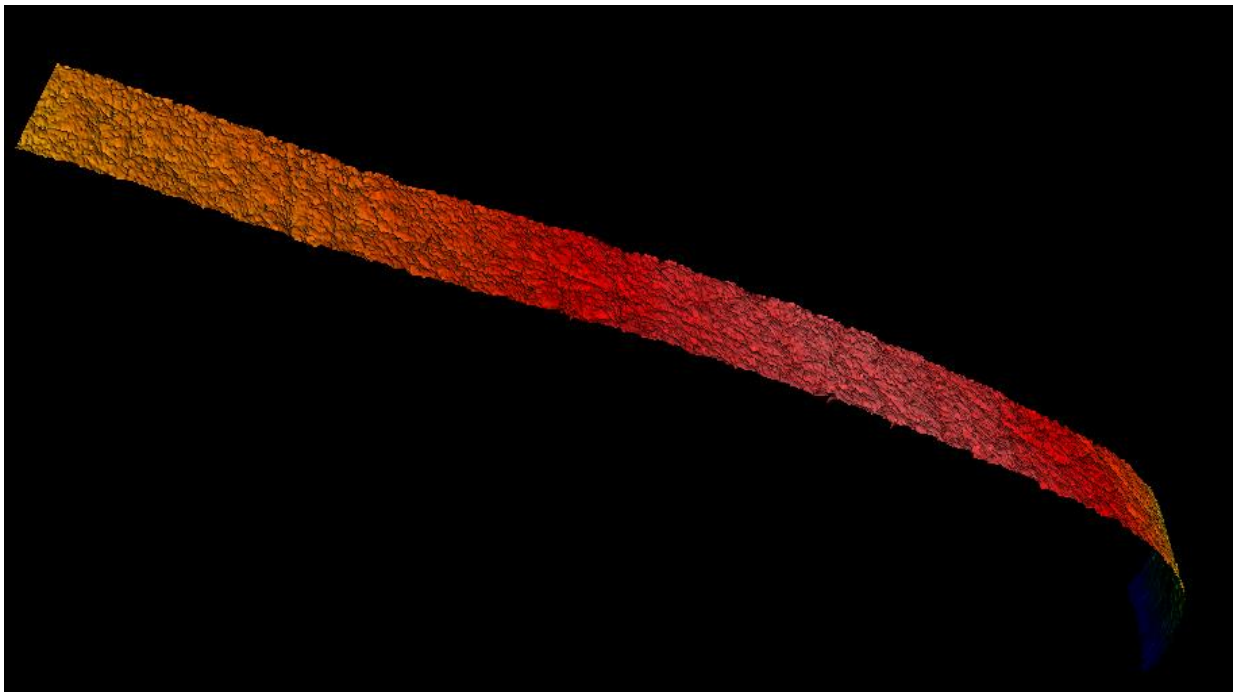

Figure 2.16: 3-D model of the first section of the centerline scan

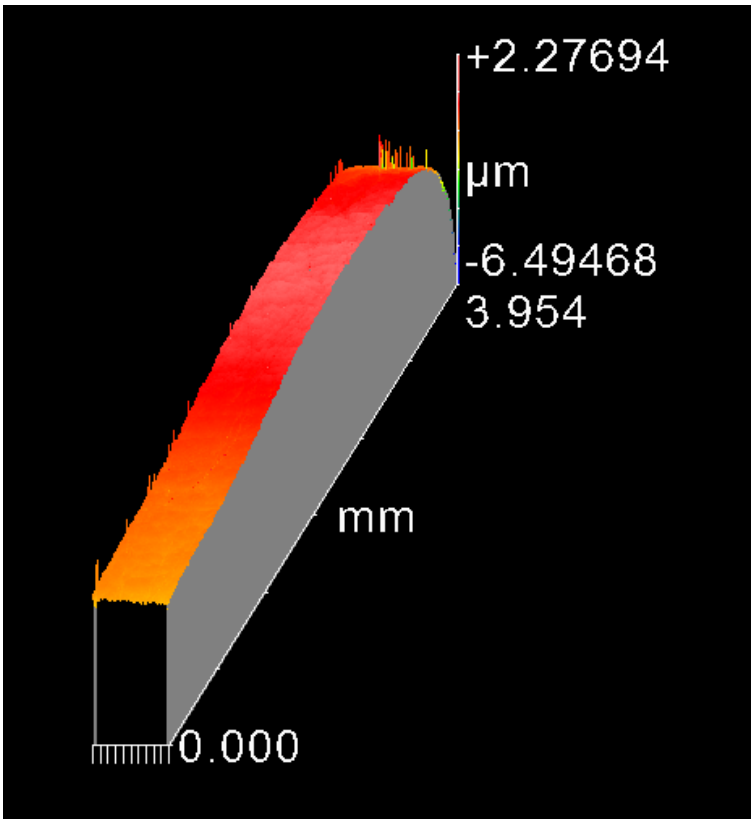

Figure 2.17: Oblique view of 3-D model of the first section of the centerline scan with scale

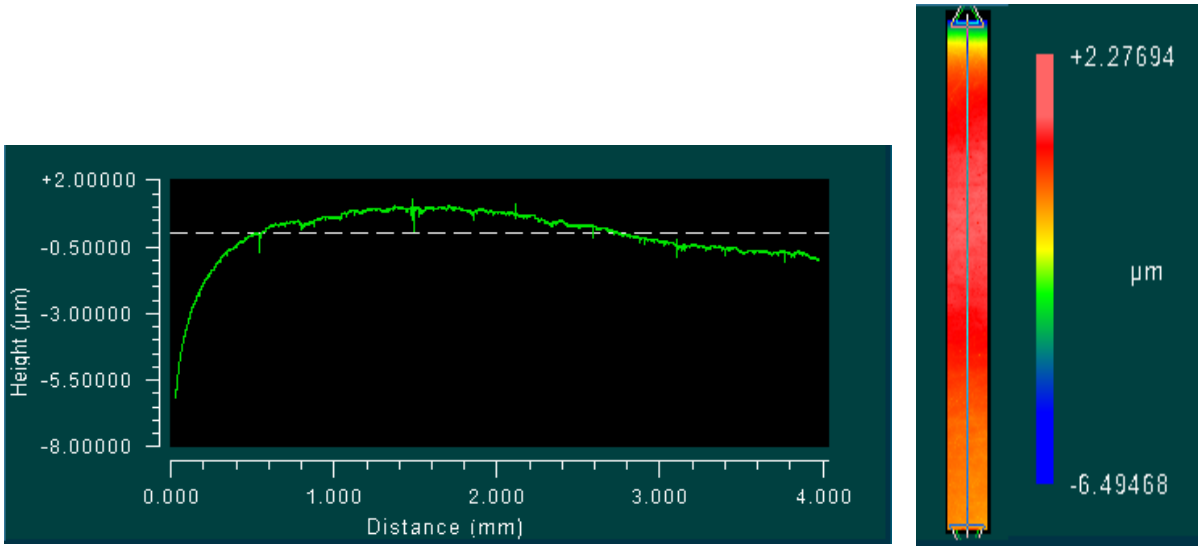

Figure 2.18: Surface profile of the first section of the centerline scan (left) and the line along which it was taken (right)

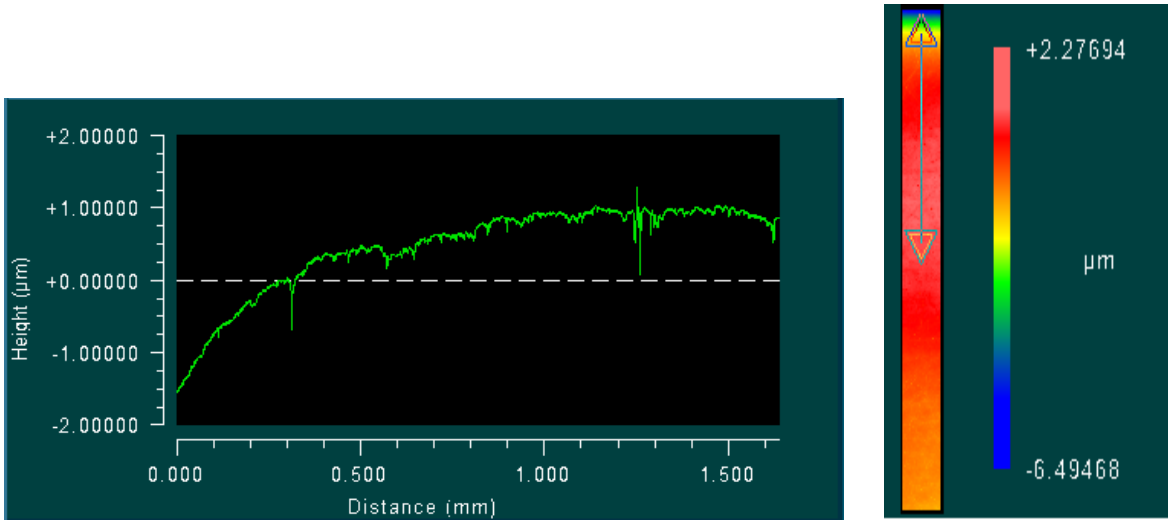

Figure 2.19: Surface profile of the sealing surface of the centerline scan (left) and the line along which it was taken (right)

Another scan was taken on a corner of the reed to ascertain the surface variation and flatness of the sealing surface in the angular direction. The line along which the profile was taken is indicated in Figure 2.20, with the surface profile shown in Figure 2.21. The analysis software does not have the capability to look at an arc, so a straight line was taken at an angle to approximate a constant radius angular track along the surface. This is an acceptable approximation since the corner is approximately 1.5 mm tall by 3.1 mm wide, and the sealing surface is approximately 1.27 mm from the edge. Therefore most of the corner scan consists of sealing surface.

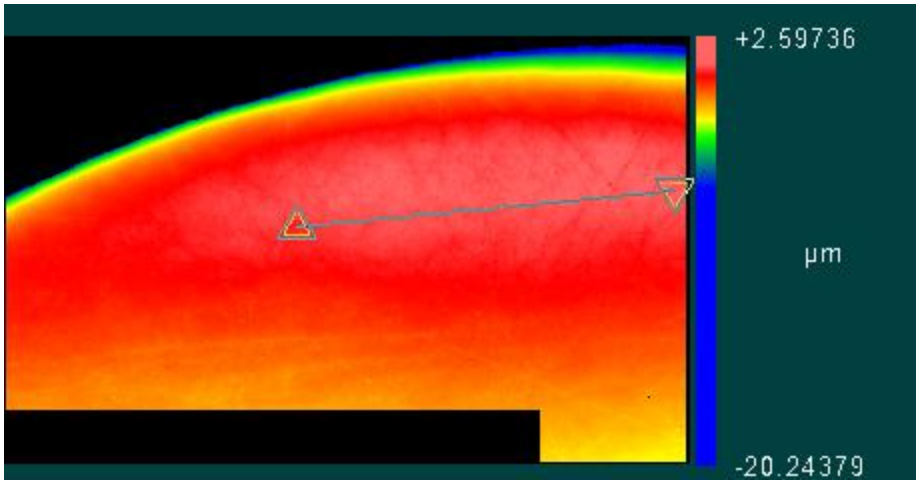

Figure 2.20: Top view of corner scan with the surface profile line indicated

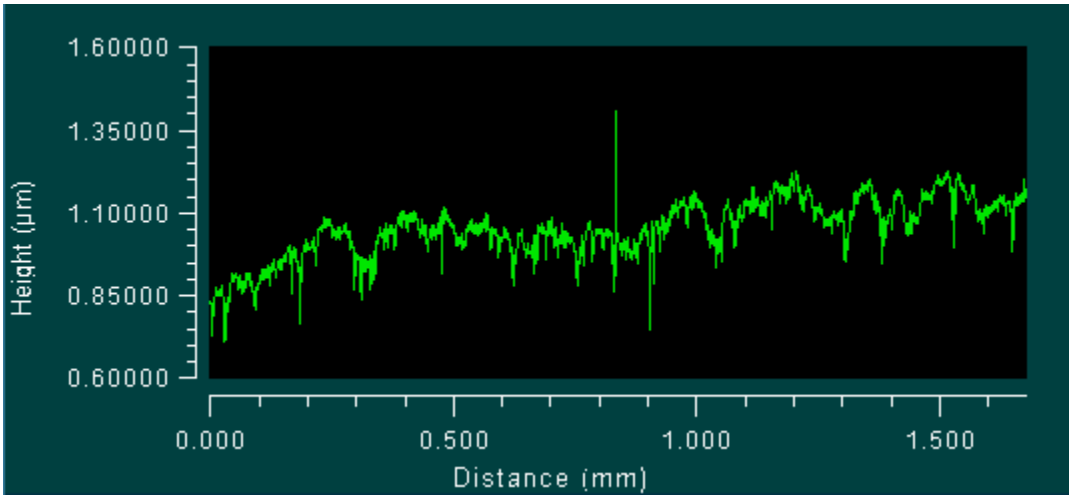

Figure 2.21: Surface profile of sealing surface in angular direction

Analysis of the surface profile shows one feature approximately .5 micron in height, but the majority of the features lie within .2-.3 microns. The net height variation is approximately .4 microns.

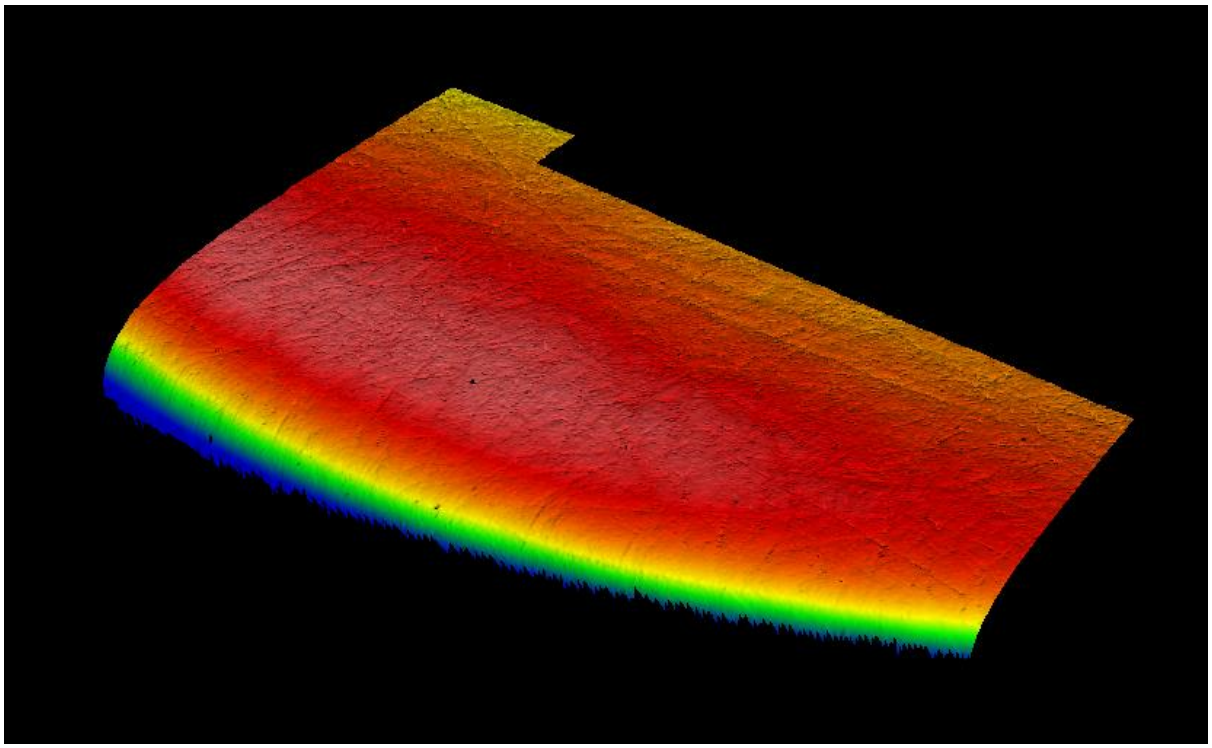

Figure 2.22: 3-D model of the first section of the corner scan

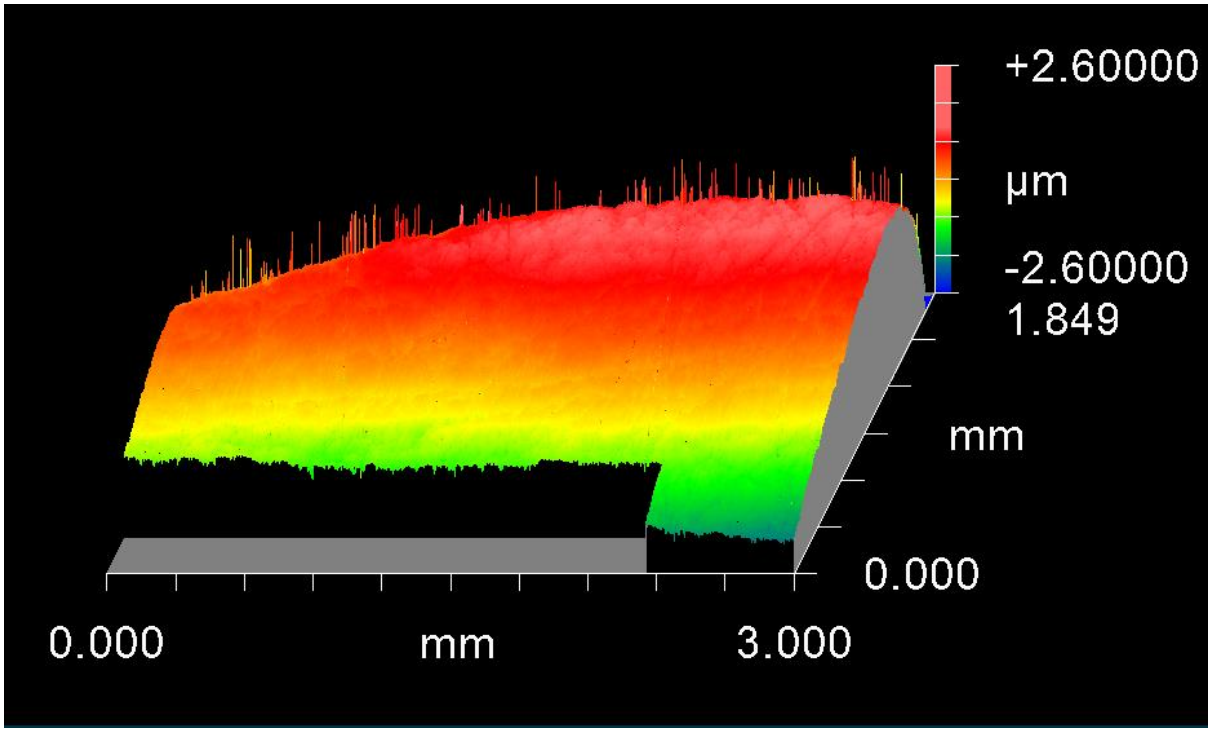

Figure 2.23: Oblique view of 3-D model of the corner scan with scale

The net result of the scans show that most surface variations where in the range of .2-.3 microns. The total flatness variation was approximately +/-1 micron from the average (magnitude of 2 micron), excluding the sharp drop off on the edge. However this flatness variation was between the center and the sealing surface. Across the sealing surface the height variation was approximately .4 microns in the angular direction and .5-.6 microns in the radial direction. Therefore, the optical profilometer scans indicate that in general the surface variation in both the angular and radial directions is much less than the 1 micron maximum feature size of the polishing paper.

2.2.5 Washer, Wave spring, and Valve top

Figure 2.24: From left to right, washer, wave spring and valve top

The remaining components of the valve, shown in Figure 2.24, are mutually dependent on each other. The washer is placed between the wave spring and the reed to apply a uniform pressure on the outer radius of the reed. Without this washer, the wave spring would apply pressure only at the points of contact and deform the reed. The purpose of the wave spring is to apply a small amount of pressure to the support ring of the reed, preventing shifting both during handling and cool down. The particulate screen is placed between the valve top and

the wave spring and, as discussed earlier, it prevents particulate from entering in the back flow direction. The valve top serves to contain all of the components and seal against the valve base, completing the valve. These features are all dependent on one another in the axial dimension. As mentioned, the wave spring must compensate for shifting during cool down. The cause of that shifting is differential thermal contraction. Both axial and radial thermal contractions have already been analyzed, but this analysis is slightly more involved. There are several different materials involved with different thermal expansion coefficients. Thus the two thermal contractions to be compared are the sum of the contractions of the internal components: the brass abutment, Teflon seat, steel reed, copper washer and particulate screen shown in Equation 2.3 and Equation 2.4 and the outer shell consisting of the inner bore depth of the brass valve top shown in Equation 2.5 was derived from Equation 2.2.

$$\Delta L_{inner,net} = \Delta L_{brass,abutment} + \Delta L_{Teflon,seat} + \Delta L_{steel,reed} + \Delta L_{copper,washer} + \Delta L_{stainless,screen} \quad \textbf{(2.3)}$$

$$\Delta L_{inner,net} = L_{brass,abutment}\int_{T_1}^{T_2}\alpha_{brass}(T)dT + L_{Teflon,seat}\int_{T_1}^{T_2}\alpha_{teflon}(T)dT + L_{steel,reed}\int_{T_1}^{T_2}\alpha_{steel}(T)dT + L_{copper,washer}\int_{T_1}^{T_2}\alpha_{copper}(T)dT + L_{stainless,screen}\int_{T_1}^{T_2}\alpha_{SS304}(T)dT \quad \textbf{(2.4)}$$

$$\Delta L_{shell,net} = L_{brass,shell} \int_{T_1}^{T_2} \alpha_{brass}(T)dT \tag{2.5}$$

The initial length of the inner components is the sum of the individual heights. Subtracting the change in length from that value will give the final length. The depth of the bore in the valve top is the initial length for the shell and again subtracting the net change due to thermal contraction from it gives the final length of the shell. The wave spring is not included since it will take up the difference between the two. Therefore the difference must not exceed the uncompressed height of the wave spring (.05"), nor can it be less than the nominal thickness of a fully compressed wave spring (.01"). Ideally the wave spring would begin the cool down slightly compressed and not be fully compressed at the final temperature. EES was again employed with internal functions to ascertain the result of the integrals in Equation 2.4 and Figure 2.25 was generated.

$$\begin{aligned}\Delta L_{inner,net} = L_{brass,abutment} \int_{T_1}^{T_2} \alpha_{brass}(T)dT \\ + L_{Teflon,seat} \int_{T_1}^{T_2} \alpha_{teflon}(T)dT + L_{steel,reed} \int_{T_1}^{T_2} \alpha_{steel}(T)dT \\ + L_{copper,washer} \int_{T_1}^{T_2} \alpha_{copper}(T)dT \\ + L_{stainless,screen} \int_{T_1}^{T_2} \alpha_{SS304}(T)dT\end{aligned} \tag{2.4}$$

It is clear with the selected dimensions of bore depth and copper washer height; the wave spring will be able to compensate for any differential thermal contraction without being over compressed.

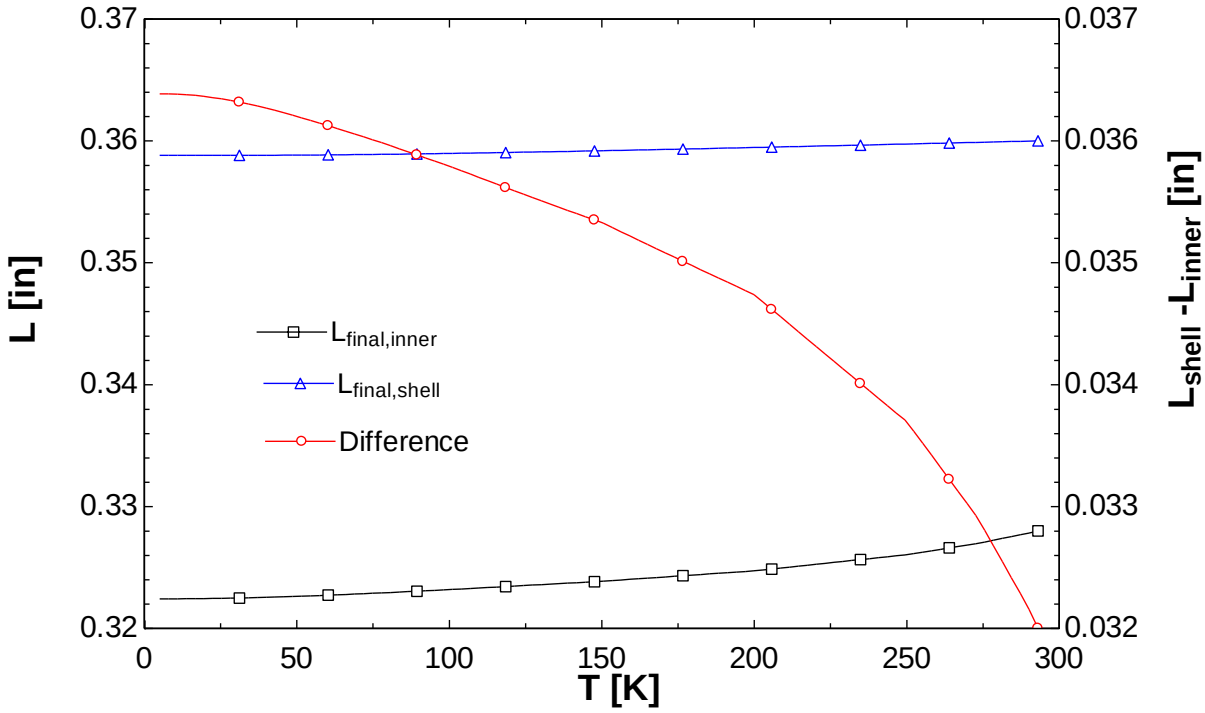

Figure 2.25: Differential thermal contraction between inner components and shell

2.2.6 Indium Seal

The final component of the valve assembly is the indium seal. Remnants of the seal can be seen in Figure 2.26 as the silvery substance radially inward from the bolt circle. Indium was selected for a sealing material both for its thermal and mechanical properties. Mechanically, indium is extremely soft and will flow into cracks and surface imperfections, blocking leak paths. Thermally, indium also provides an excellent contact between the two sections of the valve, ensuring that the whole assemble remains relatively isothermal.

To complete the assembly of the valve a ring of .05" thick indium wire was placed around the Teflon seat, against the indium abutment. The surfaces of the valve top and bottom must be cleaned with scotch bright and rinsed with methanol to ensure a good contact with the indium. The valve top was then joined to the valve bottom and the screws were tightened in a

star shaped pattern. This is done to guarantee that the indium is uniformly squeezed between the valve top and valve bottom. The star pattern was repeated until the indium is fully compressed and there was little gap (<0.005”) between the valve base and top. The indium abutment on the valve base prevents the indium from being compressed into the Teflon seat or epoxy joint and causing damage. Another consideration with indium seals is that it exhibits a great deal of creep. After initially compressing the material, the indium slowly relaxes the stress imposed by flowing outwards and flattening. To compensate for this, the bolts must be torqued again approximately an hour after the initial tightening. Lock washers are also used on the screws to maintain pressure on the indium seal during cool down. The final result is a hermetically sealed valve assembly shown in Figure 2.27.

Figure 2.26: Fabricated components of valve

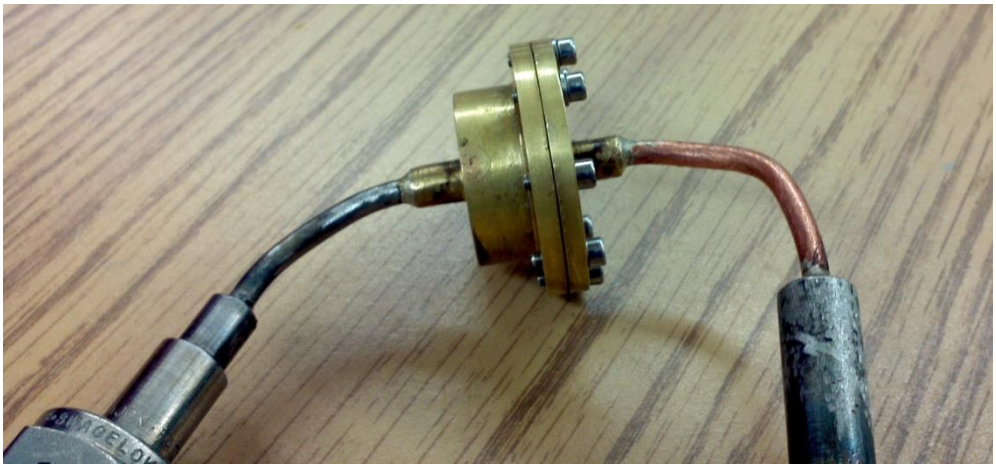

Figure 2.27: Closed valve assembly

2.3 References

Miller, F. K., & Brisson, J. G. (1999). Development of a Low-Dissipation Valve for use in a Cold-Cycle Dilution Refrigerator. *Cryogenics, 39*, 859-863.

Pobell, F. (2007). *Matter and Methods at Low Temperature.* Berlin: Springer-Verlag.

Rae, P. J., & Dattelbaum, D. M. (2004). The properties of poly(tetrafluoroethylene) (PTFE) in compression. *Polymer*, 7615-7625.

Du Pont. (n.d.). Teflon PTFE Properties Handbook. Wilmington, Delaware, USA.

Acton Technologies. (2003). *Acton Technologies FlouroEtch*. Retrieved from http://www.actontech.com/

Optical profiling: how optical profilers work. (n.d.). Retrieved from Zemetrics: http://zemetrics.com/optical-profilers-about.shtml

3 Valve Model

The purpose of the valve model is to accurately predict the leak flow rate of a ^{3}He-^{4}He mixture in the CCDR at l.8K with a pressure differential of 10-20 kPa. However, since the valve was fabricated and tested as an individual component and ^{3}He is difficult to obtain, the valve tests were conducted with pure ^{4}He. As will be discussed in greater detail, the model must accurately predict the flow based on known fluid properties so that the testing results with ^{4}He could be transferred to the conditions in the CCDR.

3.1.1 Constraints

In the development of a predictive model, constraints must first be established. The simple constraints are the temperature and pressure. These values are made to match the set points seen in the actual valve. The temperature and pressure provide the physical properties of the fluid, such as density (ρ) and viscosity (μ). If the temperature and pressure contribution to the model can be computed according to these physical properties, there is hope that results using pure ^{4}He can be scaled to ^{3}He-^{4}He mixtures. As will be discussed, the temperature ranges from room temperature (293 K) to approximately 6 K and the pressure across the valve was held at 10 psi in the valve test. The CCDR set points of 1.8 K and 10-20 kPa pressure difference must be employed to obtain the fluid properties of ^{3}He-^{4}He mixtures.

Another constraint is the physical geometry of the flow area. Ideally, in the back flow direction, there would be no cross sectional area through which the fluid can flow. However in the real situation, the sealing surfaces on both the reed and the seat are not perfectly flat or matching. Predicting the level to which the two surfaces are mismatched can be attempted using the data from the optical profilometer. The opacity of Teflon is such that the surface

profile obtained by an optical profilometer can be very inaccurate. The surface can be coated with a metal to improve results, but this would modify the surface. Therefore, the surface profile data was only taken for the steel reed. It was assumed that the Teflon would have a similar order of magnitude of surface asperities since it was polished with the same method. Practically, it is likely that the seat had slightly higher surface roughness due to the difficulty of polishing softer materials like Teflon. Referring to the previous section, the surface in both the radial and angular directions consists mainly of features approximately 0.2-0.3 micron in size. Mirroring this onto the Teflon seat, a net difference between the two surfaces could be expected to be approximately 0.5 micron. This neglects the deformation of the Teflon under pressure and, in fact, this deformation was intentionally imposed to reduce the difference between the two surfaces. However in the development of the model, the measured difference, based on surface profiles, was used and in the results this deformation will be discussed further.

Beyond the magnitude of surface differences, the geometry shape itself must be established. Figure 3.1 shows a zoomed 3-D view of a section of the sealing surface on the reed from the optical profilometer.

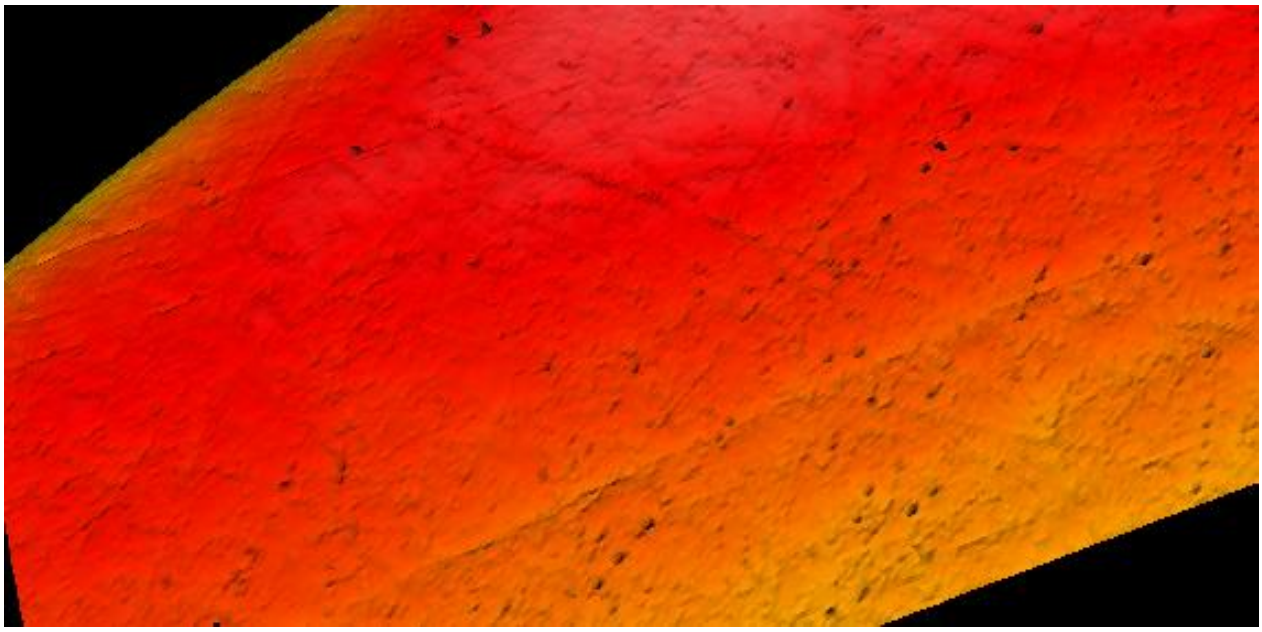

Figure 3.1: Zoomed view of 3-D surface profile

The main surface features seem to be straight channels on the surface. Likely due to features on the polishing paper catching and leaving grooves in the steel. These channels can then be approximated as circular ducts. In the worst case these ducts could span the entire length of the sealing surface. Qualitatively estimated, in the worst case, approximately 50% of the sealing surface would be spanned by these micron sized ducts. The number of these parallel ducts can be found by taking the inner circumference and dividing by the diameter of the duct and dividing that number by two, resulting in approximately 30000 parallel ducts. Thus the flow geometry can be fully specified and a parallel series of circular ducts with a diameter of approximately 0.5 micron and a length of .1" (the difference between the orifice diameter and the reed diameter, see section 2).

3.1.2 Flow Regime

With an established geometry, the flow can be described. An important parameter in identifying any internal flow problem is the Reynolds number indicated in Equation 3.1.

$$Re = \frac{\rho v d_h}{\mu} \tag{3.1}$$

In this equation, ρ is the density of the fluid, v is the mean velocity, μ is the viscosity of the fluid and d_h is the hydraulic diameter. The hydraulic diameter is further defined in Equation 3.2 as four times the ratio of cross-sectional area over the wetted perimeter.

$$d_h = \frac{4A_c}{Per} \tag{3.2}$$

The relations of Equation 3.1 and Equation 3.2 can be applied to the situation of flow through many parallel microchannels, resulting in Equation 3.3.

$$Re = \frac{4\dot{m}_{tot}}{n_{ch}\pi d_{ch}\mu} \tag{3.3}$$

Where $\dot{m}_{tot}$ is the total mass flow rate through all of the channels, n_{ch} is the number of micro channels, d_{ch} is the diameter of the individual channels and μ is the viscosity of the fluid.

The Reynolds number is the ratio of the inertial forces over the viscous forces and indicates whether the flow is likely to be laminar or turbulent. In general, for internal flow, the transition Reynolds number is 2300-4000 for internal pipe flow. A Reynolds number of less than 2300 indicates laminar flow, similarly the flow is fully turbulent if the Reynolds number is above 4000. One problem with approaching the Reynolds number first is that the leak back in the reverse direction is not known, thus the velocity is not known. At the same time, the Reynolds number is needed to determine whether the flow is laminar or turbulent. Knowing

this, the flow rate can be computed with a known pressure drop and geometry. The solution to this "Catch 22" is to first assume a laminar flow regime then use the flow rate to check the Reynolds number. If it is much less than 2300, the flow can be assumed to be laminar.

3.1.3 Laminar Flow Model

A diagram of a general internal duct flow problem is found in Figure 3.2. From this problem a relation for pressure drop to flow rate can be derived. However, some important assumptions must first be employed. First the flow is incompressible and steady, meaning that the density is constant and the mass flow rate at point 1 is the same as point 2 giving a constant velocity profile across the section length.

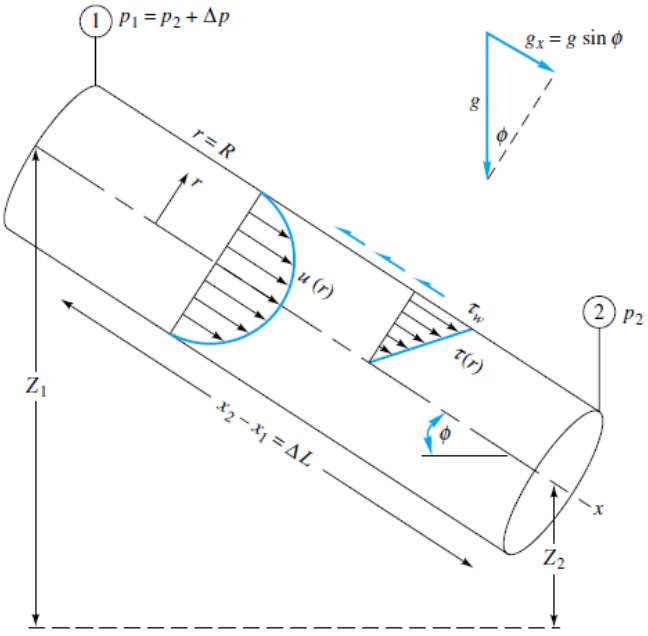

Figure 3.2: General internal flow situation (White, 2006)

An energy balance on this section yields Equation 3.4.

$$\frac{v_1^2}{2} + z_1 g + \frac{P_1}{\rho} = \frac{v_2^2}{2} + z_2 g + \frac{P_2}{\rho} + \frac{\Delta P_{loss}}{\rho} \quad \textbf{(3.4)}$$

In this equation, *v* is the velocity, *z* is the height change parallel to gravity, *P* is the pressure, and ΔP_{loss} is the non-recoverable pressure drop. For the valve, helium has a very low density and will be changing height by a very small amount so the gravity contribution can be neglected. The flow is also fully developed and incompressible so v_1 is equal to v_2 and the velocities cancel. Therefore, the equation is simplified to Equation 3.5.

$$P_1 - P_2 = \Delta P_{loss} \quad \textbf{(3.5)}$$

The energy balance can be coupled with a balance on the forces in the x direction shown in Equation 3.6.

$$\Sigma F_x = \frac{(P_1 - P_2)\pi d^2}{4} + \frac{\rho g \pi d^2}{4}(z_1 - z_2) - \tau_w \pi d L = \dot{m}(v_2 - v_1) \quad \textbf{(3.6)}$$

Here τ_w is the wall shear stress. Recall that the gravity forces are being neglected and steady flow ensures that the velocities are equal. Thus combining Equation 3.5 and Equation 3.6 gives Equation 3.7.

$$\Delta P = \frac{4\tau_w L}{d} \quad \textbf{(3.7)}$$

For turbulent flows there is a known correlation between wall shear and the velocity and the equation simplifies to Equation 3.8.

$$\Delta P = f \frac{L v^2 \rho}{2d} \quad \textbf{(3.8)}$$

The friction factor, *f*, is experimentally determined as a function of the Reynolds number, the relative roughness of the surface, and the duct shape.

For laminar flow, the wall shear stress can also be represented as the change in x velocity (parallel to the wall) with respect the direction perpendicular to the wall (y), multiplied by the viscosity. In the situation of flow through the micron sized ducts, those ducts can be approximated as circular. An analytical solution for laminar flow through a circular duct (Poiseuille flow) is readily available in Fluid Mechanics by White. To apply this to the general solution for internal duct flow in Equation 3.8, the analytical solution can be rearranged to provide the friction factor for laminar flows, shown in Equation 3.9.

$$f_{lam} = \frac{64}{Re_d} \tag{3.9}$$

Equation 3.8 and Equation 3.9 can be combined with the known relation between mass flow rate and velocity to yield a more tractable form for use in the valve flow model in Equation 3.10.

$$\Delta P = \frac{128 \mu L \dot{m}}{\rho^2 d^4 \pi} \tag{3.10}$$

However, for the case of backflow there is not a single duct, but a series of parallel circular ducts. In this case the pressure drop across all of them can be approximated to be the same and the total mass flow rate is the sum of all of the mass flow rates through individual channels. The pressure drop and flow through and individual channel is shown in Equation 3.11.

$$\Delta P = \frac{128 \mu L_{ch} \dot{m}_{ch}}{\rho^2 d_{ch}^4 \, \pi} = \frac{128 \mu L_{ch} \dot{m}_{tot}}{\rho^2 d_{ch}^4 \, \pi n_{ch}} \tag{3.11}$$

The total leak rate is $\dot{m}_{tot}$ and the number of small channels is n_{ch}. With the known geometry relations and pressure drop, this can be applied across the sealing surface to find the expected

mass flow rate across the valve. In Equation 3.11, the density and viscosity are assumed to be constant over the pressure drop.

First, the model was run for the ^{3}He-^{4}He mixture. The density was found based on the equation of state Chaudhry developed for ^{3}He-^{4}He mixtures. The molar specific volume was found at 1 bar (the expected charge pressure of the CCDR) and a molar concentration of 6% ^{3}He and combined with the molar mass of the mixture to yield the mass density. A Matlab model of the equation of state shows that the specific volume does not change significantly if the pressure varies by 10-20 kPa from the charge pressure. Therefore the assumption of constant density flow through the micro ducts is valid. The viscosity was found from a curve fit based on experimental data taken by Meyer of the viscosity of ^{3}He-^{4}He mixtures at various concentrations and temperatures. The viscosity is primarily a function of concentration and temperature. In the CCDR, the valves will be at a point of relatively constant concentration (5-6% ^{3}He) and a constant temperature of 1.8 K. Therefore constant viscosity can also be assumed across the sealing surface. Therefore, the relation between mass flow rate and pressure should be linear as seen in Figure 3.3. The EES code that solves for the mass flow rate based on the specified parameters is shown in Appendix C. (Chaudhry & Brisson, 2009)

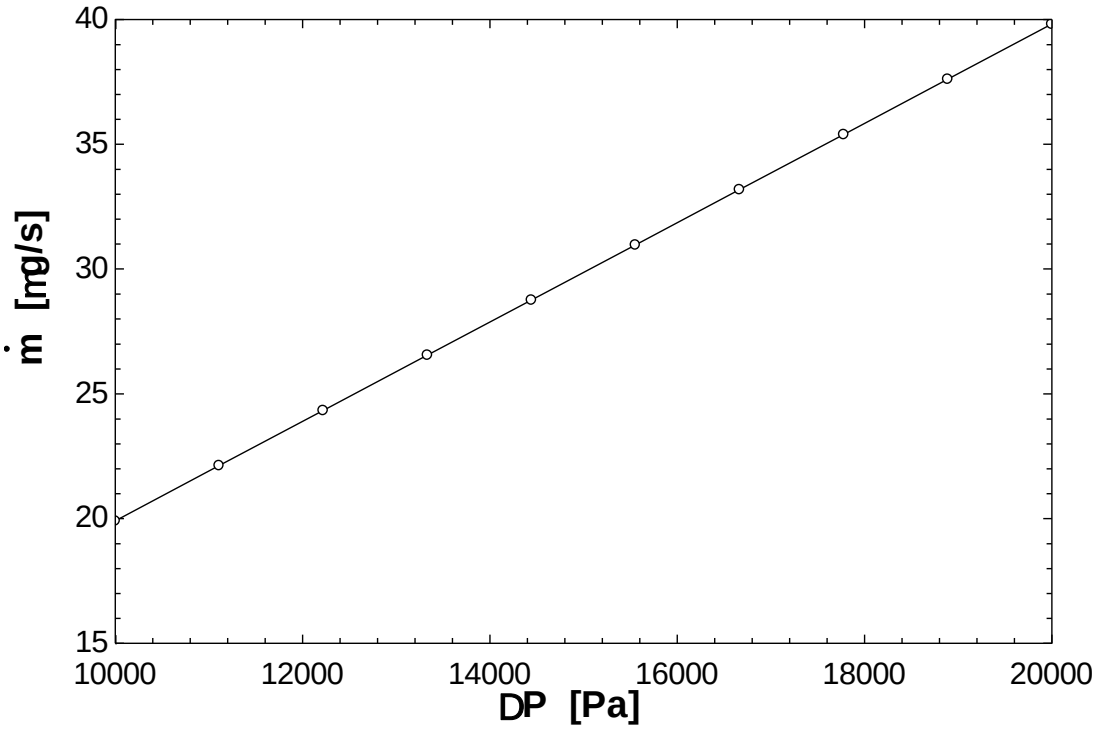

Figure 3.3: Laminar model mass flow rate vs pressure for ^{3}He-^{4}He mixtures at 5.5% ^{3}He concentration and 1.8 K

According to the prediction of this model, the mass flow rate of the valve with a mixture of ^{3}He-^{4}He and at the sealing back pressure is 20-40 µg/s. This is well inside the requirements laid down by the CCDR model of 39.4-92.0 µg/s.

After the flow rate based on the laminar flow model is evaluated, the Reynolds number can be revisited. The Reynolds number for each microchannel with a ^{3}He-^{4}He mixture and a pressure difference of 20 kPa is found to be 2.606. This is well inside the laminar regime and validates the use of a laminar friction factor.

It is clear that the variation of mass flow with respect to pressure is linear since the density and viscosity does not change with respect with pressure. Though this assumption is valid with ^{3}He-^{4}He mixtures at a constant temperature and small pressure differentials, it is not

valid with the test fluid at the test conditions. As will be discussed in greater detail in the testing section, the difficulty of obtaining ^{3}He requires that the valve is tested with the pure ^{4}He and limitations of the equipment resulted in an ultimate low temperature of 6 K. However, as mentioned earlier, if the flow can be predicted accurately passed purely on the flow properties of ^{4}He, then the model will be portable to ^{3}He-^{4}He mixtures.

At the test conditions of a 10 psi (~70 kPa) pressure differential, the density of gaseous ^{4}He at ~6 K will change significantly from 16.85 to 9 kg/m^{3}. Another test of the model's accuracy is how well the flow rate is predicted as the valve is cooled down. Therefore, a final approximation must be made to improve the accuracy of this model. In Equation 3.11, the density is assumed as constant, but this equation can be evaluated for smaller differential control volumes. The properties of each volume can be evaluated at the given pressure. The pressure at each volume is then the pressure of the previous volume minus the pressure drop due to the flow across the length of the differential control volume. As seen in Equation 3.12, the form of the equation is very similar, but the length is now a differential length.

$$\Delta P = \frac{128 \mu \Delta L \dot{m}_{tot}}{\rho^2 d_{ch}^4 \pi n_{ch}} \tag{3.12}$$

The mass flow rate is constant from one control volume to the next as the total mass flow rate, since the volumes are in series. The initial and final pressures are then fixed according to the total pressure drop. The greater the number of the control volumes, the greater the accuracy and the greater the computational requirements. When the test results where compared to the model, it was run for many different temperatures and flow rates. Therefore the number was selected to be 20 to balance accuracy and computational time. EES can

easily evaluate the convergence of this model by simultaneously solving the large set of equations this approach generates for the mass flow rate. The EES code that evaluates this model can be found in Appendix D.

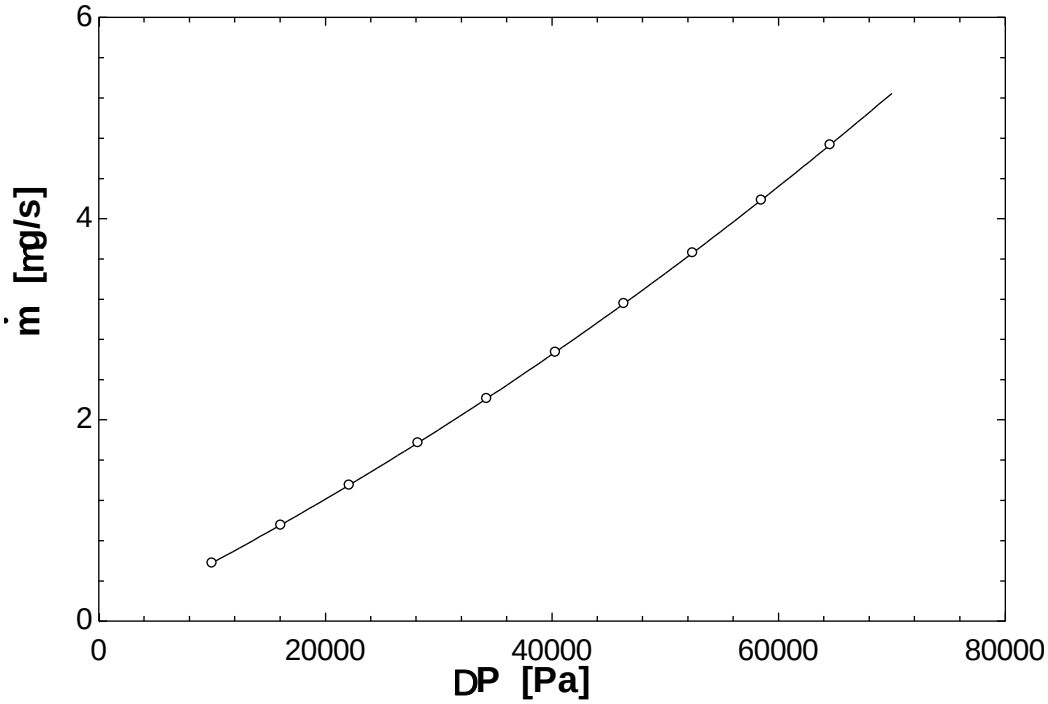

Figure 3.4: Laminar model mass flow rate vs pressure for pure ^{4}He at 6 K

A second way the model can be validated beyond predicting the flow at the ultimate low temperature is to predict the mass flow rate as a function of temperature as the valve cools down. Figure 3.5 shows the mass flow rate at temperatures ranging from room temperature (293 K) down to 6 K with a pressure differential set to be 10 psi (70 kPa).

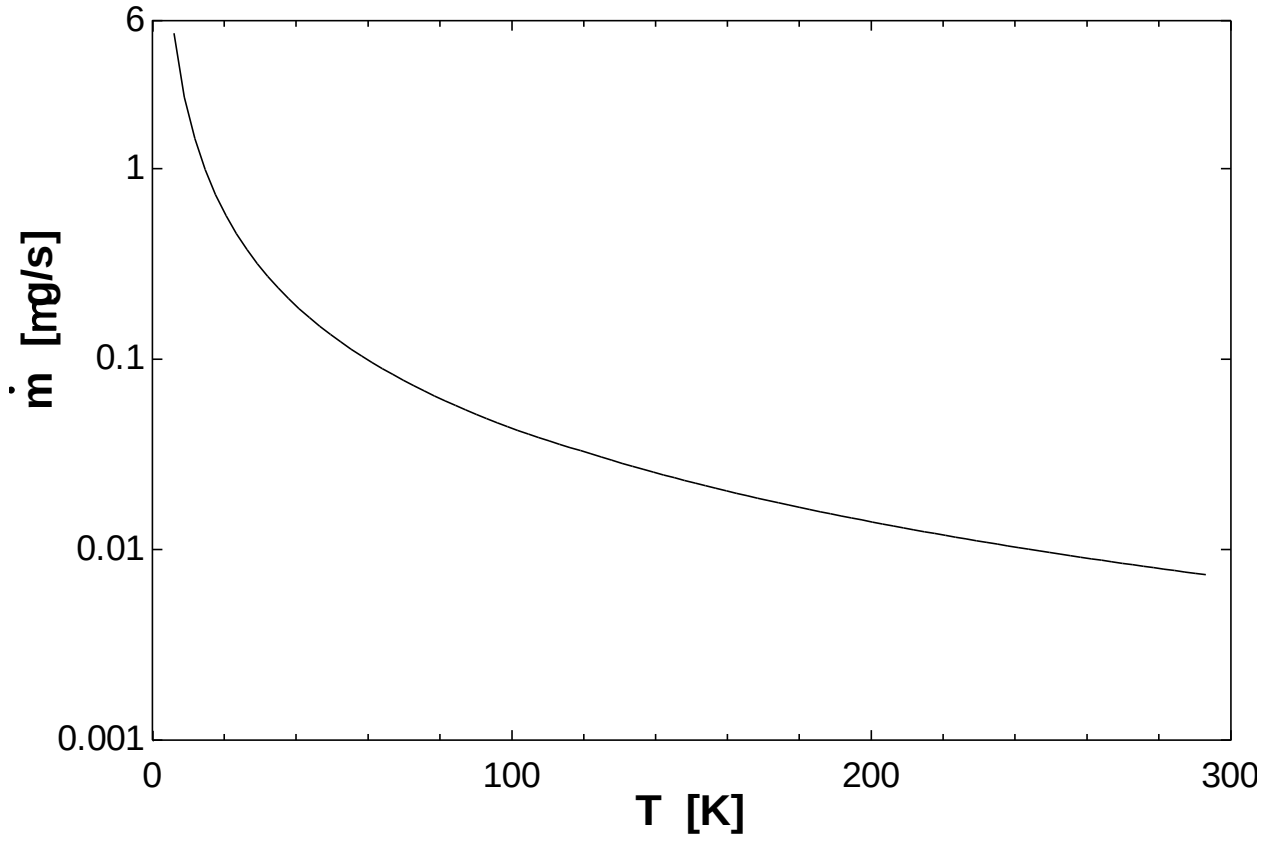

Figure 3.5: Laminar model mass flow rate vs temperature for pure ^{4}He with a pressure differential of 70 kPa (10 psi)

Again the Reynolds number was generated using **Error! Reference source not found.**, but this time at the set point resulting in the maximum flow rate of pure ^{4}He (10 psi/70 kPa pressure differential and 6 K). The Reynolds number was found to be 0.4888, again solidly in the laminar regime.

Based on the results of the flow model for both pure ^{4}He and ^{3}He-^{4}He mixtures, the original assumption to use a laminar pressure drop is valid. In addition, the model can be validated with pure ^{4}He tests at different temperatures and pressures. Since the same assumptions where made with the model for ^{3}He-^{4}He mixtures based on known properties of the mixture, this model can be at least partially validated with the test results discussed in a later section.

3.2 References

White, F. M. (2006). *Fluid Mechanics* (6th ed.).

Chaudhry, G., & Brisson, J. G. (2009, June). Thermodynamic Properties of Liquid 3He-4He Mixtures Between 0.15 K and 1.8 K. *Journal of Low Temperature Physics*, *155*(5-6), 235-289.

4 Test Facility

In this section, the test facility design and fabrication will be discussed. During the course of this research, there were two test facilities fabricated and employed. Initially, the research was funded from the NASA SBIR (Small Business Innovation Research) program in conjunction with Atlas scientific. In this first phase of research a test facility was designed for installation in a liquid ^{4}He dewar. However, given time constraints of the phase 1 research, a liquid nitrogen test was conducted to find initial indications of a successful test. This was deemed acceptable, since the temperature of liquid nitrogen at atmospheric pressure is approximately 78 K, which is far below the phase transition of Teflon at 173 K discussed in the design section. After the phase 1 funding expired, given the cost and volume of liquid helium required for a test, a second test facility was fabricated and mounted on a Cryomech PT-410 cryocooler. This meant a reduction in cooling power but enabled flow measurements over a continuous temperature range. As will be discussed later in this section, this limited the ultimate low temperature of the test but allowed for verification of the model.

4.1 Cryostat Test Facility

The cryostat implemented in this test facility was designed for a dewar containing liquid helium. A diagram of the test facility is shown in Figure 4.1. This diagram does not include all of the components initially accommodated in the design but rather includes the components actually utilized in the liquid nitrogen test. Much of the analysis for the design (radiation shielding, heat exchangers, top plate, etc.) was done for a liquid helium dewar, and fortunately this resulted in an over design for the nitrogen tests.

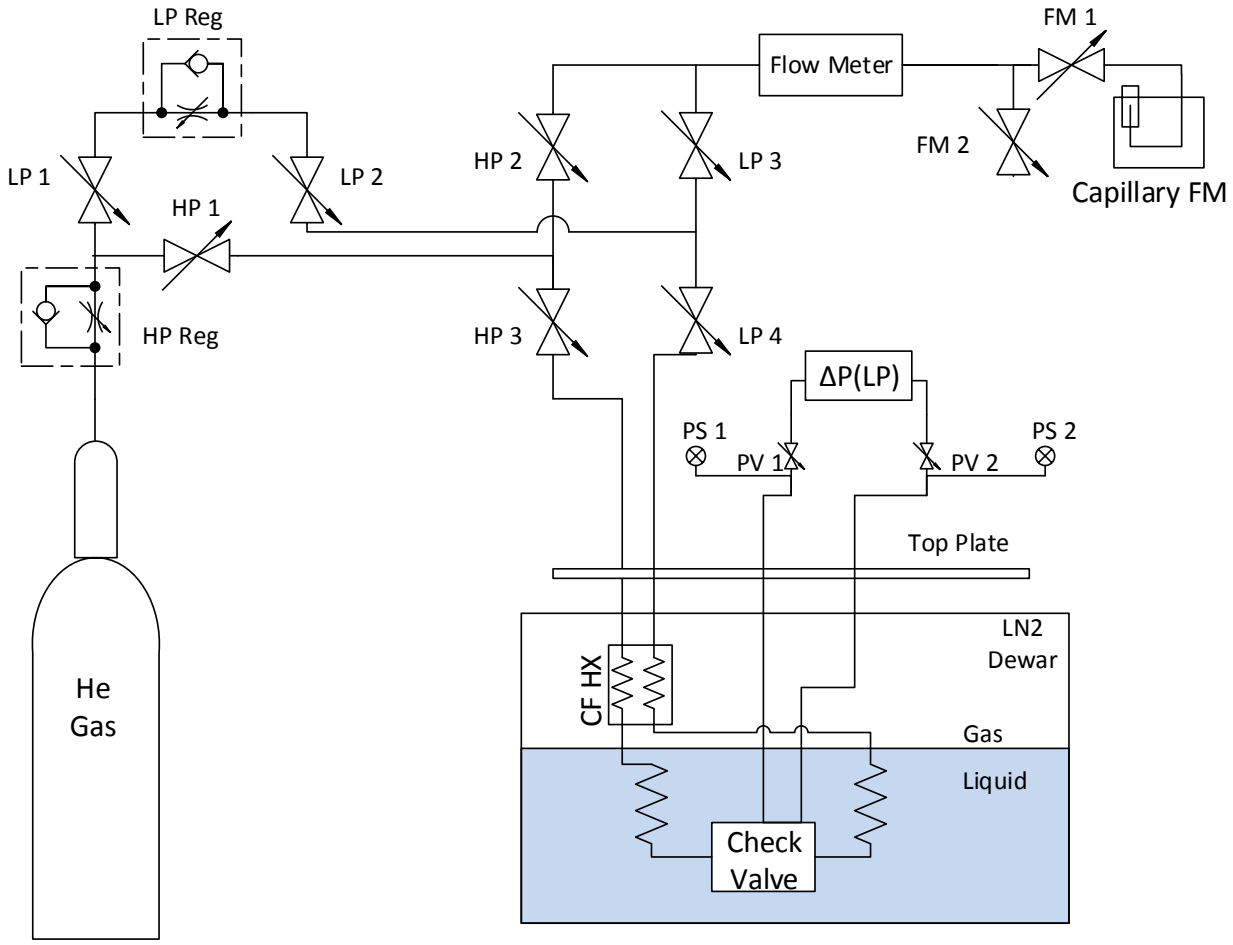

Figure 4.1: Diagram of cryostat test facility

4.1.1 Dewar

The Cryofab Dewar the system was initially designed for is a triple jacketed stainless steel cylinder. The outer vacuum jacket insulates the middle liquid nitrogen filled jacket from the ambient air. The liquid nitrogen jacket is held at the saturation temperature of nitrogen and absorbs most of the external heat load. A second vacuum jacket insulates the inner liquid helium vessel from the nitrogen jacket. The liquid helium vessel holds the experiment and

the latent heat of the ^{4}He provides the cooling power at its saturation temperature. The saturation temperature can be controlled by pulling a vacuum on the helium bath, but the nominal saturation temperature at atmospheric pressure is approximately 4.2 K.

For liquid nitrogen tests, the same theory applies. The experiment can be held at the saturation temperature of nitrogen at a given pressure. However, the much higher saturation temperature (nominally 78 K at atmospheric pressure) required less insulation for the actual test. An open stainless steel Dewar with one layer of vacuum insulation could be employed which allowed the experiment to be visually monitored. Nitrogen also possesses a much larger latent heat of vaporization than ^{4}He, 199.3 kJ/kg versus 20.78 kJ/kg at atmospheric pressure, lending to a much larger cooling capacity. Figure 4.2 shows the open Nitrogen Dewar implemented in tests.

Figure 4.2: Nitrogen dewar used in tests

4.1.2 Top plate

For the helium tests, the top plate was to provide a hermetic seal on the liquid Dewar; however for the nitrogen tests, it provided a support for the experiment and associated plumbing. The top plate was fabricated from 6061 Aluminum; Appendix E contains the engineering drawing and Figure 4.3 shows a photo. Notice the bolt circle and multiple feed-throughs designed to ensure that the helium Dewar was hermetic. The bolt circle provided a means to hang the experiment from a crane while maintaining stability and a level platform. Another feature attached to the bottom of the top plate are the G10 rods. G10 is a fiber composite used often in cryogenics as an insulator or support between two different temperature objects due to its poor thermal conductivity. In this setup, the G10 rods provided structural support for the counter-flow heat exchanger and valve without introducing significant heat leak.

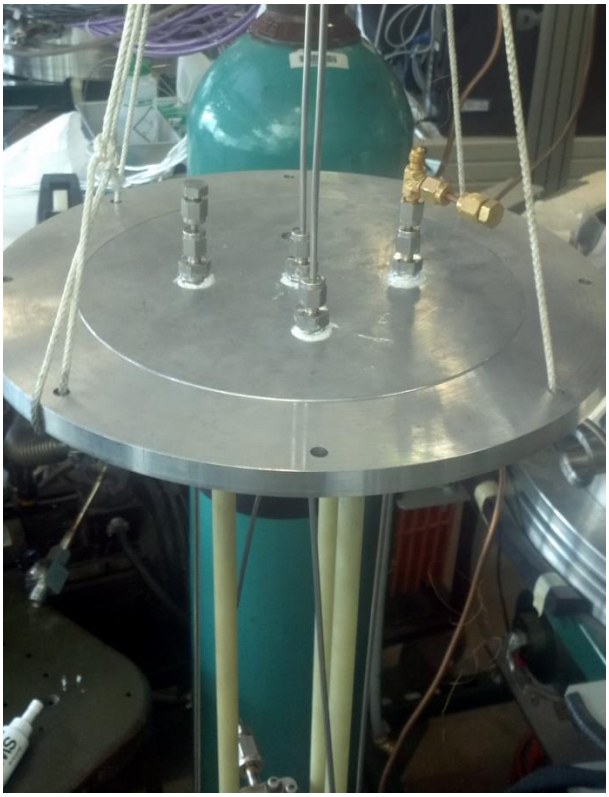

Figure 4.3 Top plate and G10 supports

4.1.3 Plumbing

The plumbing consists of the regulators and valves used to regulate and direct the flow going to and from the valve as well as the physical tubing required to connect the different components. All of the valves implemented in this test rig were Swagelok® 1/8” shutoff ball valves. The bodies of the valves were brass with the exception of PV 1 and PV 2, which were stainless steel. Figure 4.1 shows the process diagram and location of the valves for reference. Notice that all of the valves are located above the top plate. Not only does this allow access to the valves if the experiment is in a closed dewar, but it also prevents the valves from cooling down. The valves contain plastic seals and are not rated for low temperatures, so they must remain at approximately room temperature.

The valve placement was determined to allow switching between forward and back flow without opening up the system to contamination. The high pressure regulator can handle tank pressures (up to 3000 psi) and regulate down to ~ 1 psi for the back flow operation. The low pressure regulator controls forward flow in the sub 1 psi regime, but it is unable to handle the high pressure side because it must not be subject to pressures higher than 40 psi, so the high pressure regulator must be used to step down the pressure. Valves LP 1, LP 2 and HP 1 are used to switch operation between high pressure and low pressure and protect the low pressure regulator from being over pressured when the experiment was in high pressure operation. Valves HP 2, HP 3, LP 3, and LP 4 are used to switch between forward and back flow operation. Valves PV 1 and PV 2 are installed to protect the low pressure transducer from being over pressured.

The tubing above the top plate is all 1/8" outer diameter, 1/16" inner diameter copper tubing. This was selected because of its high ductility and consequent easy workability, as well as its low cost. However, copper has high thermal conductivity. Therefore, below the top plate the tubing is all 1/8" outer diameter, 1/16" inner diameter annealed stainless steel tubing. The thick wall and annealing gives the stainless better ductility, but the thermal conductivity is still low. The heat leak into the liquid was estimated using an integrated thermal conductivity for stainless steel 304 and the estimated height above the liquid of approximately 1 meter. The net heat leak through the 2 pressure sense lines and inlet and outlet feeds to the valve was then found to be 2.79 Watts if the test were done with helium and 2.48 Watts for Nitrogen. Smaller tubing would have less heat leak but would have higher pressure drop.

Pressure drop through a tube is a well understood problem and the basic equations where presented with the valve model earlier. Therefore, a basic analysis on the selected tubing was conducted using EES. There is a built in routine for dealing with the convection characteristics of internal flow including pressure drop. The routine is executed by the line Call PipeFlow('Helium',T,P,m_dot,D,L,RelRough:h_T, h_H ,DELTAP, Nusselt_T, f, Re). It takes a string argument for the fluid type, 'Helium' in this case, the temperature, T, of the fluid, the absolute pressure, P, of the fluid, the diameter, D, of the pipe, the length, L, of the pipe, and the relative roughness RelRough of the inner surface of the tube. This analysis assumes a constant temperature and pressure. To provide an upper limit on the pressure drop, the highest temperature of 293 K and lowest pressure of 100 kPa were used. This ensures both the highest viscosity and lowest density and therefore the greatest pressure drop, providing an upper bound estimate. Ten times the forward mass flow rate of ^{3}He-^{4}He mixtures was used to provide an additional buffer (since ^{4}He is not the same fluid and may result in less pressure drop). The relative roughness was taken to be .0009 based on information in White. The resultant pressure drop from the top plate down to the heat exchangers in nitrogen is less than 7757 Pa (1.125 psi). This is a large pressure drop relative to the difference to be held across the valve (~10 psi). However, the regulator can supply much more pressure than 10 psi and pressure sensors where positioned such that this pressure drop could be compensated for. (White, 2006)

The final consideration for plumbing is the joints between the tubing. All of the room temperature joints are brass Swagelok® compression tube fittings. However these joints become unreliable at low temperatures due to differential thermal contraction between the

ferrule and the tube. Below the top plate, Swagelok® VCR joints were used to connect the heat exchanger and valve. VCR joints use a metal gasket, in this case copper, compressed between two glands. The glands are soldered to the tubing providing a reliable seal through all temperatures. To feed the tubing through the top plate, a Swagelok® compression fitting to ¼" NPT was used. The core was bored out to allow the tubing to feed through, when the appropriate amount was feed through, the compression fitting could be tighten to ensure hermeticity.

4.1.4 Heat exchangers

The heat exchangers are an integral component to ensure that the gas is isothermal at the saturation temperature of nitrogen when it reaches the valve.

The first heat exchanger was a premade counterflow heat exchanger left from a previous experiment. This heat exchanger was implemented primarily to reduce boiloff for the helium tests, but since it was already integrated in the system, it was kept for the nitrogen tests. The effectiveness was measured when it was created to be approximately 60%. Using this in the effectiveness-NTU method of heat exchanger analysis yields a warm side outlet temperature of 166 K, assuming the cold inlet is at 77 K. This reduces the load on the second heat exchanger, thereby decreasing the amount of nitrogen boiled off.

The two heat exchangers to be immersed in the liquid nitrogen before and after the check valve were designed to condense Helium gas. When the heat exchanger was sized, it was done to cool and condense helium from 166 K down to saturation at 4.2 K. Since it was used in liquid Nitrogen, the analysis was simplified to be for gas flow through a tube with a constant wall temperature at 77 K. The analysis for the length of both heat exchangers was

essentially identical, however one was designed to cool the Helium in back flow (~.1 mg/s) and the other was designed for forward flow (~10 mg/s). Again, this system was designed to condense helium gas in a bath of liquid helium. From the condensation analysis, a length of 1.5 m was required for the forward flow and only 20 cm was required for back flow and so the heat exchanger was fabricated with those lengths. It is clear that if the exchangers were designed for the condensation of helium from room temperature down to saturation, the helium will reach 77 K well before the valve. Additional pressure drop through the heat exchangers must also be considered and can be mitigated with the installation of pressure taps, as will be discussed in the next section. Figure 4.4 shows the two heat exchangers. They are coiled together for structural support.

Figure 4.4: Liquid heat exchanger

4.1.5 Instrumentation

The final components in the test setup are the instruments. The setup must be able to accurately record pressure and flow data for both forward and back flow conditions. Since the forward and back flow conditions have such drastically different flow rates and pressure drops across the valve, two different sets of instruments must be integrated into the test rig.

As discussed earlier, there is significant pressure drop through the lines leading to the heat exchangers, as well as through the heat exchangers. To mitigate this pressure sense lines were installed directly before and after the valve. Since these sense lines have no flow through them, there is no intrinsic pressure drop and the pressure difference can be accurately measured only across the valve.

For the higher pressure difference back flow condition, two Endevco 8510B-500 pressure transducers where installed on the two pressure sense lines at room temperature. The sensors then measure the gauge pressure both upstream and downstream of the valve. From the gauge pressure, an absolute pressure can be found to determine fluid properties. These sensors operate by measuring the voltage generated by the deflection of a piezoelectric membrane. An excitation voltage of 10 volts is required and the measured voltage is between 0 and 300 millivolts. The measured voltage scales linearly with a calibration coefficient. The pressure transducer can handle a pressure differential of up to 500 psi with a published accuracy of .5% of full scale (2.5 psi) (Endevco). However, Maddocks manually recalibrated the transducers and, with care taken for noise reduction, achieved an effective accuracy of .1 psi. An important issue to monitor with the Endevco pressure transducers is drift. Over time, the zero offset of the transducers will slowly change. This can be dealt with by simply

checking the pressure of each transducer with no flow and adjusting the zero offset (added in the LabView code) so that the two pressures to match. Since this experiment focused mainly pressure differences, the small error this introduces with the absolute pressure was deemed acceptable.

In the forward flow condition, the pressure drop was expected to be very small, so a very accurate low pressure transducer was installed to measure the pressure difference between the two sides of the valve. The transducer used was an Omega PX277-05D5V with a selectable pressure range of 0-1.25, 0-2.5, or 0-5 inH2O and an accuracy of +-1% of full scale. (Omega) For this test, the range of 0-5 inH2O (0-1245 Pa) was selected giving an accuracy of .05 inH2O (12.45 Pa).

The flow meter used in the forward flow direction was an Omega FMA1700/1800 series; 0-5 slpm (standard liters per min). It operates on a similar principle to a hot wire anemometer. A small tube redirects some of the flow through a heater. With known fluid properties and calibrated correlation the consequent temperature rise in the fluid indicates a given flow rate. The sensor used was calibrated with Nitrogen gas, but could be scaled to helium gas using relations involving the heat capacity of the two gases. Equation 4.1 shows the result of this scaling. The variable $\dot{m}_{He}$ is the mass flow rate of Helium gas at room temperature and $\dot{m}_{meas}$ is the mass flow rate measured with the omega flow meter.

$$\dot{m}_{He} = 1.454 * \dot{m}_{meas} \quad \textbf{(4.1)}$$

Both of the mass flow rates in Equation 4.1 are in standard liters per minute. To convert the flow rate of helium to kg/s the result must be multiplied by the density of helium at standard conditions (1 bar and 21.1 C). Conducting the same conversion on the upper and lower limits

of the flow meter in standard liters per minute (slpm) yields a range of 0-21.2 mg/s. The flow meter has a published accuracy of .25% of full scale, giving an absolute accuracy of .05 mg/s. This was confirmed against the bubble flow meter described in the next paragraph.

The Omega flow meter is accurate enough for forward flow measurements, however if the valve were to be successful, the flow rate would be far below the accuracy of the meter. Therefore a second flow metering device was installed, a bubble capillary flow meter. The flow is redirected through a capillary into an upended graduated cylinder. The cylinder is filled with water and the open end is submerged in a larger container. This way, as the helium bubbles out of the capillary, it displaces the water in the graduated cylinder. The volume the gas displaces as well as the time it takes to do so can be measured. The gas is assumed to be at atmospheric temperature and pressure to find the density. The pressure difference of caused by the column of water only changes the density and consequently the mass flow rate by approximately 1 percent, therefore this assumption was deemed acceptable. Assuming the volume change can be measured to .5 mL, and setting a lower limit on the time the user will wait to measure it at 30 min, this method can accurately measure approximately .09 μg/s of flow (.1-.2% of the sealing flow rate). Simply waiting longer will improve the resolution. The effective range of this method is governed by the size of the graduate cylinder. For the 100 mL graduated cylinder, a volume chance of approximately 50 mL over the course of 30 seconds can accurately be measured, corresponding to a mass flow rate of .28 mg/s of ^{4}He. The flow metering setup is shown in Figure 4.5.

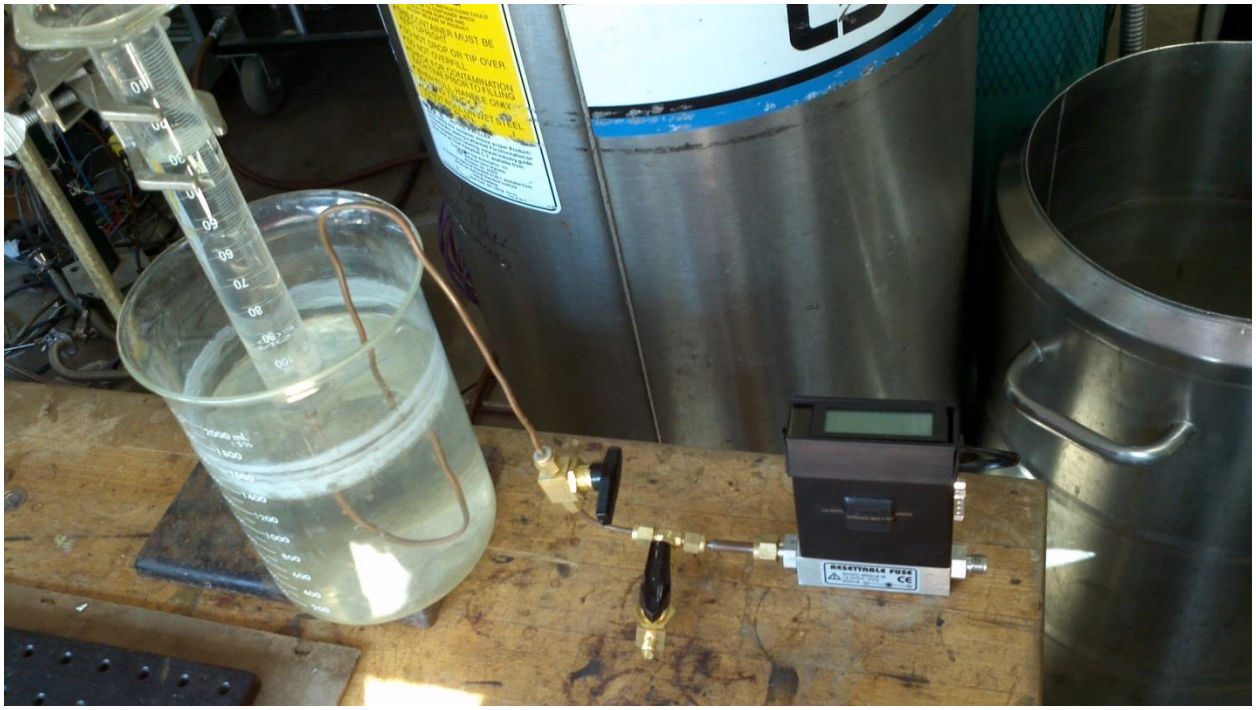

Figure 4.5: Liquid Nitrogen test flow metering setup

4.2 Cryocooler Test Facility

As mentioned earlier a lack of funding precluded tests with liquid helium, however a Cryomech PT-410 Cryocooler was available to continue tests. As will be discussed in the results section, the liquid nitrogen test verified that the pressure drop due to flow in the forward direction is negligibly small. Therefore, for the Cryocooler test, only back flow will be measured, with the ability to flow helium in the forward direction implemented simply to verify that there are no blockages. Figure 4.6 shows the process diagram for the cryocooler test setup. Note the "1 K pot" in the diagram. Designed as part of Jahromi's facility, it is an open loop Joule-Thompson cycle implemented to provide cooling down to 1.4 K beyond the 3 K attainable with the cryocooler. However, in that temperature range, a significant portion of ^{4}He becomes a superfluid. Since the valve is not intended for controlling superfluid, the

Joule-Thompson loop was not run and the 1 K pot was thermally strapped to the 3 K plate to ensure that it remained approximately isothermal.

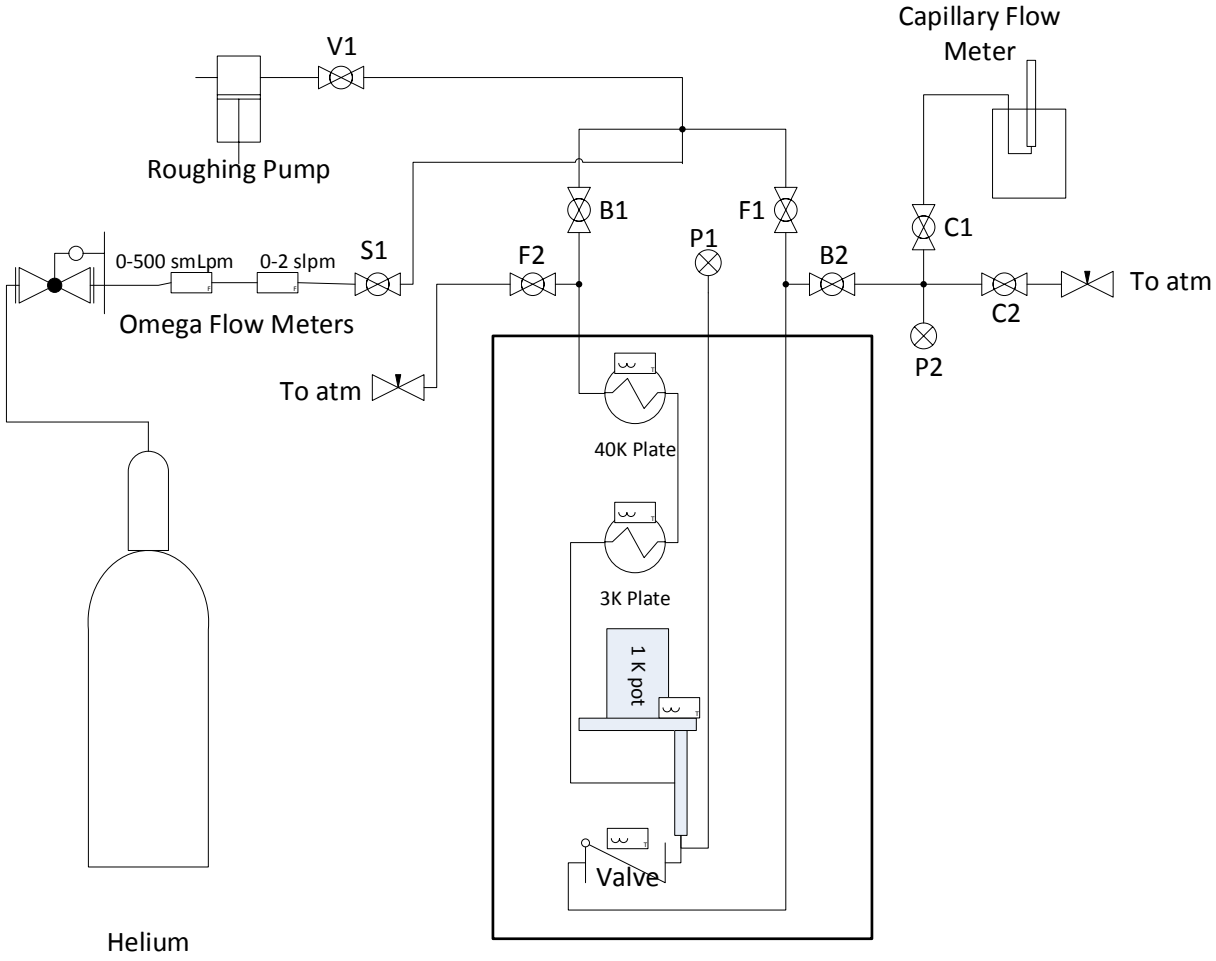

Figure 4.6: Cryocooler process diagram

4.2.1 Cryomech PT- 410

The facility was set up by Amir Jahromi and his Master's thesis can be consulted for more specific information beyond what is presented here about this facility. (Jahromi, 2011) The Cryomech PT-410 is a pulse tube type cryocooler with a nominal 2nd stage and 1st stage combined cooling power of 1 Watt at 4.2 K with 35 Watts at 45 K respectively. The 0 Watt

load, ultimate low temperature is 2.8 K. The actual final temperature is dependent on the load on each stage, therefore the performance map in Figure 4.7 must be consulted for the actual cooling power. This map can really only be used as an estimate, since the conductive and radiative heat leak will vary between setups, affecting the available cooling power. (PT410 Cryorefrigerator)

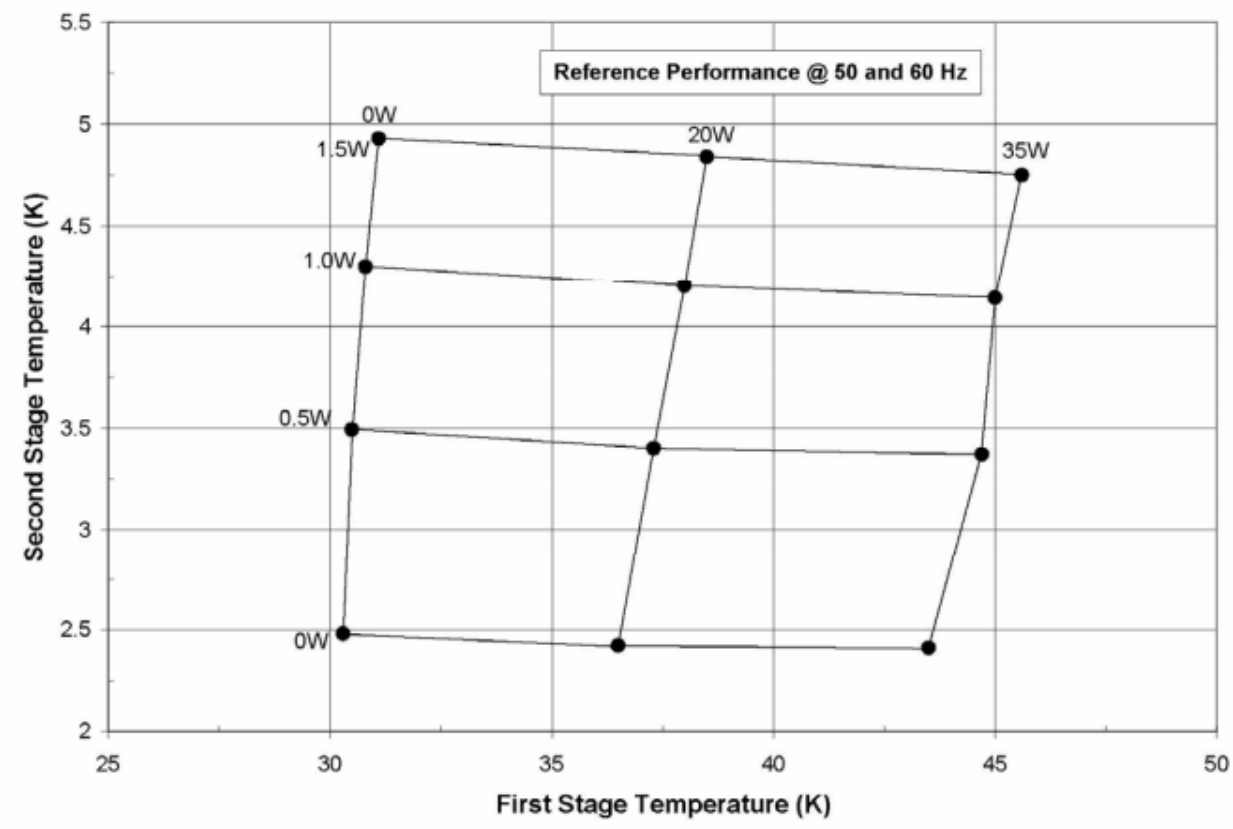

Figure 4.7: PT-410 Capacity Curve

To find the expected final temperature for the valve tests, an estimated mass flow rate must first be established. Since back flow is the only condition being tested, the flow rate must be less than the forward flow rate; therefore the forward mass flow was taken as an upper limit on the expected flow rate. For this analysis, it was assumed the heat exchangers are

sufficiently long to bring a flow rate of up to 9.2 mg/s of ^{4}He to a constant temperature with the plate. A "guess and check" procedure can be implemented by guessing the temperature of the higher temperature platform, then finding the corresponding change in enthalpy to bring 9.2 mg/s of Helium from 293 K down to that temperature. Here the pressure is at the high pressure side of the closed valve, selected to be 10 psig for the tests. The difference between this and the 10-20 kPa indicated in the valve requirements will be discussed in the testing section. Repeat until the load and enthalpy change due to temperature match. This procedure results in a temperature of approximately 35 K with a cooling power of approximately 12 Watts for the first stage.

This can then be repeated with the second stage with the inlet temperature equal to the outlet temperature of the first stage. The cooling powers of the two stages are linked, so the power line of the first stage must be followed down the chart to find the various possible second stage cooling powers. Another issue to be aware of with the second stage is the possibility of two phase flow. It is important for the tests to be completely liquid or completely vapor on both sides of the valve, since the properties of density and viscosity are well known and the laminar model can be verified. However if the flow is two phase, temperature and pressure alone do not fully specify the state and the density and transport properties of two phase substances can vary widely. The guess and check procedure was conducted again but this time it yielded a temperature above the range of the chart corresponding with the required cooling power. The temperature was extrapolated to be approximately 5 K with a cooling power of 1.51 Watts. At this temperature with a pressure of 10 psig the Helium gas is

superheated therefore two phase flow is not a concern. These results also provide a baseline for the heat exchanger analysis shown later in this section.

4.2.2 Plumbing

The room temperature plumbing and valves are similar to the liquid nitrogen test setup. All of the room temperature joints are brass Swagelok® compression tube fittings and the valves are Swagelok® brass ball valves. The system connects to a gas panel that allows access to a roughing pump. The intricacies of the panel are not shown in the diagram, since the only function utilized is the roughing pump access. Again, the room temperature tubing used was 1/8” outer diameter, 1/16” inner diameter copper tubing to allow malleability and ensure a small pressure drop. The valves were again arranged to allow flow in both the forward and reverse directions. At the outlet of both the forward and back flow orientations a needle valve was installed to provide additional flow control and ensure a positive pressure in the system. The positive pressure prevents air from being sucked back in to the system.

The cold platforms of the cryocooler are in vacuum, so feed-throughs must be utilized to connect the plumbing to the inside of the vacuum can. The outer vacuum can has several Swagelok® KF 50 vacuum ports on the body. The copper tubing was brazed into holes in a Stainless Steel KF 50 blank and the blank was sealed to a port using a rubber O-ring. Figure 4.8 shows a picture of this feed through. Note, two extra feed-throughs where added and capped off for future use.

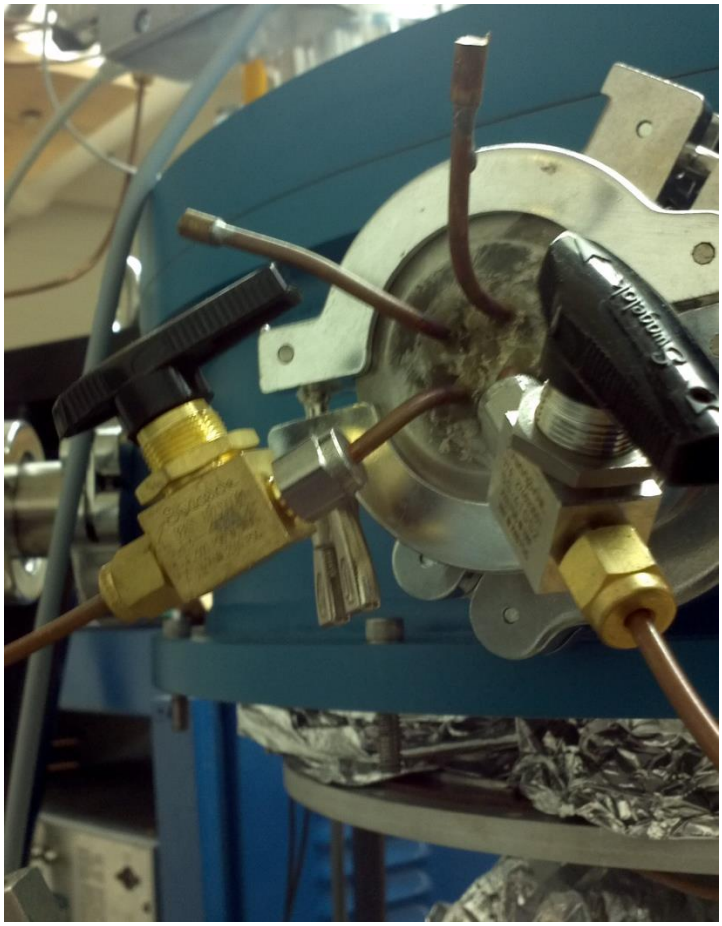

Figure 4.8: KF 50 vacuum feed-through

Inside the vacuum space, compression fittings were not utilized for the same reasons mentioned earlier (there is a possibility for large temperature gradients). Instead, solder slip joints with 1/16” outer diameter, .025” inner diameter stainless steel tubing and Swagelok® VCR joints were used. The stainless slip tubing not only provided a robust joint, but also minimized the heat leak between platforms, since the cross sectional area is small and stainless has poor thermal conductivity. Walking through the joints, the stainless tubing was used to join the room temperature feed through to the 40 K platform heat exchanger. Another section of tubing was used to connect the 40 K heat exchanger to the 3 K platform heat exchanger. The final length was used to connect the 3 K heat exchanger to the buffer volume.

From the buffer volume, a three way joint was soldered in to provide an access point for a pressure tap. The pressure tap line was 1/16” stainless steel tubing that went directly to ambient through KF feed-through. This functioned in the same manner as the pressure taps in the liquid nitrogen setup. The valve was then mounted in using 1/8” VCR joints with copper gaskets. From the valve, 1/8” outer diameter, 1/16” inner diameter stainless steel tubing ran back up through a KF feed through and to the room temperature plumbing. 1/8” Stainless tubing was used to both minimize heat leak and pressure drop. A rough pressure drop analysis similar to the nitrogen analysis was conducted on the entire assembly with EES. The code is shown in Appendix F. As can be seen, there were several very liberal approximations made with the length of the heat exchangers and average temperature of the fluid. A more in depth analysis was done on the heat exchangers and will be detailed in the next section; however this analysis was adequate to give an estimation of whether the pressure drop would be significant in the design. The results indicate there is a large pressure drop (~6.39 psi) through the heat exchangers and 1/16” stainless tubing, verifying the need for a pressure tap after the heat exchangers, but before the valve. However a second pressure tap in the vacuum space directly after the valve was not required since the pressure drop in the 1/8” tubing was found to be small (~.3 psi). The pressure after the valve (in the back flow direction) was measured at room temperature.

The final plumbing feature in this setup is the buffer volume. In the back flow direction, it was installed after the heat exchanger, before the pressure tap. It served two purposes; one is to provide a buffer to stabilize the flow into the valve. The other was to accumulate and verify the presence of liquid helium in the line. Though the cryocooler does not possess the

cooling power necessary to liquefy a flow rate of 9.2 mg/s, this is the worst case mass flow rate. There was a good chance that the flow rate would be far below that if the test is a success. At lower flow rates, the load on the cryocooler is lower and final temperature of the second stage could fall below the saturation temperature of helium at 170 kPa absolute. The buffer volume physically consisted of a copper cylinder 9” long with a ½” diameter. It also had an indium sealed cap with a Stycast epoxy feed-through to accommodate a 6 in liquid helium detector. Unfortunately, as will be discussed in the testing section, the flow rate never fell to a level where the liquid level detector was utilized and therefore its operation will not be covered in depth.

4.2.3 Heat exchangers

The analysis on the heat exchangers for each of the stages was similar to that done for liquid nitrogen test apparatus. However, where the nitrogen had a constant temperature platform, the cryocooler cooling power and temperature are not independent. To do a proper heat exchanger analysis the temperature and some flow characteristics must be known. The energy balance used to find the final temperature of each stage assumed a mass flow rate of 9.2 mg/s in the worst case for back flow so this was maintained for the heat exchanger analysis. The energy balance also provided the approximate temperature each stage would equilibrate to with the given mass flow rate. Some assumptions of the geometry must also be established. The copper tubing selected for the heat exchanger had an inner diameter of 1/16” and outer diameter of 1/8”. The tubing was soldered to 1/32” thick copper plate, which was cut to an appropriate shape to fit the available area on each platform. A bolt pattern was drilled to tightly hold the copper to the platform. The thickness of the copper plate and bolt

pattern serve to both minimize thermal contact and conduction resistance between the platform and the fluid. Also, at the lower temperature stage, indium foil was compressed between the copper plate and the platform to further reduce contact resistance. The length of each heat exchanger must be solved for to produce an outlet temperature approximately equal to that of the platform.

The walls of the tubing used in the heat exchanger where therefore assumed to be constant at that platform temperature. A cursory examination of the convection thermal resistance versus the conduction thermal resistance with the given mass flow rate and tubing dimensions show a ratio of $R_{conv}/R_{cond}=5630$ for the 1st (higher temperature) stage and $R_{conv}/R_{cond}=1210$ for the 2nd (lower temperature) stage. This indicates the resistance to heat transfer is heavily convection dominated, validating the claim of isothermal walls.

The length required to bring the temperature of helium close to the isothermal walls at each respective platform temperature can be found using known inlet and outlet temperatures, the mass flow rate and the tubing diameter. The analysis for both stages was essentially the same. Given that the lowest temperature obtainable at this mass flow rate is 5 K, which is above the saturation temperature at 10 psig ($T_{sat}=4.8$ at ~170 kPa absolute for Helium), the helium was assumed to remain fully gas. However the helium drastically changes properties through both of the heat exchangers, therefore a slightly more complex analysis is required. A method of sub-heat exchangers as discussed on page 876 in Nellis and Klein's Heat Transfer text was implemented. Unlike other, more traditional, methods of heat exchanger analysis such as ε-NTU and LMTD, this does not assume constant capacity rates. The EES code used to implement this method can be found in 0. (Nellis & Klein, 2009)

The analysis on the first stage with an inlet temperature of 293 K and and outlet temperature of 35.1 K indicated that a length of .47 meters was required. The second stage with an inlet temperature of 35.1 K and an outlet temperature of 5.1 K required a length of .44 meters. The first stage heat exchanger was fabricated by soldering a length of 36” of 1/8” outer diameter, 1/16” diameter to the 1/32” thick copper plate with 60-40 lead tin solder. The plate was cut into three crescent shaped sections, each with an arc length of 10” to complete a total length of 30” (.76 m). This is an additional factor of safety over the required .47 meters to assure that the helium exits at the temperature of the platform. The difference in length between the plate and the tubing allowed for a slight bend in the tubing between each section to provide some flexibility in mounting the plate to the first stage platform. The plate had a circular bolt pattern to mount the heat exchanger securely. Figure 4.9 shows one of the sections of the fabricated heat exchanger.

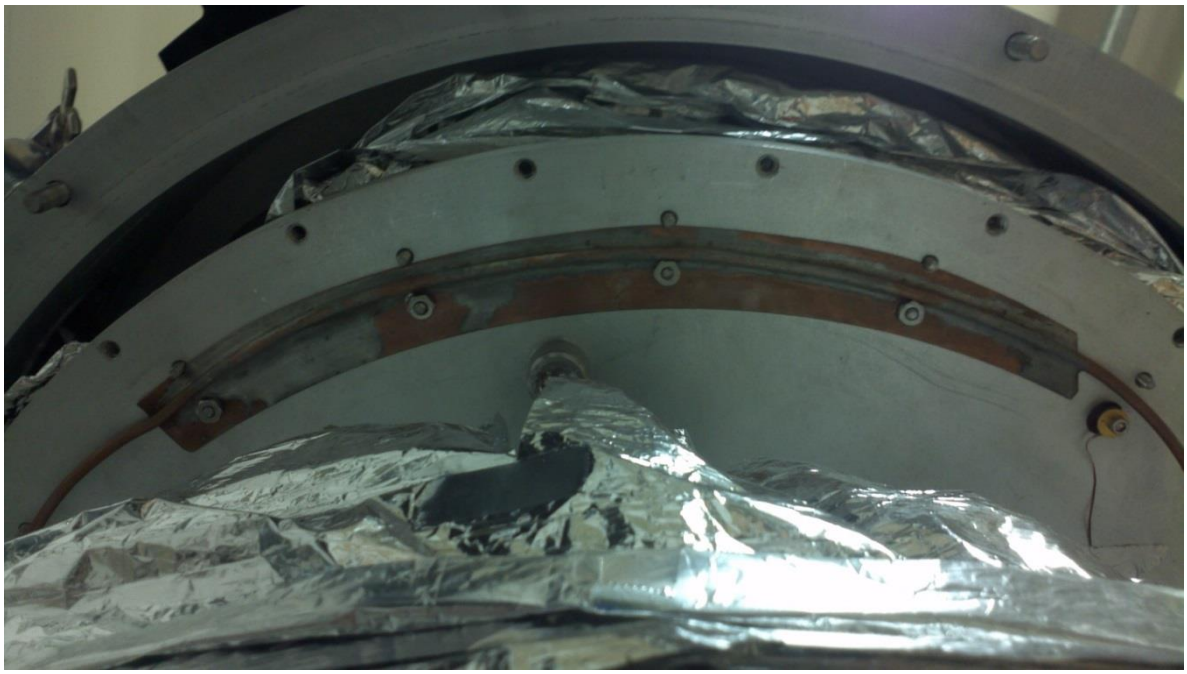

Figure 4.9: First Stage heat exchanger on Cryocooler

The second stage heat exchanger was fabricated using the same materials of the first, but a different bolt pattern and available area changed the geometry. For this heat exchanger the tube was laid back and forth 10 times on a 6” by 3” square plate. This resulted in a continuous flow path with a net length of approximately 60” or 1.52 m, much greater than the required .44 meters. Another feature of this heat exchanger is indium foil placed between the platform and the plate to reduce the contact resistance. Figure 4.10 shows the fabricated second stage heat exchanger.

Figure 4.10: Second Stage heat exchanger on Cryocooler

4.2.4 Instrumentation

Much of the instrumentation on the cryocooler was similar to the liquid nitrogen test rig. There were however several refinements, such as series flow metering and various temperature sensors to give an accurate temperature profile of the valve performance.

In the cryocooler setup, there were in fact three flow meters; two omega flow meters in series with ranges of 0-500 standard milliliters per minute and 0-2 standard liters per minute respectively and a capillary bubble flow meter on the outlet. The 2 omega flow meters shown in Figure 4.11 are in series to accurately measure the flow from 2 standard liters per minute (8 mg/s ^{4}He) down to 30 standard milliliters per minute (.12 mg/s ^{4}He) when the capillary bubble flow meter can be used. The accuracy of the gauges are .25% of the full scale, therefore the 0-500 smlpm (2 mg/s ^{4}He) has an accuracy of 1.25 smlpm (.005 mg/s ^{4}He) and the 0-2 slpm meter has an accuracy of .005 slpm (.021 mg/s ^{4}He).

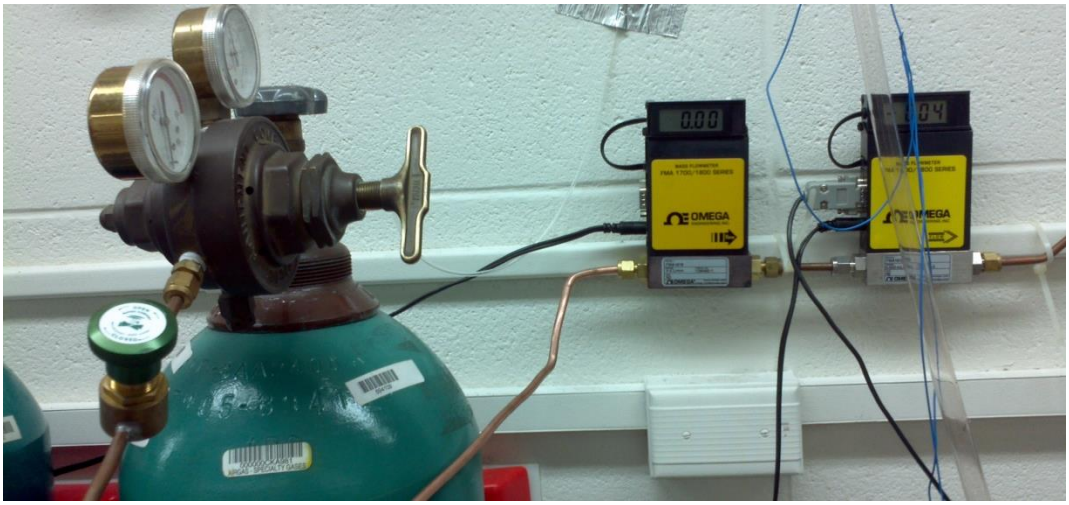

Figure 4.11: Omega flow meters in cryocooler setup

The capillary flow metering setup was the same as the liquid nitrogen test with an accuracy of .09 µg/s and an effective range of 0-.28 mg/s of ^{4}He. The implementation for the cryocooler setup is shown in Figure 4.12.

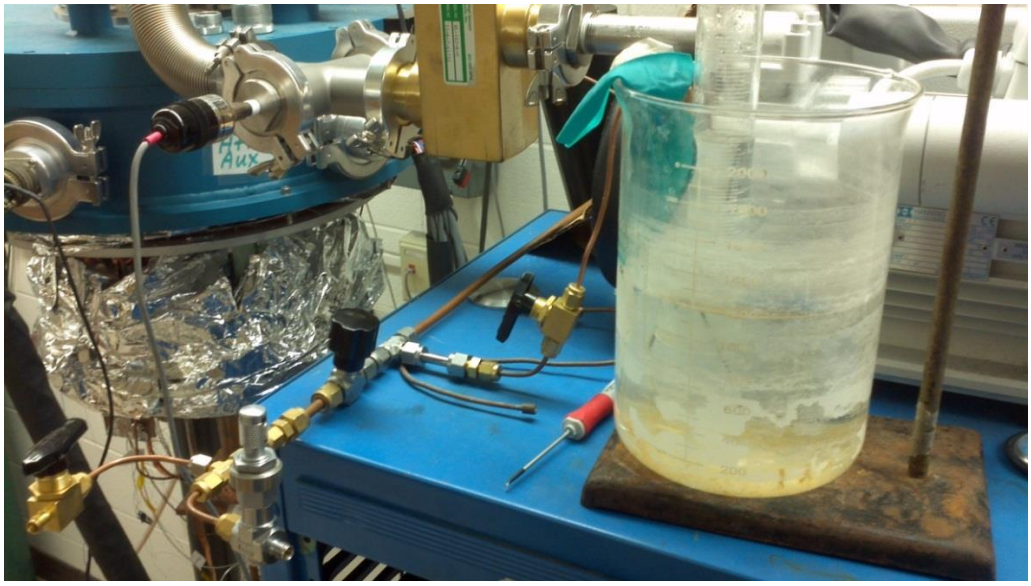

Figure 4.12: Capillary flow meter in cryocooler setup

The cryocooler was instrumented for earlier experiments with Cernox and Silicon diode sensors on the various components of the rig. A detailed description of the calibration of these sensors can be found in Jahromi's thesis. A spare Cernox sensor was used to measure the temperature of the valve. Cernox sensors are a type of resistance temperature device (RTD), where the temperature is correlated with a resistance. The advantage of these RTDs in particular is the large change in resistance associated with a change in temperature at low temperatures. The accuracy of the Cernox sensor used on the valve is +/-.025 K in the temperature range of .1 to 77 K and +/-.153 K from 77 to 300K.

The sensor package is a gold coated bobbin with a mounting hole through the center. The gold coating provides low contact resistance between the sensor and the object to which it is attached. To mount the sensor onto the valve, a standoff was created shown in Figure 4.13. A final image of the complete test setup is shown in Figure 4.14.

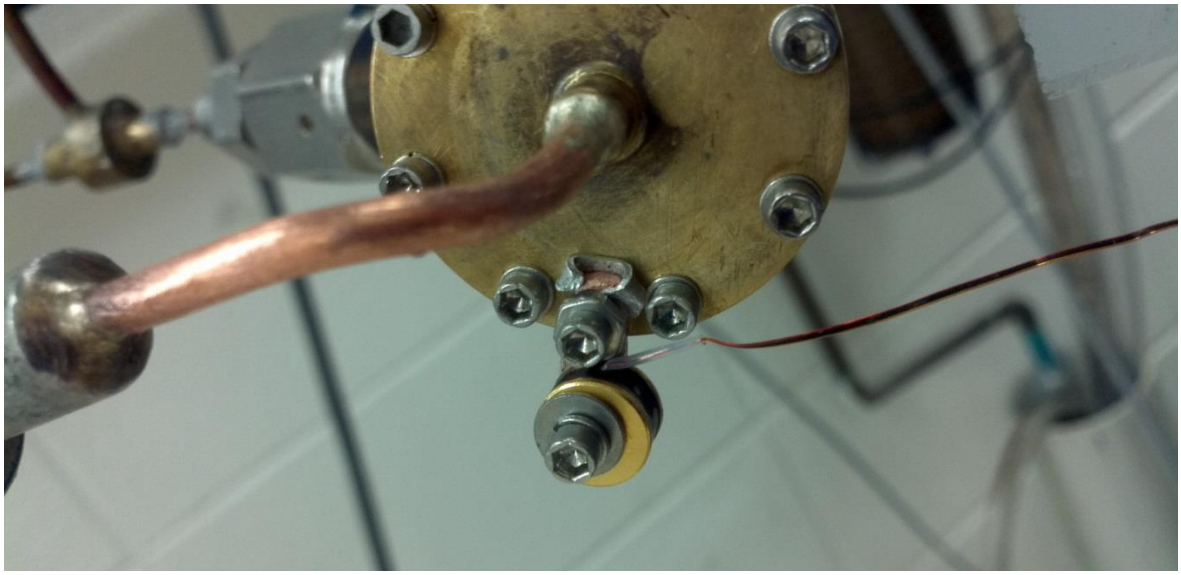

Figure 4.13: Check valve temperature sensor mounting

Figure 4.14: Completed cryocooler test setup

4.3 References

White, F. M. (2006). *Fluid Mechanics* (6th ed.).

Endevco. (n.d.). Piezoresistive Pressure Transducer Model 8510B-500.

Omega. (n.d.). Differential Pressure Transducer with Field Selectable Range.

Jahromi, A. (2011). Development of a 1 K facility and modeling of a superfluid magnetic pump with no moving parts. University of Wisconsin - Madison.

PT410 Cryorefrigerator. (n.d.). Retrieved from Cryomech: http://cryomech.com/PT410.php

Nellis, G., & Klein, S. (2009). *Heat Transfer*. Cambridge University Press.

5 Test Results

As mentioned previously, the testing was done on two separated setups, a liquid nitrogen dewar and a cryocooler. This section details both of those tests and relates them to the laminar flow model.

5.1 Liquid Nitrogen Test

Given the time and budgetary restrictions at the beginning of this project, the liquid nitrogen test allowed for a simple, quick test to verify the performance of the valve at 78 K. At this temperature, much of the thermal contraction has occurred as has the final phase transition of Teflon (173 K). Therefore this test was excellent for finding initial indications of a successful valve while allowing for rapid modifications to be implemented and tested.

5.1.1 Procedure

After the valve was installed, a simple, yet rigorous procedure was followed. Here the process diagram is revisited in Figure 5.1. First, the lines were flushed with Helium gas, to be sure that there is no lingering water vapor in the lines to freeze and block flow. To do this valves HP 1-3, LP 1-4 and PV 1-2 were all opened. FM 1-2 remained closed. The HP regulator was barely cracked to allow a pressure of approximately 1 psig of Helium to fill the system. HP 1 and LP 1 were then closed and FM 1 was opened to allow the pressure to blow down to atmospheric. FM 1 was then closed and the procedure to fill and blow down the system was repeated two more times.

Following the purge, the preload was applied to the valve. Valves LP 1-2 and HP 2 were closed while HP 1 and 3 and LP 3-4 remained open. Valves FM 1-2 were initially closed

after the purge. Though the check valve eventually sealed with an adequate preload pressure, there was always some leak through the valve. If the system were not allowed to vent (FM 1-2 closed), this leak would eventually build up the pressure on the low pressure side of the valve. If the pressure on the low pressure side increased too much, the sealing would eventually fail. Therefore after the desired preload pressure differential was applied and the downstream pressure began to build, FM 2 was opened to allow the flow to vent. The pressure differential across the valve could then be held with a flow in the sealing direction.

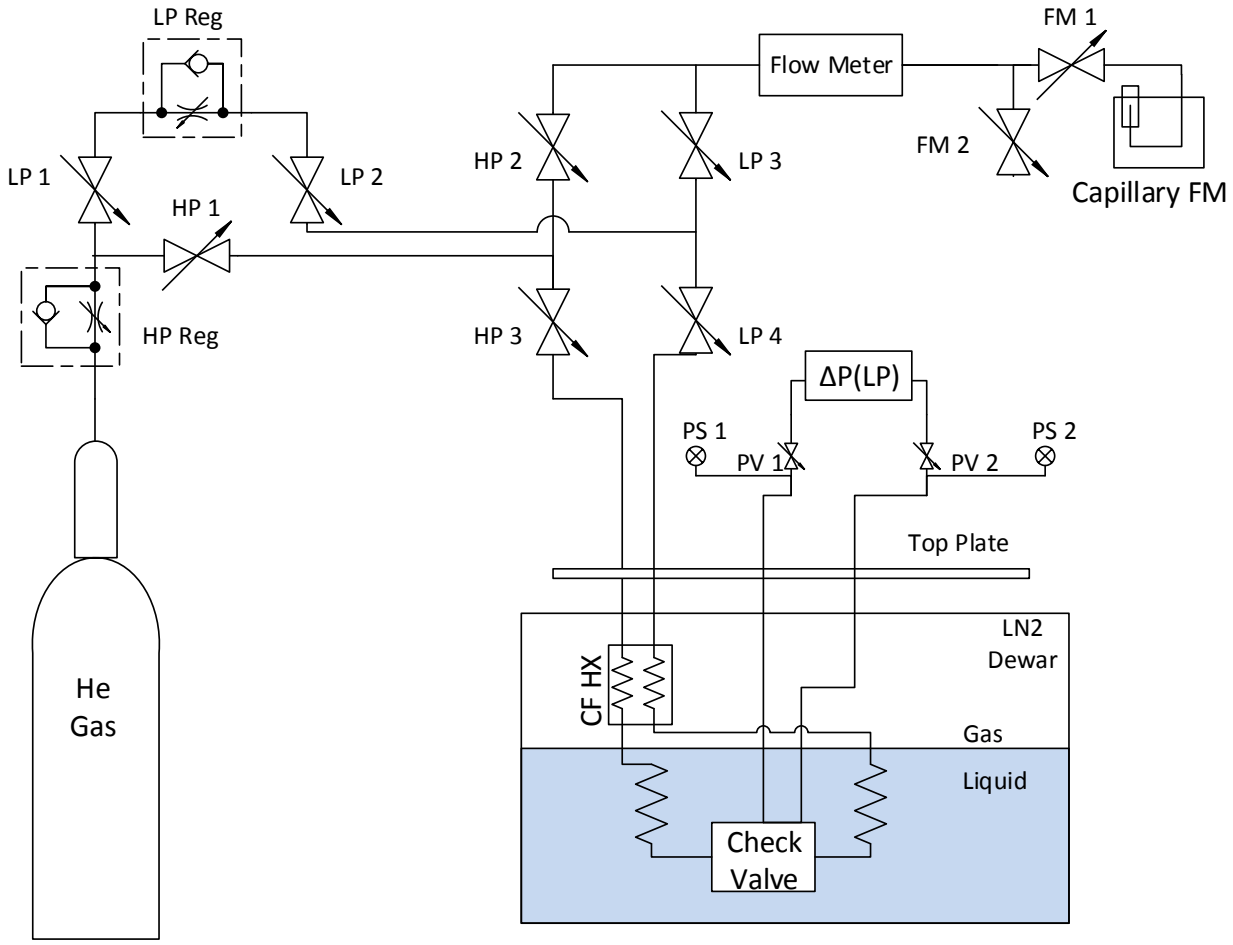

Figure 5.1: Liquid nitrogen process diagram revisited

Next, the dewar was filled with liquid nitrogen. The nitrogen was filled to approximately 6" inside the dewar to ensure the valve was entirely immersed in liquid. Since the entire test rig was suspended from a crane, the valve could be slowly lowered into the liquid. The valve was assumed to be isothermal with the liquid after the film boiling visually became nucleate boiling (the nitrogen boiled vigorously than visibly calmed to a steady state). After the valve

cooled, the forward and back flow tests could be conducted, with care taken to ensure helium remained flowing through the system to prevent water vapor from being pulled in.

5.1.2 Results

5.1.2.1 Back flow tests

A difficult criterion to establish in these tests is the mass flow rate of ^{4}He that indicates sealing. This is true since the criteria established at the beginning of this thesis was for ^{3}He-^{4}He mixtures. When these tests were undertaken a scaling argument had not yet been confirmed. The sealing criterion for the mixture was established to be 39.4-92 µg/s or less than 1% of the forward flow. Therefore, in order to roughly account for the difference between the fluids, a flow rate of less than 4 µg/s of pure ^{4}He was selected (less than .05 % of forward flow). Another difference with the criteria established at the beginning of this thesis is that the desired sealing pressure differential was selected to be 10 psi. The initial testing was done before the model of the CCDR was completed and this was thought to be the pressure difference attainable by the pump. Though the final model results lower the pressure differential to 10-20 kPa, 10 psi was retained as the desired sealing pressure since much work had already been done with this assumption and it provided a good basis for comparison between different iterations of the valve. Later using the cryocooler test apparatus a scaling argument was solidified and the nitrogen results were revisited. With this new lower sealing criteria established for pure ^{4}He, the valve was tested at room temperature as shown in Figure 5.2. It was clear from these results that the selected sealing criteria was not met until the pressure difference was 25 psi, so the valve was cooled down with this pressure as the preload to keep the valve closed. After the valve had cooled, the preload was

released and the flow of the valve was tested at various pressures applied to close the valve. Since the valve seemed to seal better as the preload pressure differential was increased, preloads of 45 psi and 65 psi were also tested. The results are shown in Figure 5.3.

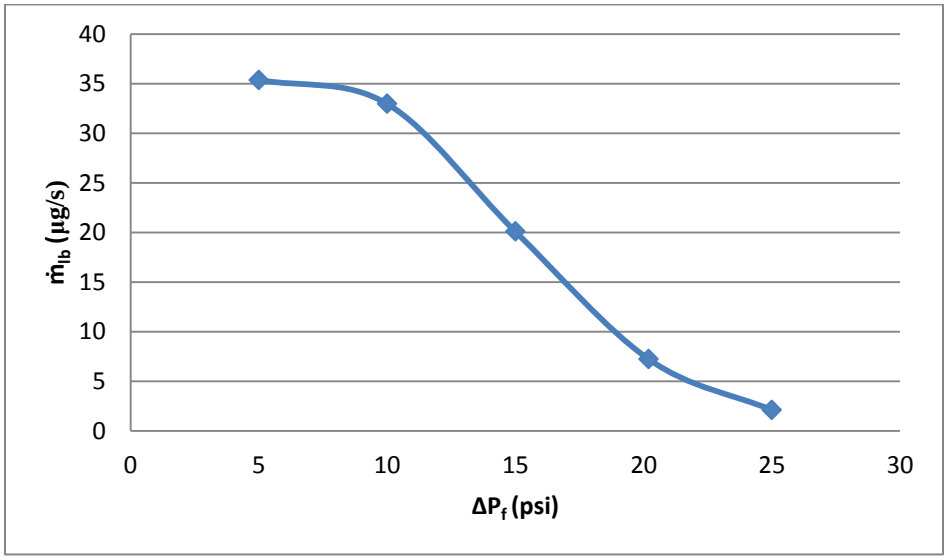

Figure 5.2: Mass flow rate vs back flow pressure difference at room temperature

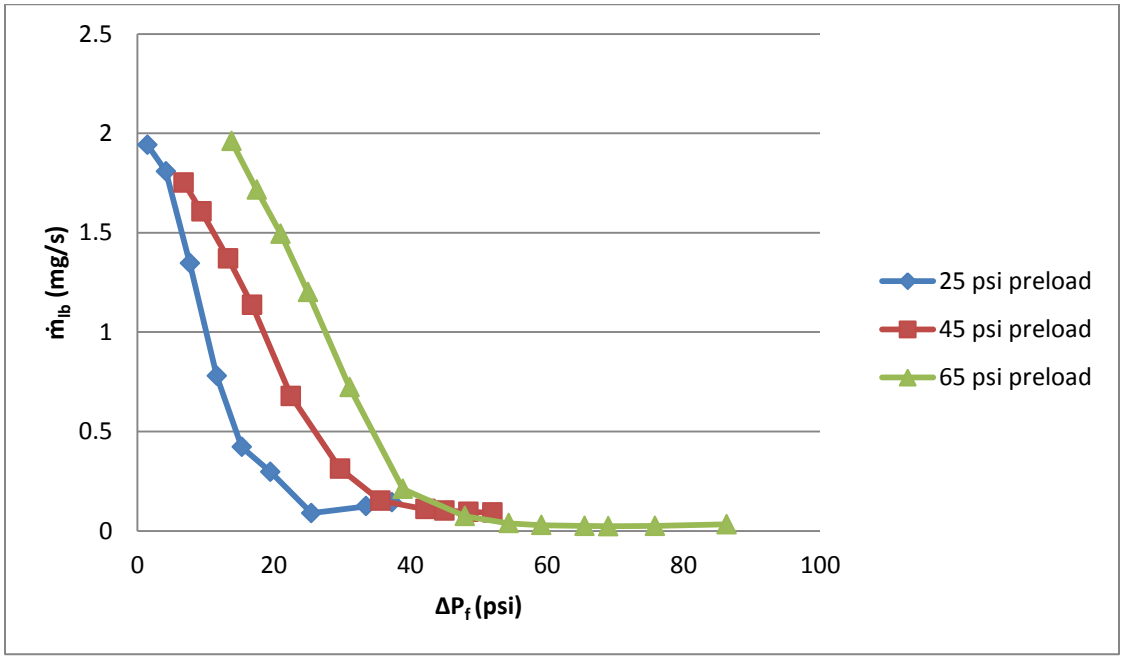

Figure 5.3: Mass flow rate vs back flow pressure difference at 78 K with preloads of 25, 45, and 65 psi

Figure 5.3 indicates that sealing can be accomplished, but at very high preload pressures. Another lesson from these tests is that the best sealing occurs at the preload pressure. At the high preload pressures, it was likely that some amount of permanent deformation had occurred. To confirm this, the valve was warmed and the room temperature flow rate at a pressure difference of 10 psi was found to be 13 µg/s, far less than before the 65 psi test and close to the selected sealing criteria. The preload was held at 10 psi and cooled down again resulting in Figure 5.4.

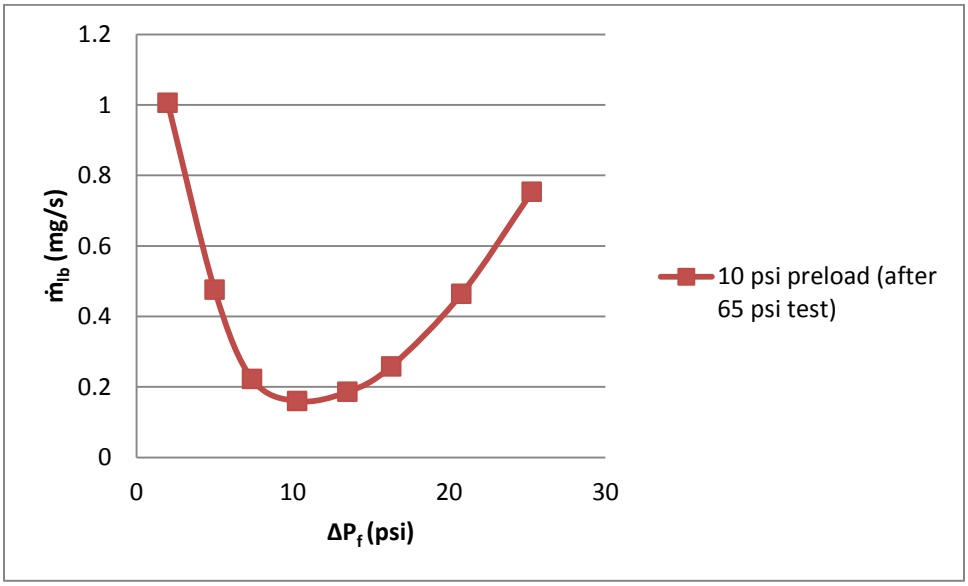

Figure 5.4: Mass flow rate vs pressure at 78 K with 10 psi preload after the 25, 45 and 65 psi tests

The mass flow rates shown in Figure 5.4 are still above 4 µg/s but are far lower than the leakage flow rates that occurred at low pressures after high pressure preloads. This solidifies the idea that the best sealing occurs at the preload pressure, but some permanent deformation occurred in the seat from the high pressure 65 psi preload tests. The best sealing at the preload pressure can be described by the radius of curvature of the reed under pressure. It is obvious that with high pressure preloads, the radius of curvature will be small. When the

valve is cooled down and the pressure is released to test at lower pressures, the high pressure radius of curvature is frozen into the seat and sealing surfaces no longer matches. A simple illustration of this principle is shown in Figure 5.5.

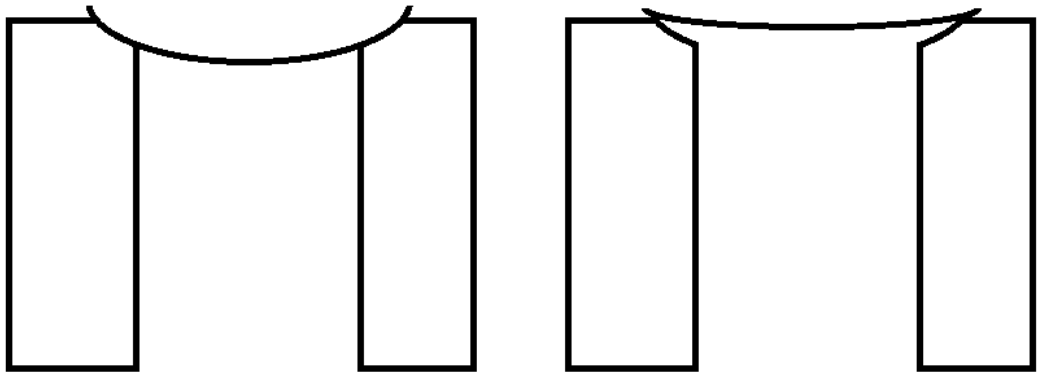

Figure 5.5: Sketch of changing radius of curvature, left is the high pressure preload, right is the low pressure tests.

Ideally, permanent deformation could be accomplished with a large radius of curvature so the shape of the sealing surface would match at the low pressure differentials desired in the valve. Therefore it was postulated that a thicker reed could be installed and a high pressure differential applied to achieve the permanent deformation. Since it is well known that the radius of curvature is also a function of the thickness of the reed, the radius of curvature of this thicker reed could be made to match the low pressure radius of curvature of a thinner reed at low pressures. The thicker reed could be removed and the thinner reed installed for actual operation at low pressures. To find the required pressure differential to apply to the thicker reed to align with the shape of the thinner reed at low pressures, the Theory of The Flexure of plates must be employed. The maximum deflection of a circular plate under a distributed load with fixed edges can be found using Equation 5.1, where ν is poisons ratio, *F*

is the distributed load, *a* is the radius of the plate, *E* is the Young's modulus of the material, and *th* is the thickness of the plate.

$$w_{max} = \frac{\frac{3}{16}(1-\nu)(5+\nu)Fa^4}{Eth^3} \quad \textbf{(5.1)}$$

Equation 5.1 can be simplified to the proportionality in Equation 5.2, since the only characteristic of the reed that will be changing is the thickness and the pressure difference. It is also assumed that the maximum deflection is proportional to the radius of curvature. In this proportionality ΔP is the pressure difference across the reed, R_c is the radius of curvature and *th* is the thickness of the reed.

$$R_c \propto \frac{\Delta P}{th^3} \quad \textbf{(5.2)}$$

From this the radius of curvatures of the two reeds can be set equal. If the desired shape in the seat is optimized for a .004" thick reed at 10 psi, then a pressure difference of 80 psi must enforced across a .008" thick reed.

The .008" thick reed was installed and an 80 psi pressure difference was held. The reed was then replaced with a .004" thick reed and the valve was cooled down with a preload of 0 psi and 10 psi respectively, resulting in Figure 5.6.

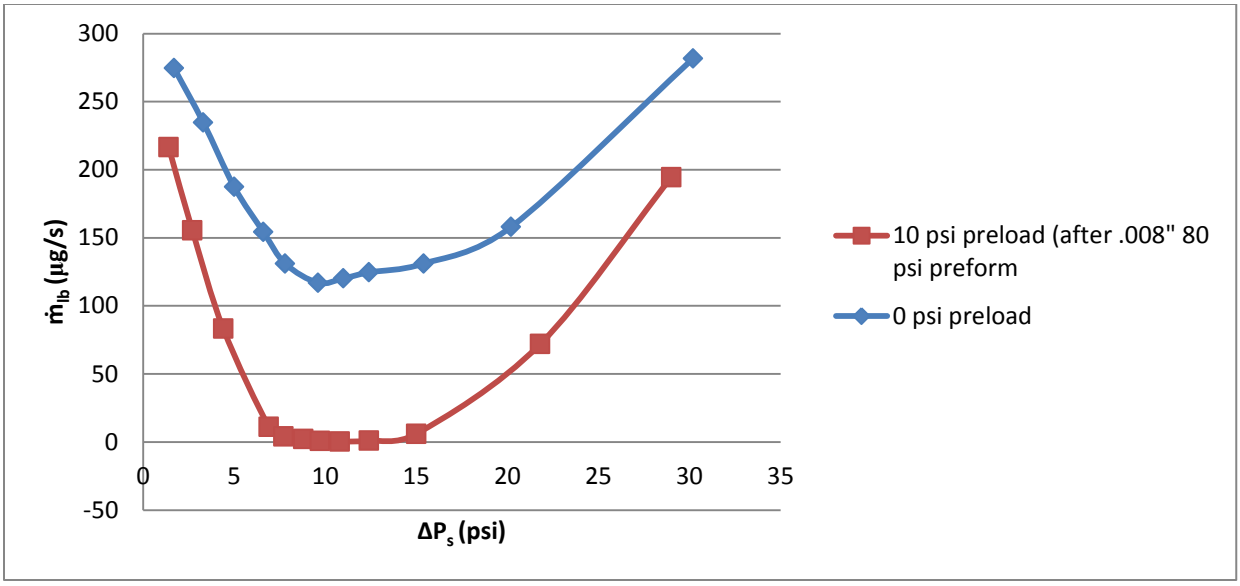

Figure 5.6: Mass flow rate vs pressure at 78 K for .004" reed after preforming at 80 psi with .008"

It is clear that even with no preload the leakage gets close to the desired value and with a preload of 10 psi the leakage goes below the selected criteria, with a minimum at 10.8 psi of .3 µg/s. The results of the liquid nitrogen test confirm that favorable permanent deformation can be accomplished with a thick reed at a pressure calculated according to the desired operation pressure and thin reed thickness. Excellent sealing at low temperatures and low pressures can be accomplished if the thinner reed is then swapped into the valve and cooled down with the desired operation pressure as the preload.

5.1.2.2 Forward flow test

After the valve was confirmed in back flow, the forward flow was tested while the valve was still immersed in liquid nitrogen. Valves PV 1 and PV 2 were opened to allow access to the pressure taps for the low pressure transducer. To configure the flow loop for forward operation, FM 1 and 2 were closed to prevent air from being pulled back in as the valves where reconfigured. Valves LP 3 and HP 1 were closed and LP 1-2 and HP 2-3 were opened.

After a low pressure (~1 psi) was provided with the low pressure regulator, FM 2 could be opened again. The flow was then tested at various low pressures shown in Figure 5.7.

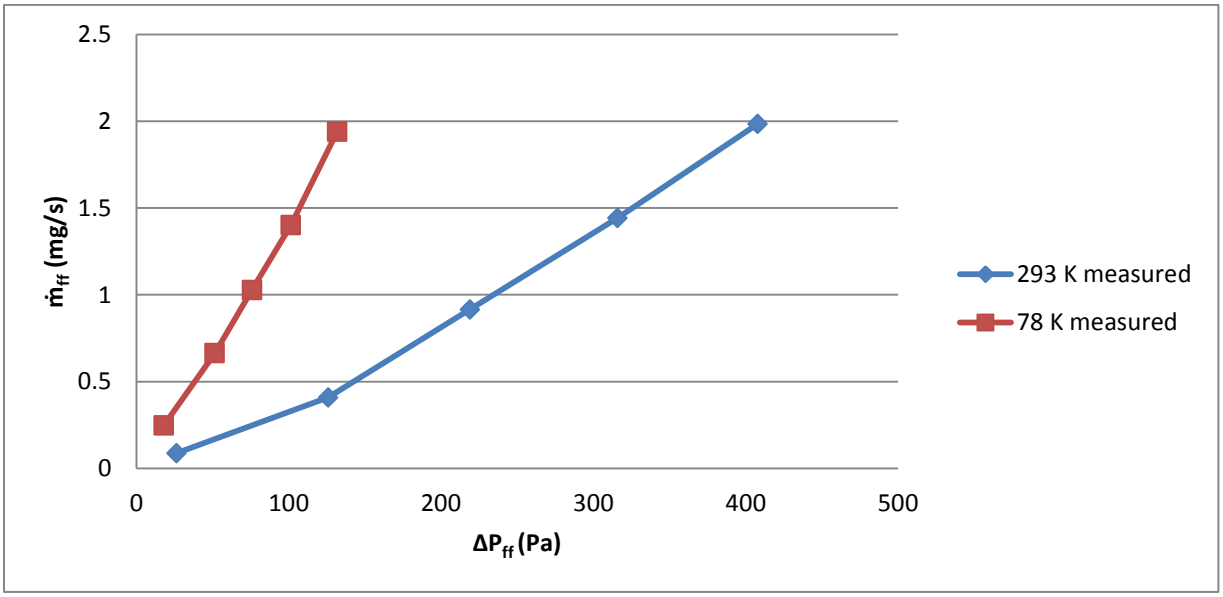

Figure 5.7: Mass flow rate vs pressure in forward flow at 78 K

Though the flow rate was not increased to 9.2 mg/s, it is clear that at both room temperature and nitrogen temperatures, the pressure drop is on the same order as the selected 100-200 Pa. As can also been seen, as the temperature is decreased, the pressure drop is decreased. It can therefore be assumed that the pressure drop in the forward flow direction was acceptable.

5.2 Cryocooler Test

Though the nitrogen tests gave good indications of a working valve, the sealing criteria selected was effectively an educated guess. To verify the model and the understanding of the flow characteristics, a continuous temperature profile must be generated. If this predicted temperature and mass flow profile could be reconciled with experimental data, there are grounds to explore the scaling argument detailed at the end of this section.

5.2.1 Procedure

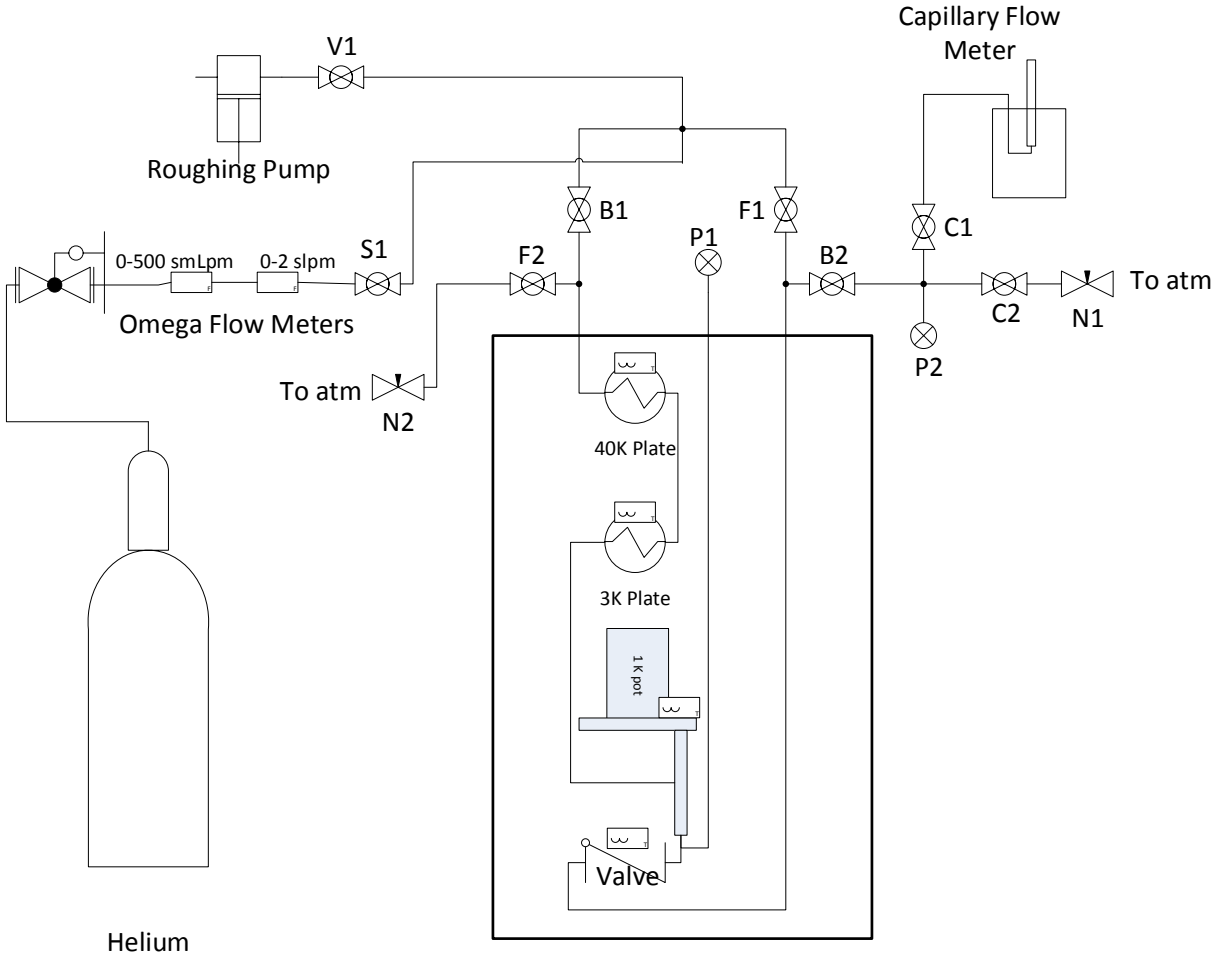

Figure 5.8: Cryocooler process diagram revisited

The process diagram for the cryocooler test facility is again shown in Figure 5.8 to aid in describing the procedure. A detailed operating procedure for the cryocooler can be found in Amir Jahromi's thesis. For the purposes of this thesis, the procedure for specifically operating the valve experiment is included.

The first step after integrating the valve into the system was to clear the lines of all possible residual gases. This is even more critical than in the nitrogen experiment since both air and

water will freeze at the temperatures the cryocooler can achieve. Valves V1, C1 and C2 were closed, while all other valves were left open. The system was then charged with 1 psi of helium gas. The roughing pump was turned on and Valve S1 was closed while V1 was opened, pumping out the system. After the system was fully evacuated, V1 was again closed while S1 was opened, purging the system. This was repeated several times.

Following the pump and purge, the preload could be applied. The liquid nitrogen tests indicated that preforming with a thicker reed at higher pressures and installing a thinner reed for low pressure operation produced the best results. However, contaminant control became a serious issue with the new setup, where a small amount of air or particulate trapped in the system could cause serious issues. Therefore another option to preform the seat was explored. As mentioned, Teflon has several phase transformations, one being at 20 C. Therefore, if the seat could be heated well above 20 C it should become more malleable and the thin reed could be used to preform the seat at low pressures. A pressure difference of 10 psi was enforced across the valve and it was immersed in 50 C water for 15 min to ensure a uniform temperature. The room temperature flow rate before the valve was heated was 0.9344 μg/s; and after the valve was allowed to cool back to room temperature it was 0.2217 μg/s. This method did improve the sealing, however not as drastically as the .008” 80 psi preform, where the room temperature flow rate was below the range of even the bubble flow meter. This course was still used since the flow characteristics across the valve did not fundamentally change between the two methods, therefore the modeling could still be confirmed and scaling could be investigated.

After preforming at a high temperature, a preload pressure of 10 psi was held across the valve. The needle valve N2 was used to hold a slight positive pressure in the line to prevent air from entering into the system during cool down. Therefore the gauge pressure before the valve was 10.5 psi and after the valve .5 psi in the closed condition. The cryocooler radiation shielding and vacuum can were closed up. A vacuum was pulled on the experiment space and the cryocooler was turned on.

5.2.2 Results

As the facility was cooled, the leakage rate was measured frequently to complete a temperature vs mass flow rate curve for the valve shown in Figure 5.9.

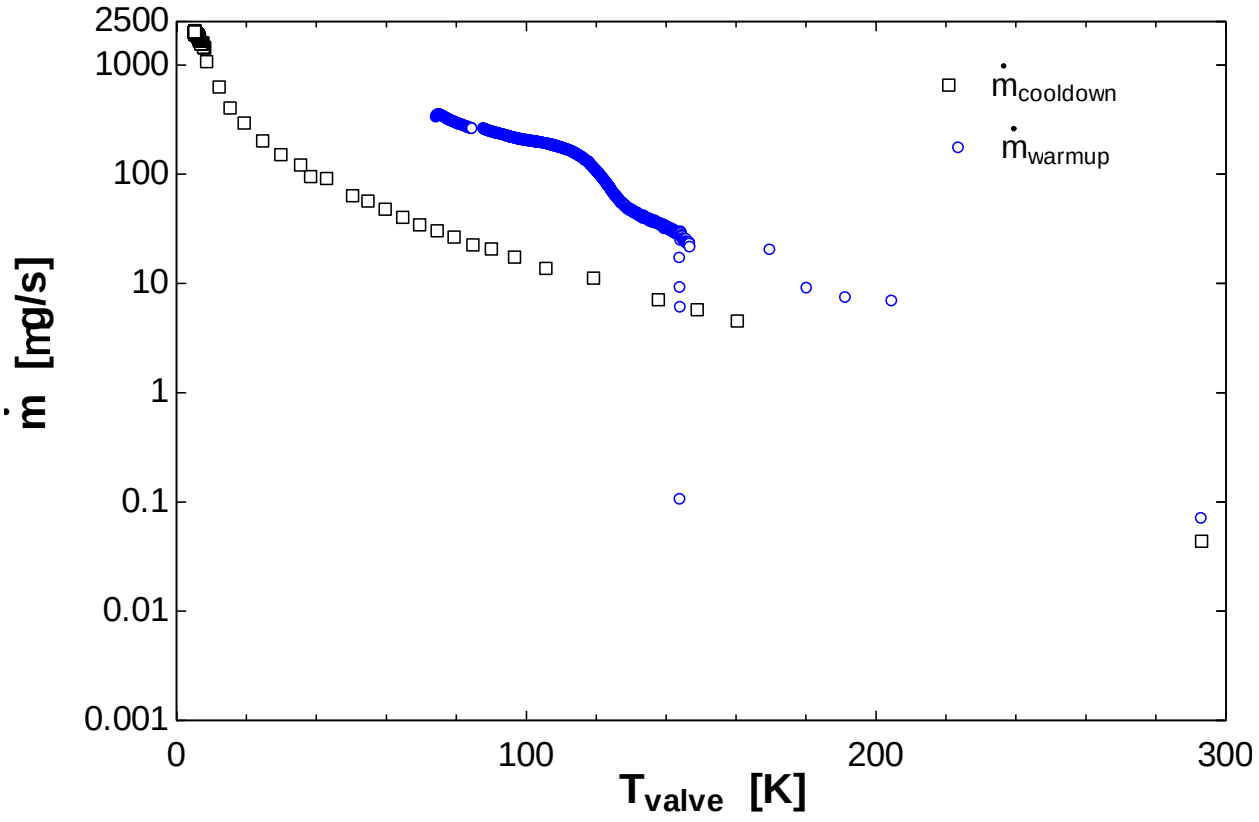

Figure 5.9: Mass flow rate vs temperature during first cool down and warm up on cryocooler

A feature to point out in Figure 5.9 is the disparity between the cool down and warm up mass flow rates. At the final low temperature of the test the flow was reversed and forward flow was tested to confirm that there were no blockages in the line. When sealing was attempted again in the back flow direction, flow simply blew through the valve beyond the range of the flow meter. After the test, the valve was disassembled and under visual inspection small particulates could be seen on the seat. Most appeared to be metal flakes, the largest was assessed under a microscope with a reference scale and found to be approximately 15 microns in size. It was at this point that the particulate screens were deemed necessary. After installation, a second test was run, shown in Figure 5.10. Figure 5.11 shows both tests on a log scale with error bars based on an uncertainty propagation conducted with EES.

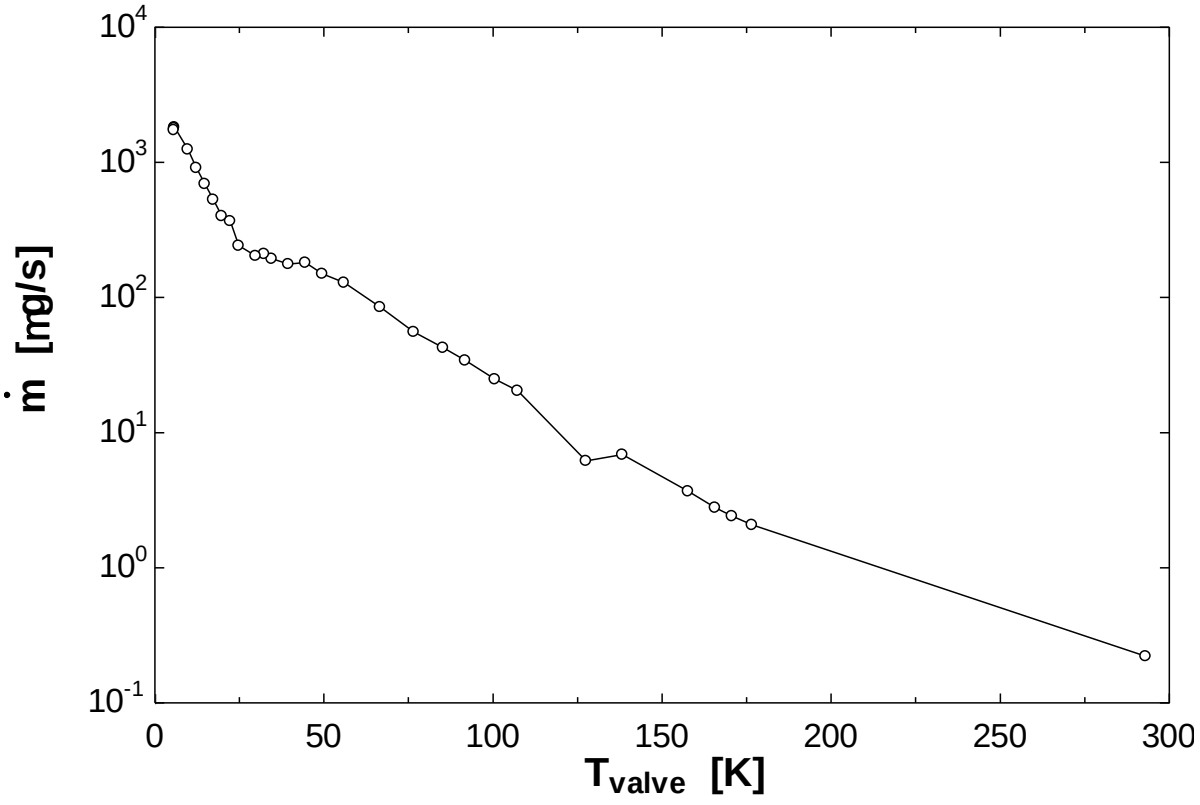

Figure 5.10: Mass flow rate vs temperature during second cool down on cryocooler

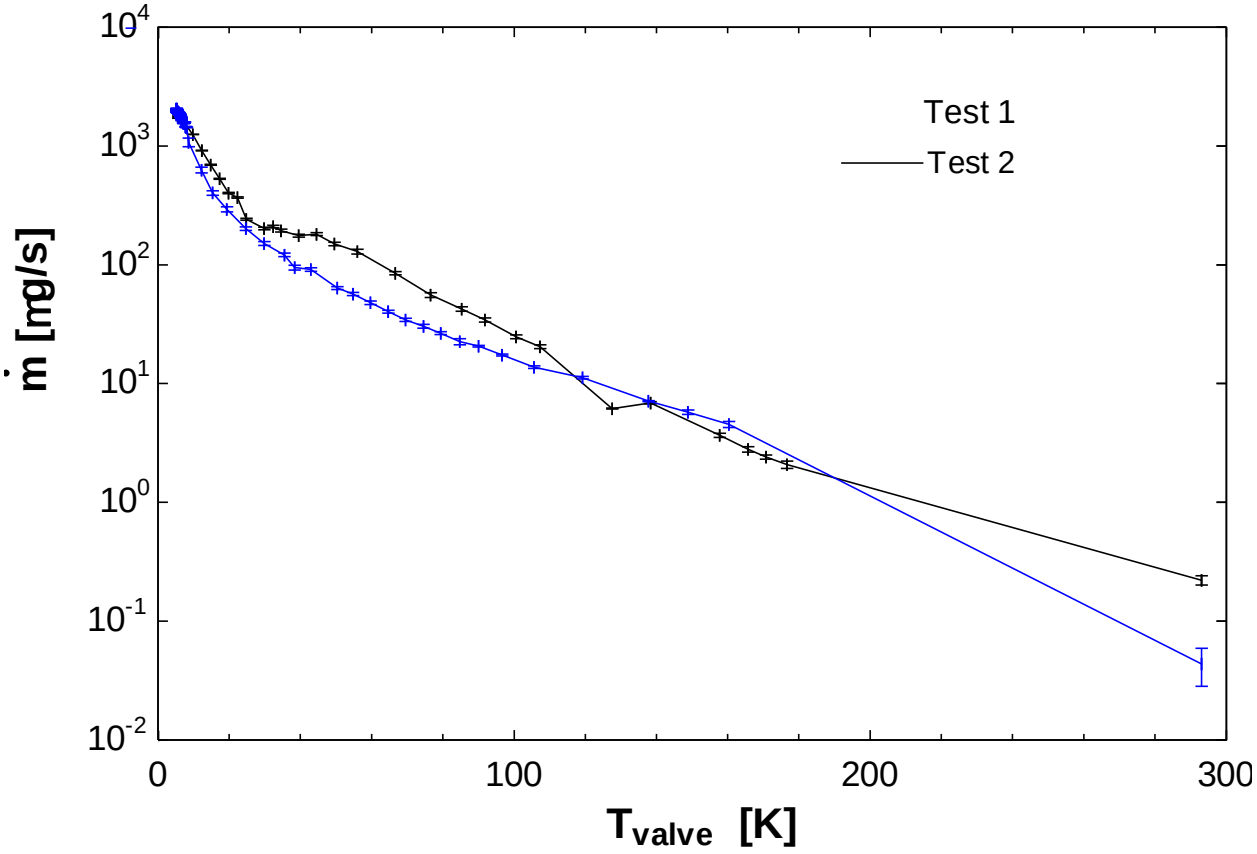

Figure 5.11: Mass flow rate vs temperature for both tests with error bars on log-linear scale

At the ultimate low temperature, the flow was reversed to confirm that there were no blockages. After the forward flow, when sealing was attempted, the flow was again above range of the flow meter. The valve was warmed up and at the flow rate was taken at room temperature and found to be 0.6431 μg/s (~3 times as higher than before cool down). The valve seat was visually inspected and again several particulates were observed in spite of the particulate screens.

It was clear that a finer mesh would be required to prevent the particulates from interfering with sealing. At this point, the cool down data was adequate to investigate the model and

develop a possible scaling argument. Also, finer screens are significantly more expensive so new screens were not installed and the data was proceeded with as is.

5.3 Comparison to model

With a profile of the mass flow rate as it changes with temperature, the model results can be compared to the experimental data in Figure 5.12.

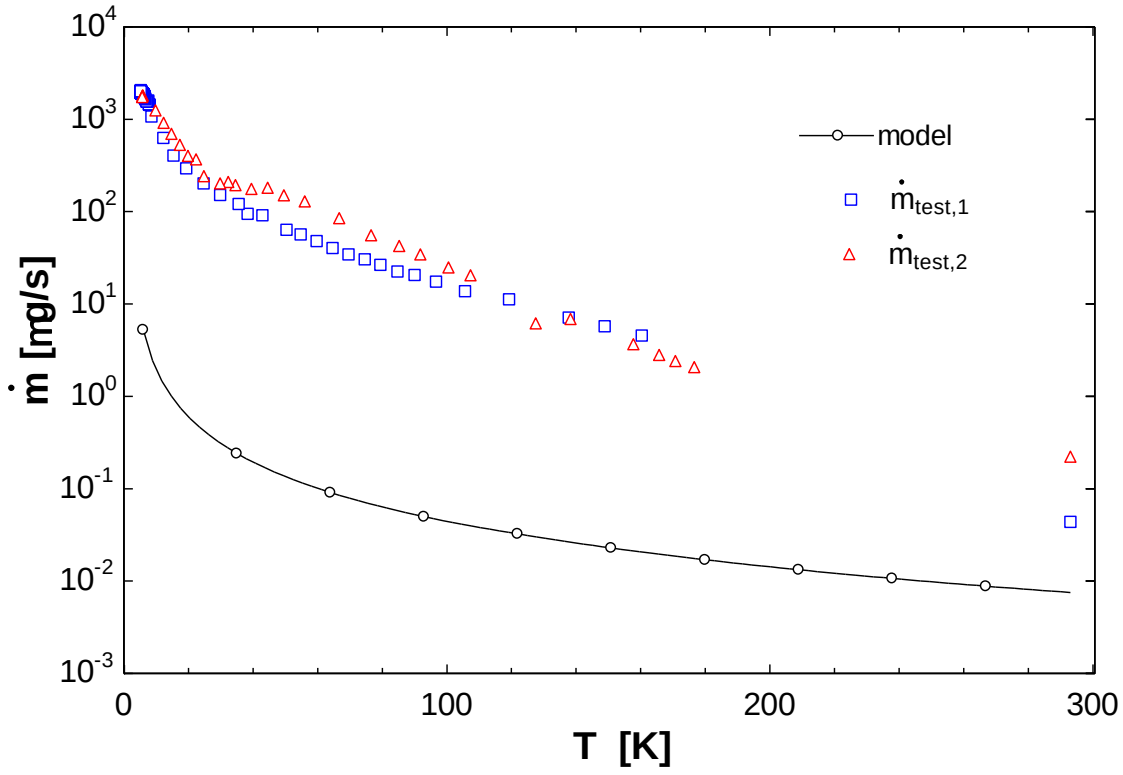

Figure 5.12: Experimental mass flow rate vs temperature compared to laminar flow model

The model drastically under estimated the mass flow rate. However, viewing the model on a different scale as in Figure 5.13, yields some interesting results. The shape of the model almost perfectly matches the shape of the experimental data. This is unlikely to be due to incorrect assumptions of the flow, since the difference between laminar and turbulent flow would not result in a simple offset.

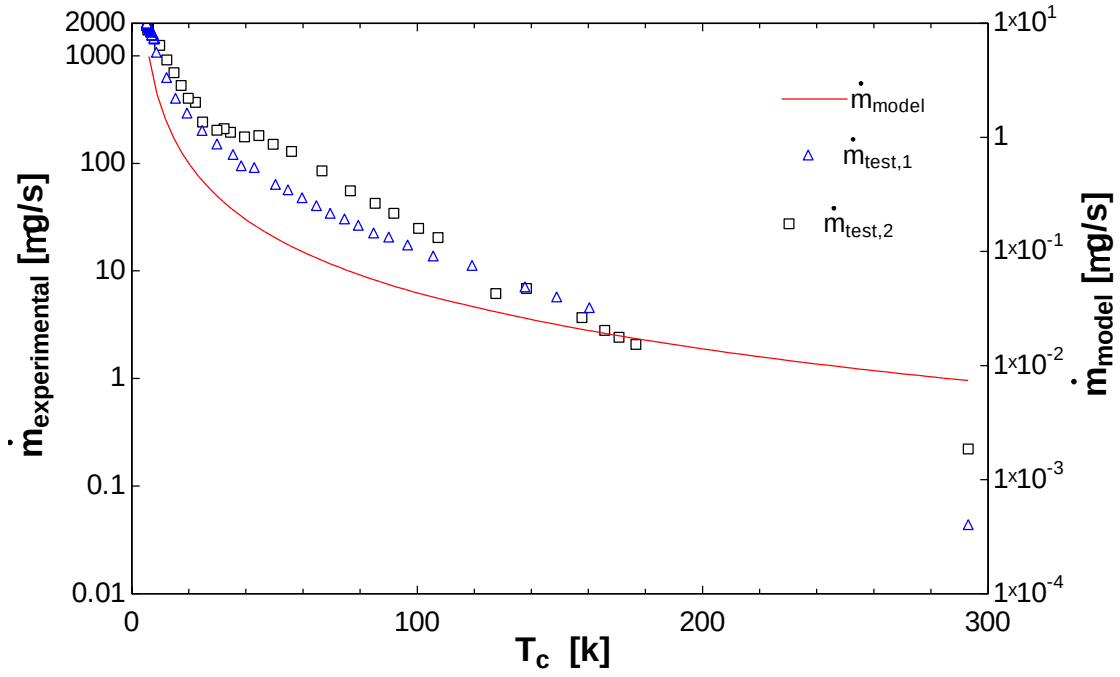

Figure 5.13: Experimental mass flow rate vs temperature compared to laminar flow model with separate axis

Reexamining Equation 5.3 for relating mass flow rate to pressure drop in the laminar case sheds light on this offset.

$$\Delta P = \frac{128\mu\Delta L\dot{m}_{tot}}{\rho^2 d_{ch}^4 \pi n_{ch}} \tag{5.3}$$

It is clear that the density and viscosity will not change linearly with temperature or provide a linear offset. However, very liberal estimations where made of the flow geometry in the original modeling efforts. The purpose of holding the pressure constant during cool down was to maintain a constant flow geometry, changing only temperature and thus the thermophysical properties of the fluid. Therefore the equation can be simplified to Equation 5.4.

$$\Delta P = \frac{m\mu \Delta L \dot{m}_{tot}}{\rho^2} \tag{5.4}$$

Here it becomes clear that a scaling argument can be introduced. If the number and size of flow channels do not change, a geometry term, *m*, can be introduced. This geometry term can be found with a reference fluid, such as ^{4}He, at a higher temperature. Knowing the properties of the fluid to be scaled for, such as a ^{3}He-^{4}He mixture, at a given temperature and pressure, the geometry term can be substituted in and the scaled mass flow rate can be found as a function of temperature. For example, in the first test, the flow rate was taken at room temperature to solve for the geometry term. The expected flow rate at a constant pressure drop was plotted against the experimental data shown in Figure 5.14.

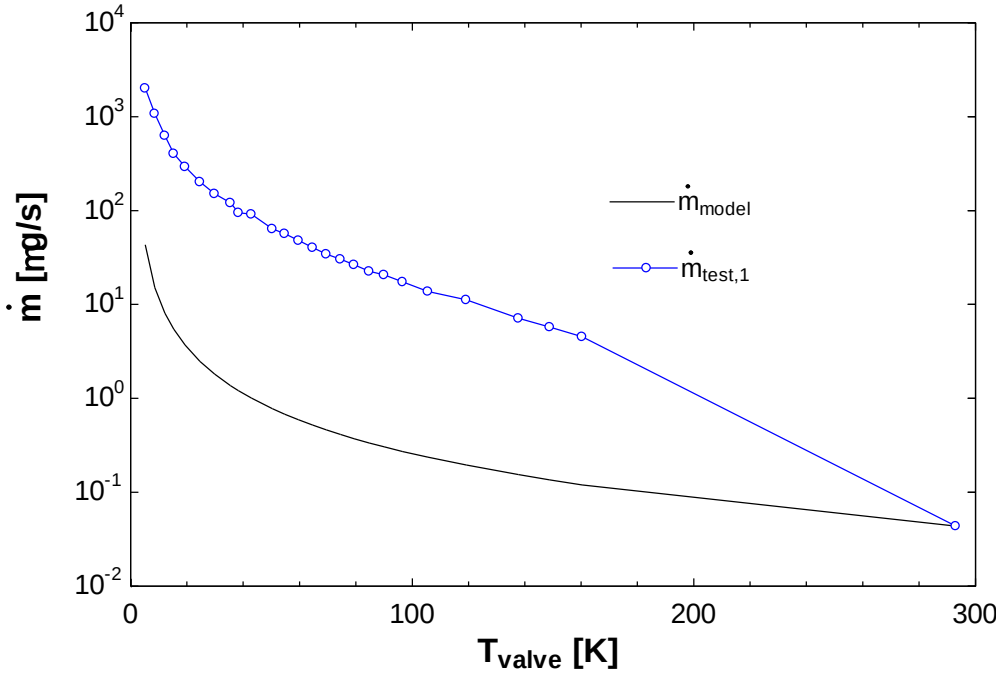

Figure 5.14: Experimental mass flow rate vs temperature compared to model scaled from room temperature

Scaling the model from room temperature still resulted in a large offset. However, the scaling assumes a constant geometry, whereas there is a great deal of differential thermal contraction

from room temperature down to low temperature. The geometry term was then found using the pressure difference, fluid properties and mass flow rates at various temperatures. The model mass flow rate was then solved for other temperatures using that geometry term and again plotted against the experimental data shown in Figure 5.15.

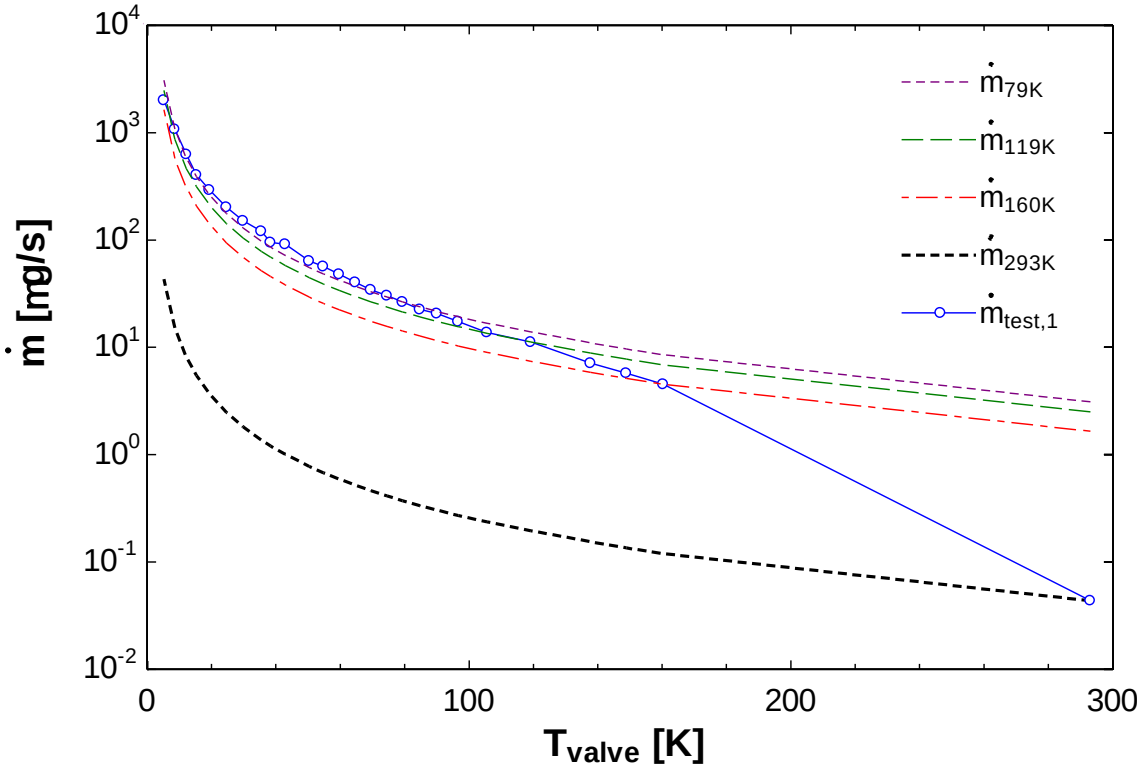

Figure 5.15: Experimental mass flow rate vs temperature compared to model scaled from various temperatures

The model becomes more accurate at lower temperatures as the scaling temperature is decreased. However with each decrease in scaling temperature, the gain in accuracy of the model becomes less. The RMS percent error of the model relative to the experimental data was found for temperatures below each respective scaling point and plotted in Figure 5.16 and Figure 5.17.

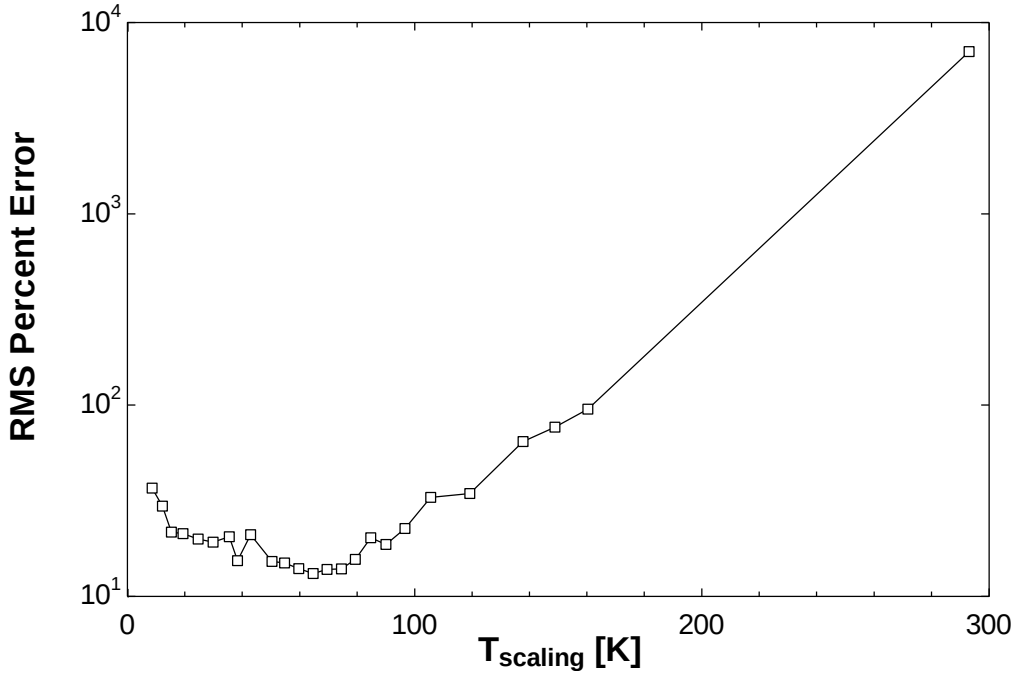

Figure 5.16: RMS error of model mass flow rate vs scaling temperature

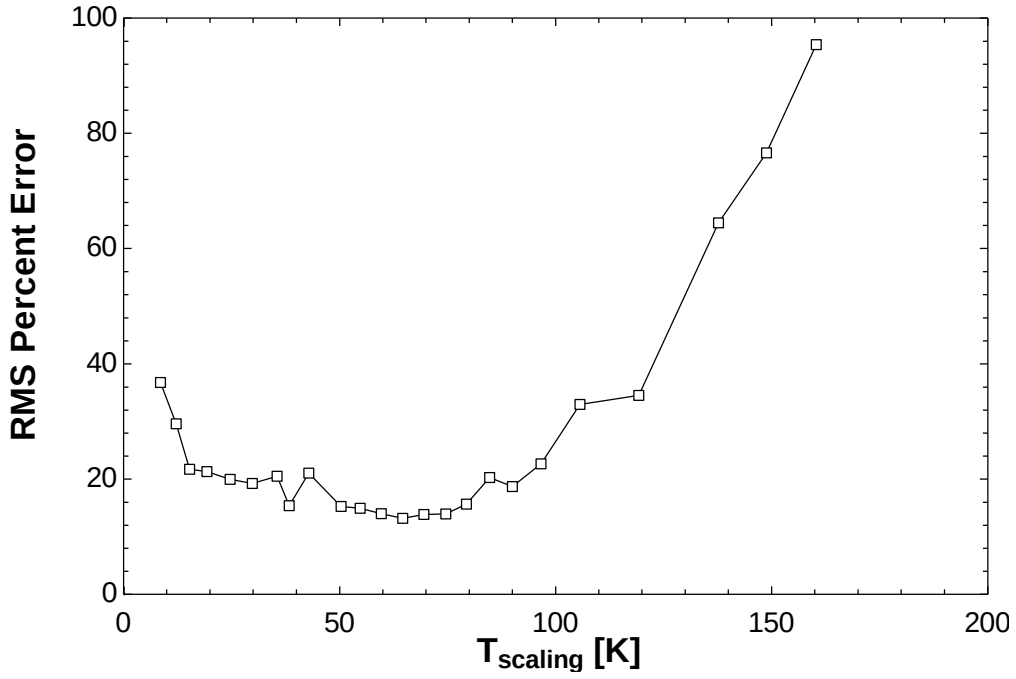

Figure 5.17: RMS error of model mass flow rate vs scaling temperature at low temperatures

These plots show that the scaling from temperatures lower than approximately 100 K does not significantly increase the accuracy of the model. Therefore, if the valve is tested at liquid

nitrogen temperatures (78 K) the geometry constant for the valve can be found and an accurate prediction can be made for the valve's performance at different temperatures. The performance with helium mixtures can also be predicted, since the model is a function of the geometry constant, which does not seem to change significantly after approximately 100 K, and the fluid properties, which are known.

For the pressure dependence of the flow rate, unfortunately the model does not agree even after applying the concept of a geometric constant. The issue is that the laminar model makes the assumption that the geometry does not change when there are clearly non-linear changes in geometry due to the flexure of the reed. Figure 5.18 shows the actual pressure dependence vs the model for the results from the liquid nitrogen test.

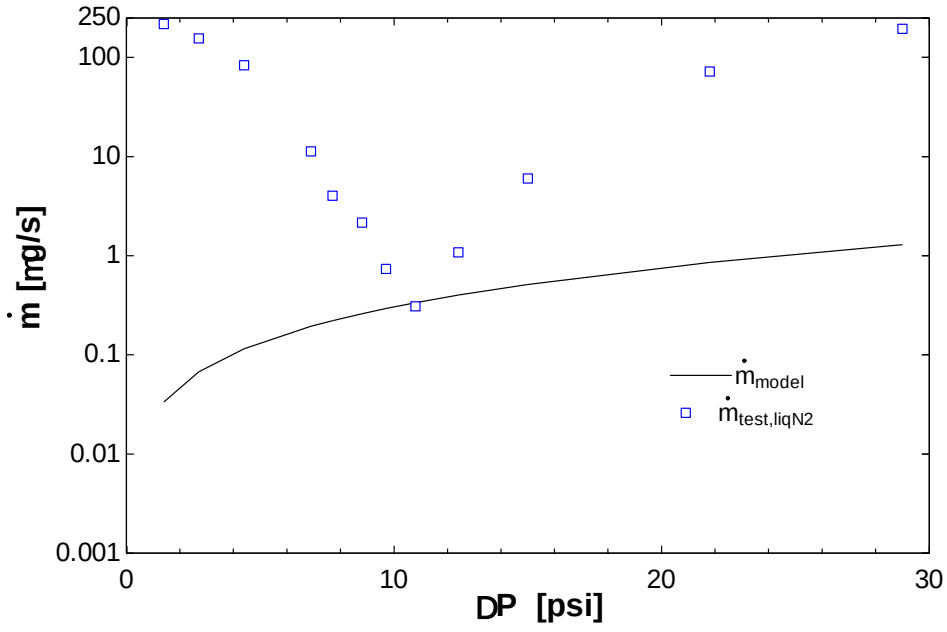

Figure 5.18 Pressure vs mass flow rate for experimental results from liquid nitrogen test compared to model

Though the model doesn't accurately predict pressure dependence, it does not mean that the results cannot be scaled to the ^{4}He-^{3}He mixture. The preloading results in excellent sealing at

the set pressure, so it can be assumed that the preload could be optimized for the lower pressure operation in the CCDR. If the sealing results of the cryocooler test, with thermal preforming employed, were scaled to using the properties of ^{3}He-^{4}He mixtures, the resulting scaled flow rate would be 9.112 mg/s of ^{3}He-^{4}He. This is far above the required 92 µg/s. However, scaling the liquid nitrogen tests, with high pressure, thick reed preforming, results in a scaled flow rate of 102.8 µg/s ^{3}He-^{4}He. This is very close to the required low flow rate established in the beginning of this thesis. In fact, 102.8 µg/s of leakage in the back flow direction is only 1.1% of the forward flow. Though this is slightly above the selected criteria of 1%, it is close enough to indicate a successful test.

6 Conclusion and Future Recommendations

For future work, the first priority should be to verify that the assumed sealing criteria and forward flow pressure drop are acceptable. The current CCDR model assumes that there is no leak back rate and no pressure drop in the forward direction, so further refinement of this model is required. Experimentally, another iteration of the valve could be fabricated with much finer filter screens and further particulate mitigation steps. If the particulate issue could be resolved, repeatability could then be tested. The final refinement could be to test the valve with the exact same fluid and set points as in the CCDR, with ^{3}He-^{4}He mixtures at 1.8 K, though with limited ^{3}He availability this would be very difficult.

In conclusion, the design, fabrication, modeling and testing of a cryogenic check valve for application in a Cold Cycle Dilution refrigerator was presented in this thesis. The check valve design and modeling efforts justified cryogenic temperature tests. Initial testing in liquid nitrogen indicated that the design was a good candidate for application in the CCDR. Further testing with a Pulse-Tube Cryocooler facility confirmed the modeling efforts and provided a temperature profile of the valve performance. Finally using the temperature profile, combined with modeling efforts, a scaling argument was presented. With this argument a valve could be tested with pure ^{4}He gas at liquid Nitrogen temperatures (~78 K) and the results could be scaled to operation in the CCDR with ^{3}He-^{4}He mixtures at 1.8 K. Revisiting the nitrogen test results and using this scaling, it was shown that the best sealing attained with those tests was only 1.1% of the forward flow rate required by the CCDR.

Appendix A

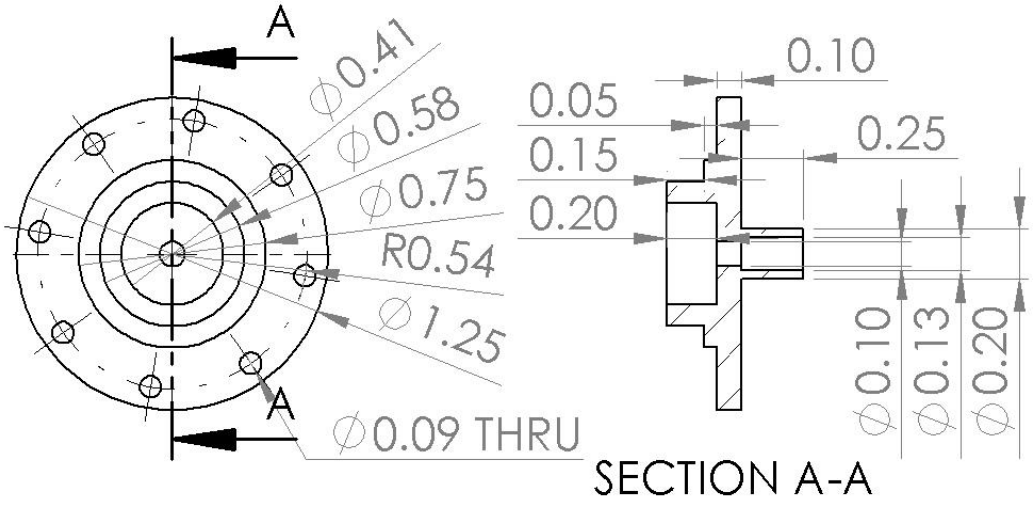

Figure A-1: Valve base dimensioned drawing

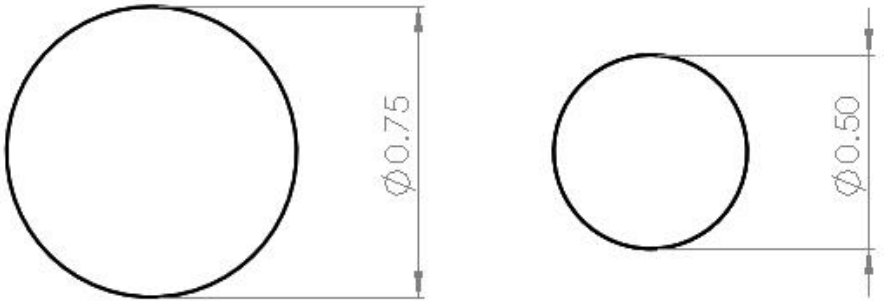

Figure A-2: Large (left) and small (right) particulate screens, both are approximately .004" thick

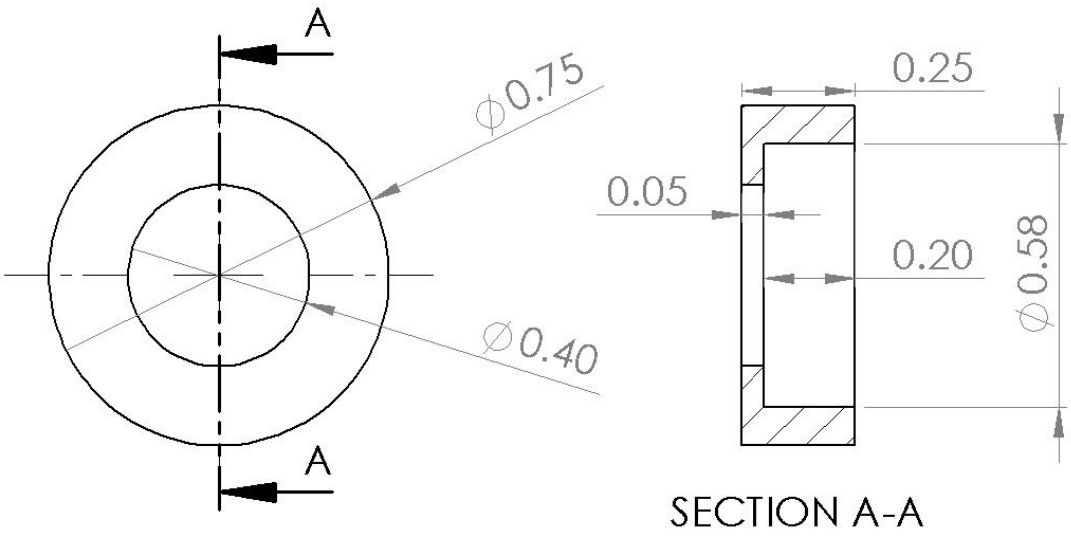

Figure A-3: Teflon seat dimensioned drawing

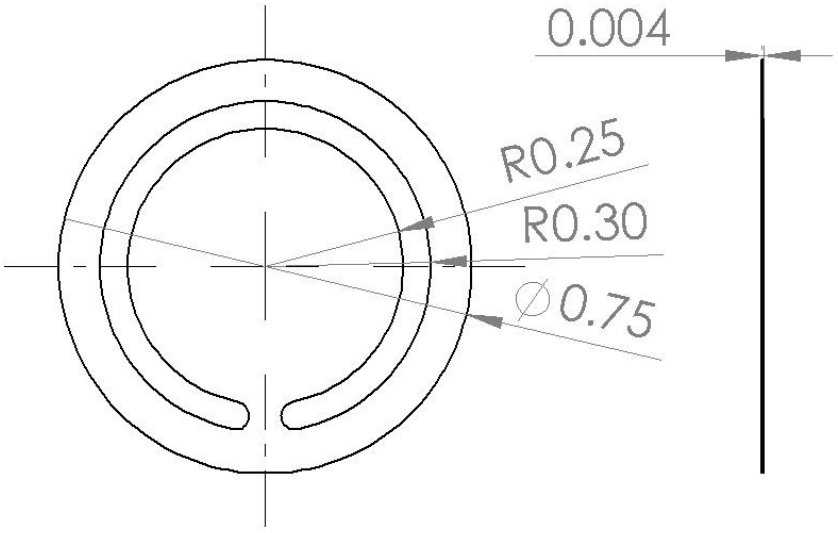

Figure A-4: Reed dimensioned drawing

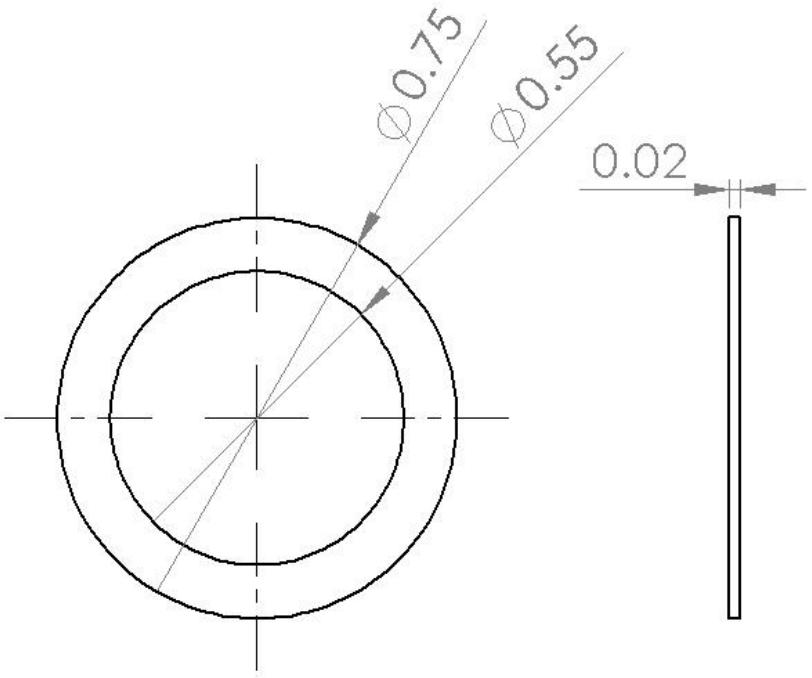

Figure A-5: Copper Washer dimensioned drawing

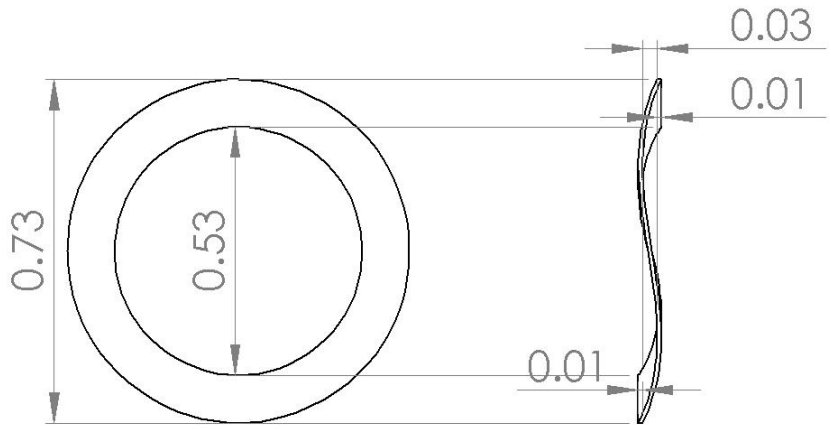

Figure A-6: Wave spring dimensioned drawing

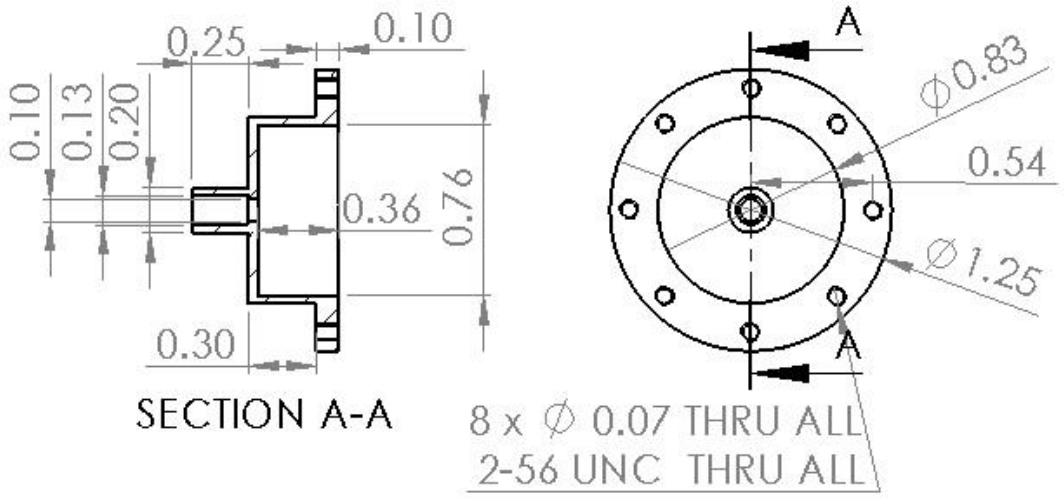

Figure A-7: Valve top dimensioned drawing

Appendix B

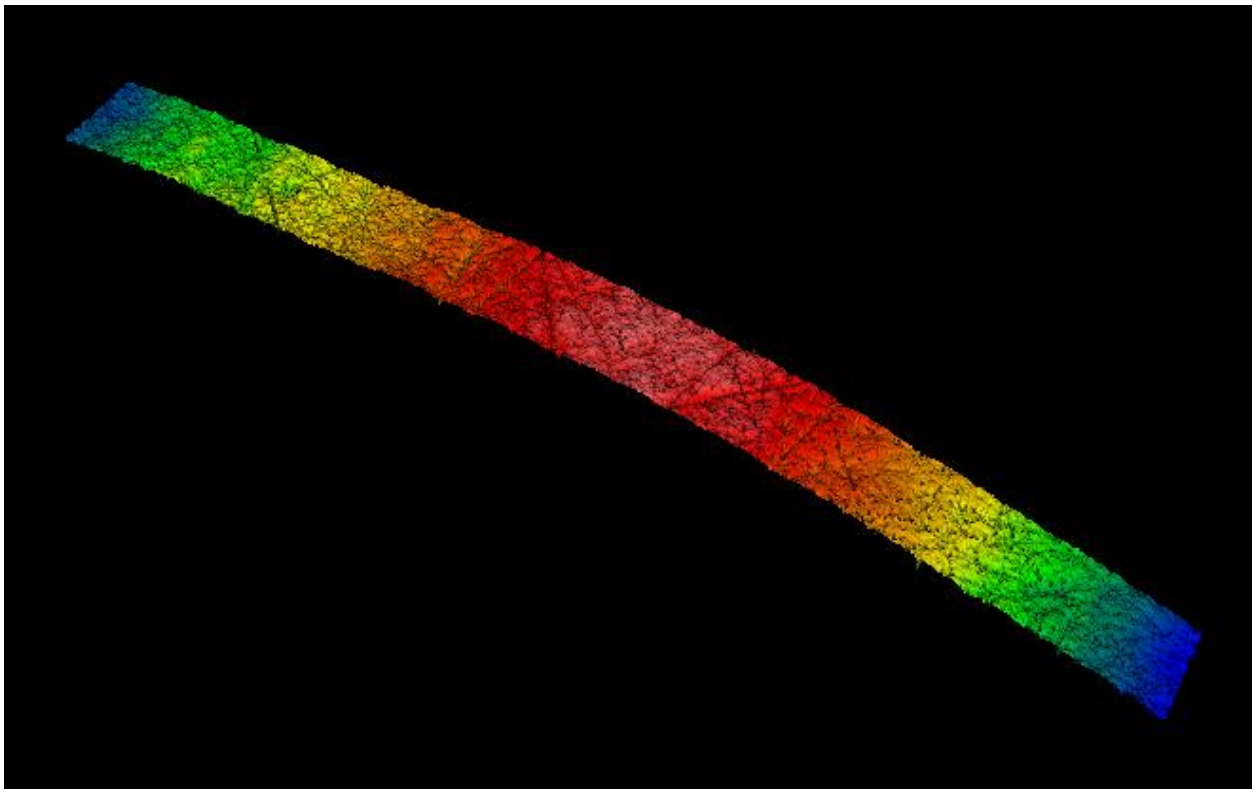

Figure B-1: 3-D model of the second section of the centerline scan

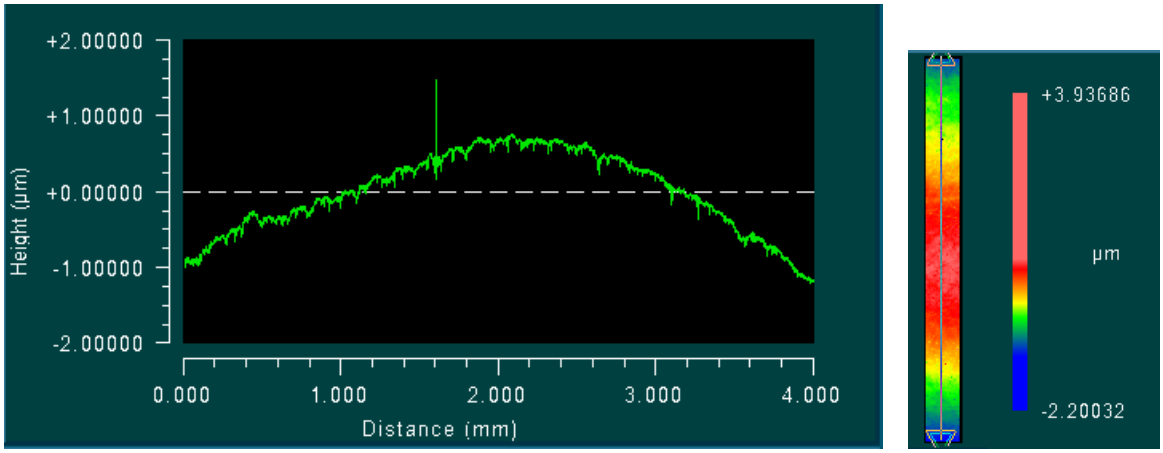

Figure B-2: Surface profile of the second section of the centerline scan (left) and the line along which it was taken (right)

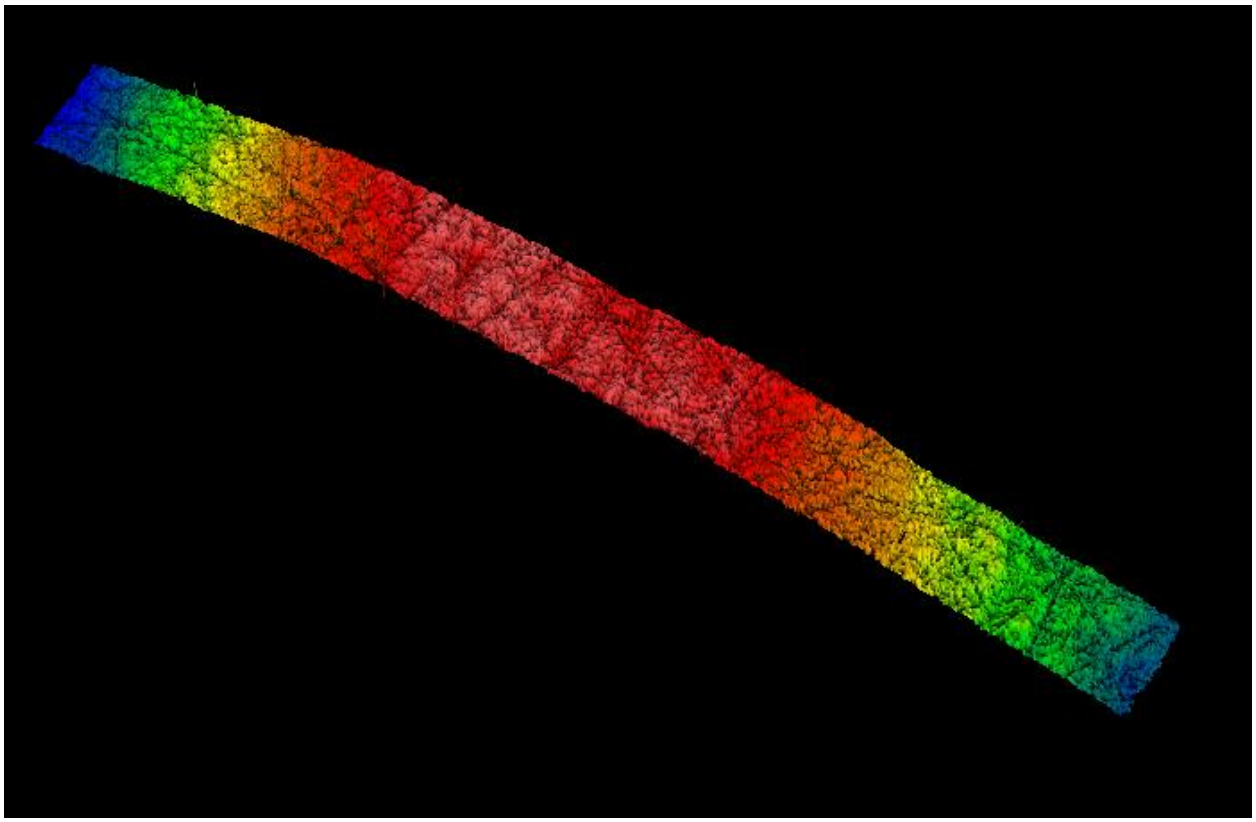

Figure B-3: 3-D model of the third section of the centerline scan

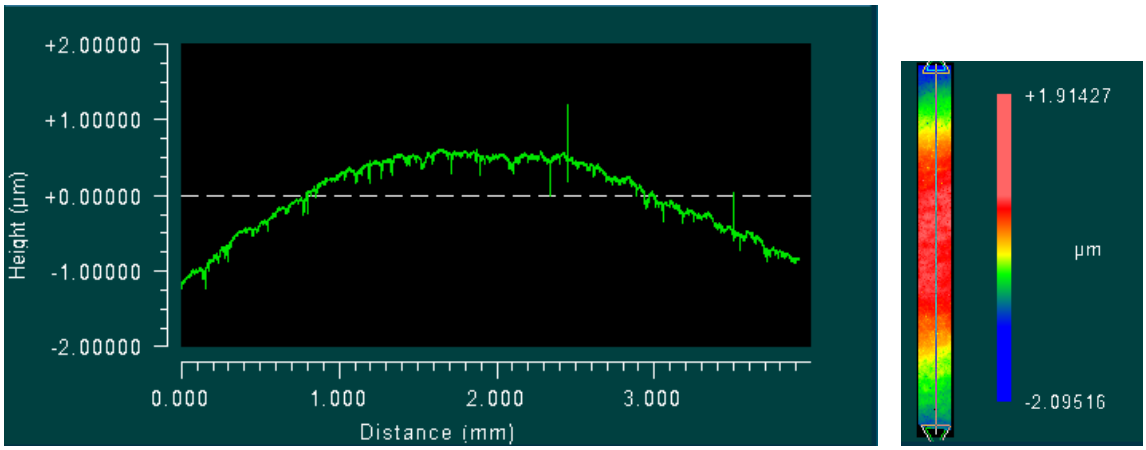

Figure B-4: Surface profile of the second section of the centerline scan (left) and the line along which it was taken (right)

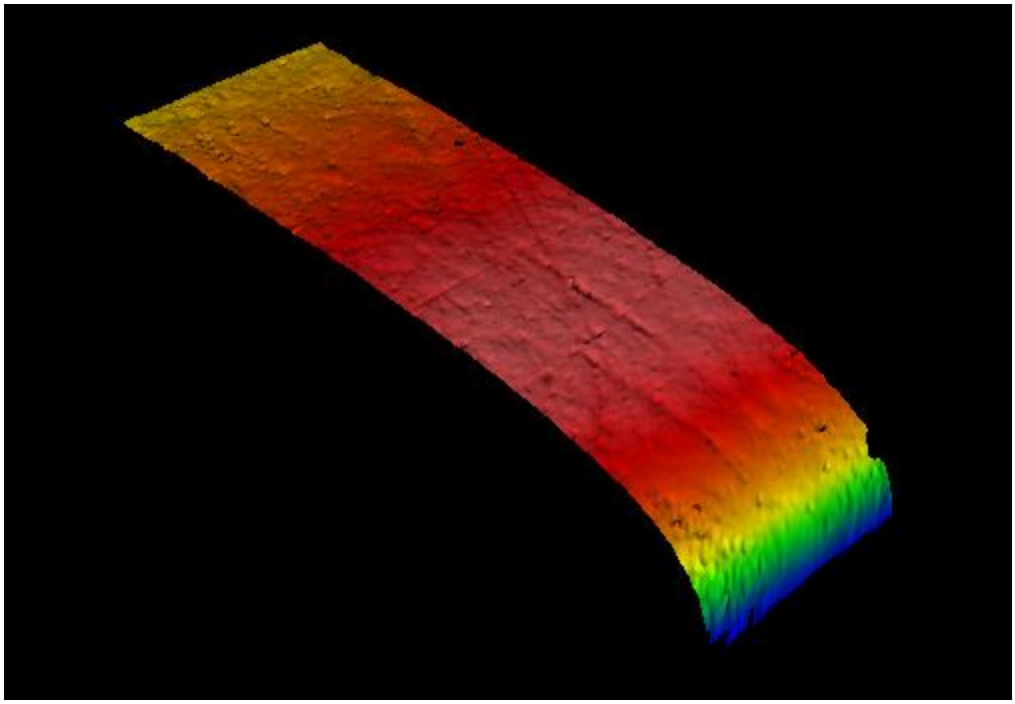

Figure B-5: 3-D model of the fourth and final section of the centerline scan

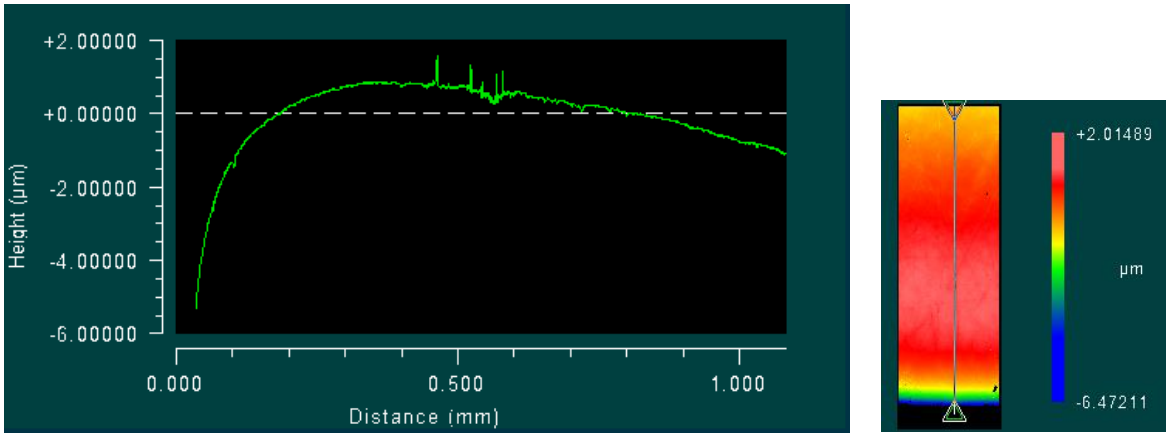

Figure B-6: Surface profile of the fourth and final section of the centerline scan (left) and the line along which it was taken (right)

Appendix C

```
$Unitsystem SI, J, K, Pa, rad

"Laminar flow model 3He-4He mixture"

"Curve fit from Meyer's data"
Function mu_mix(T)
    a:=    2.42043e-06
    b:=    -4.8511e-06
    c  :=  -5.5577e-06
    d  :=  3.08947e-05
    e  :=  8.1608e-05
    f   := -0.00025280
    g  :=  -0.00032014
    h  :=  0.001138017
    i   := -6.412e-05
    j   := -0.00153212
    k  :=  0.000961198
    mu_mix=(a+b*ln(T*1[1/K])+c*(ln(T*1[1/K]))^2+d*(ln(T*1[1/K]))^3+e*(ln(T*1[1/K]))^4+f*(ln(T*1[1/K]))
^5+g*(ln(T*1[1/K]))^6+h*(ln(T*1[1/K]))^7+i*(ln(T*1[1/K]))^8+j*(ln(T*1[1/K]))^9+k*(ln(T*1[1/K]))^(10))*1[
Pa-s]
end

v_34_mol=lookup('v', 281,'Column12') "Specific volume at x_3He=.055, (approximately same as .05
and .06) and T=1.8 from Chaudhry"

MM_3=3.0160293191 [g/mol]                          "Molar Mass 3He"
MM_4=4.00260325415 [g/mol]                         "Molar Mass 4He"
MM_tot=.06*MM_3+.94*MM_4                           "Total Molar Mass of Mixture"

rho_34_mass=(MM_tot/v_34_mol)*convert(g/m^3,kg/m^3)"Mass density of mixture"
mu_34=mu_mix(T)                                    "Viscosity of mixture"

DELTAP=20000 [Pa]                                  "Pressure difference across valve"
T=1.8 [K]                                          "Temperature of valve"

L_tot=.1[in]*convert(in,m)                         "Length of sealing surface"
d_ch=.5E-6 [m]                                     "Diameter of micro channels"
n_ch=30000                                         "Number of micro channels"

DELTAP=128*mu_34*L_tot*m_dot_34/(rho_34_mass*d_ch^4*pi*n_ch)"Laminar pressure drop across
valve"

Re=4*m_dot_34/(n_ch*pi*d_ch*mu_34)                 "Reynolds number for flow"

m_dot_micro=m_dot_34*convert(kg/s, microgram/s)    "mass flow rate in microgram/s"
```

Appendix D

```
$Unitsystem SI, J, K, Pa, rad

P_amb=98000 [Pa]                                    "ambient pressure the helium will be vented
to"
P_high=10.25[psi]*convert(psi,Pa) +P_amb            "high pressure at the test conditions"
P_low=.25[psi]*convert(psi,Pa)+P_amb                "low pressure at the test conditions (held
constant)"
DELTAP_tot=P_high-P_low                             "pressure difference across valve"

T_c=6 [k]                                           "Temperature of the valve"

L_tot=.1[in]*convert(in,m)                          "total length of the sealing surface"
d_ch=.5E-6 [m]                                      "diameter of the micro channels"
n_ch=16000                                          "number of micro channels"

Num=20[-]                                           "number of differential control volumes"

dL=L_tot/(Num-1)                                    "Length of each differential CV"

P[1]=P_high                                         "setting first differential control volume to the
high pressure"

"loop runs through all of the differential CVs"

duplicate i=2,Num

    mu[i]=viscosity(Helium, T=T_c, P=P[i])          "viscosity at each pressure"

    rho[i]=density(Helium, T=T_c, P=P[i])           "density at each pressure"

    DELTAP[i]=128*mu[i]*dL*m_dot_tot/(rho[i]*d_ch^4*pi*n_ch) "Pressure drop from flow"

    P[i]=P[i-1]-DELTAP[i]                           "evaluate the pressure at this node"

end

P[Num]=P_low                                        "final CV set to the low pressure"

Re=4*m_dot_tot/(n_ch*pi*d_ch*mu[2])                 "Reynolds number for flow"

m_dot_micro=m_dot_tot*convert(kg/s, microgram/s)    "converting the flow to microgram/s"
```

Appendix E

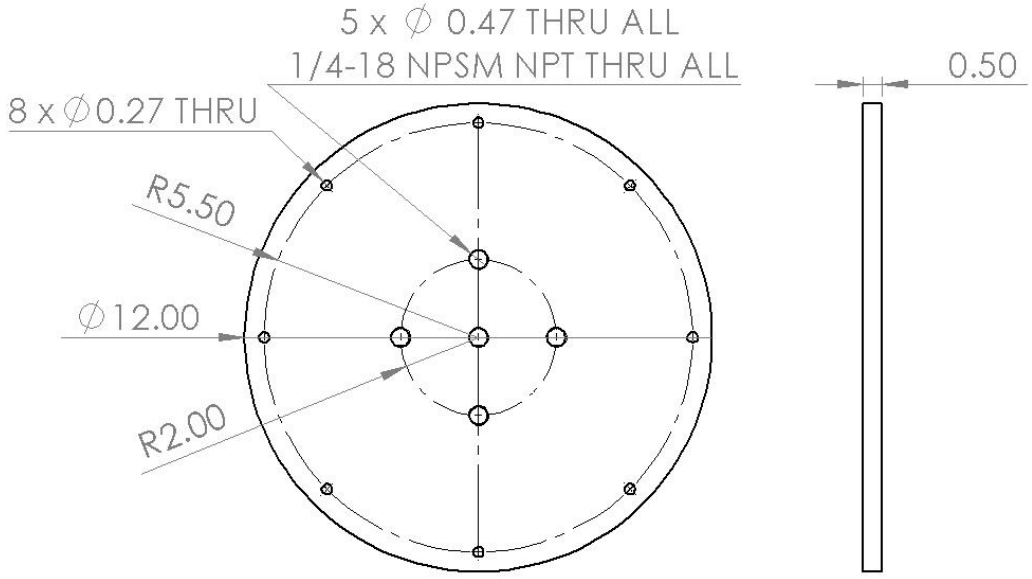

Figure E-1: Dimensioned drawing of aluminum top plate

Appendix F

```
$UNITSYSTEM SI, J, K PA, Radian

"mass flow rate"
m_dot=9.2E-6 [kg/s]
"Lengths of pipes"
L_pre40=7 [in]*convert(in,m)
L_40=.3
L_pre4=7 [in]*convert(in,m)
L_4=50 [in]*convert(in,m)
L_prev=7 [in]*convert(in,m)
L_out=1
"Pressure upstream and downstream of the valve"
P_up=1 [atm]*convert(atm, pa)+10 [psi]*convert(psi,pa)
P_dn=1 [atm]*convert(atm, pa)
"average temperatures at various points"
T_pre40=300 [K]
T_40=((300+40)/2) [K]
T_pre4=40 [K]
T_4=((6+40)/2) [K]
T_prev=6 [k]
T_out=((6+300)/2) [k]

"Diameters and areas of tubing"
D_lg=.065 [in]*convert(in,m)
D_sm=.025 [in]*convert(in,m)
A_lg=pi*D_lg^2/4
A_sm=pi*D_sm^2/4

"line from room to 40k plate"
call PipeFlow('Helium',T_pre40,P_up,m_dot,D_sm,L_pre40,0:h_T_p40, h_H_p40 ,DELTAP_p40,
Nusselt_p40, f_p40, Re_p40)
"HX on the 40k plate"
call PipeFlow('Helium',T_40,P_up,m_dot,D_lg,L_40,0:h_T_40, h_H_40,DELTAP_40, Nusselt_40,
f_40, Re_40)
"line from 40k to 4k plate"
call PipeFlow('Helium',T_pre4,P_up,m_dot,D_sm,L_pre4,0:h_T_p4, h_H_p4,DELTAP_p4,
Nusselt_p4, f_p4, Re_p4)
"4 k plate "
call PipeFlow('Helium',T_4,P_up,m_dot,D_sm,L_4,0:h_T_4, h_H_4,DELTAP_4, Nusselt_4, f_4,
Re_4)
"post 4k plate"
call PipeFlow('Helium',T_prev,P_up,m_dot,D_sm,L_prev,0:h_T_pv, h_H_pv ,DELTAP_pv,
Nusselt_pv, f_pv, Re_pv)
"DeltaP of outlet"
call PipeFlow('Helium',T_out,P_dn,m_dot,D_lg,L_out,0:h_T_out, h_H_out ,DELTAP_out, Nusselt_out,
f_out, Re_out)

"total pressure drop"
DELTAP_pre=(DELTAP_p40+DELTAP_40+DELTAP_p4+DELTAP_4+DELTAP_pv)*convert(pa,psi)
DELTAP_post=DELTAP_out*convert(pa,psi)
```

Appendix G

```
$Unitsystem J, K, Pa, Rad

N=250[-]                                        "Number of sub heat exchangers"
m_dot=9.2e-6[kg/s]                              "Mass flow rate of helium"
D=(.065)*convert(in,m)                          "Diameter of tubing"
P=170000[Pa]                                    "Pressure in line"
T_in=35.1[K]                                    "Inlet temp, 293 K 1st stage, 35 K 2nd stage"
T_w=5.1 [K]                                     "Wall temp, 35 K 1st stage, 5 K 2nd stage"
T_out=T_w+.1 [K]                                "Outlet temperature, .1 K above wall temp"

h_in=enthalpy('Helium', T=T_in, P=P)            "inlet enthalpy"
h_out=enthalpy('Helium',T=T_out, P=P)           "outlet enthalpy"

q_dot=m_dot*(h_in-h_out)                        "total heat transfer, should line up with
cooling power curve at temp"

"finding the heat transfer from each sub hx"
duplicate i=1,N
    q_dot[i]=i*q_dot/N
end

T[1]=T_in                                       "initial node temp"
h[1]=h_in                                       "initial node enthalpy"

"Energy balance on each sub hx"
duplicate i=2,(N+1)
    h[i]=h[i-1]-q_dot/(N*m_dot)
    T[i]=Temperature('Helium', h=h[i], P=P)
end

x[1]=0[m]                                       "initial length"
RelRough=0.02                                   "assumed relative roughness of copper
tubing"

"Finding the neccessary length of each sub-HX to achieve heat transfer found earlier"
duplicate i=1,N
    call PipeFlow_local('Helium',T_ave[i],P,m_dot,D,x_avg[i],RelRough:h_T_x[i], h_H_x[i], dPdx[i])
    x_avg[i]=(x[i]+x[i+1])/2
    h_bar[i]=h_H_x[i]
    T_ave[i]=(T[i]+T[i+1])/2
    dx[i]=m_dot*(h[i]-h[i+1])/(h_bar[i]*pi#*D*(T_ave[i]-T_w))
    x[i+1]=x[i]+dx[i]
    position[i]=x[i]
    P_loss[i]=-dPdx[i]*dx[i]
end

"Checking to be sure an iterative pressure is not required"
P_drop=SUM(P_loss[i],i=1,N)
"Guesses for length"
duplicate i=1,N
    guess[i]=x[i]+0.001[m]
end
```